

**Palaeoenvironmental variabilities: A multi-proxy study of
lacustrine sediments from salt lakes in the Antequera region
(Andalusia), Southern Spain**

by

Tabea Schröder

A thesis submitted for the Degree of Master of Science

in Applied Geosciences

at the RWTH Aachen University

September 2013

Supervision by

Prof. Dr. Klaus Reicherter & Dr. Margret Mathes-Schmidt

Institute of Neotectonics and Natural Hazards, RWTH Aachen

Statement of authorship

I hereby affirm that this master thesis has been composed of myself and describes and constitutes my own work, unless otherwise acknowledged in the text. All references and verbatim extracts have been quoted, and all sources of information have been specifically acknowledged.

_____, the _____

Contact

B.Sc. Tabea Schröder

Dennewartstr.5

52068 Aachen; Germany

Email: tabea.schroeder@rwth-aachen.de

Phone: +49 (0)157 85927066

Acknowledgement

I would like to express my great appreciation to Prof. Dr. Klaus Reicherter and Dr. Margret Mathes-Schmidt, my research supervisors, as well as the other academic staff of the Institute of Neotectonics and Natural Hazards for useful critiques of this work and the possibility of contributing to the research project of the SFB 806 "Our Way to Europe". My thanks are also extended to M.Sc. Nicole Höbig for her great advice, support and the exchange of ideas. I would also like to express my deep gratitude to Prof. Dr. Frank Schäbitz and his research group for offering me their help, especially Jonathan Hense and Konstantinos Panagiotopoulos, with whom I was privileged to work with.

A special thank of mine goes to my friend Yasar Manß for his broad and nice encouragement and generous technical assistance. Finally, I would also like to extend my thanks to my parents, especially my mother, for her encouragement and great support under every circumstance throughout my studies.

Abstract

Within the framework of the work of the Collaborative Research Centre 806 which investigates the history of the humankind, a multi-proxy analysis was applied on lacustrine sediments of Andalusia, Southern Spain. In this study different methods were applied on the sediments of the Laguna Dulce, Laguna Salada, Laguna de la Ratoša and the Laguna del Gosque to gain valuable information about past climate and environment, like the magnetic susceptibility, the X-ray fluorescence method and pollen analysis. Salt lakes constitute good archives of sediments and the south-western Mediterranean region represents an excellent site for palaeoclimate reconstruction. This and the proximity to archaeological sites on the Iberian Peninsula accounted for the selection of the research area, where variations of the past climate could be detected with the use of the geochemical and geophysical methods. The pollen analysis leads to interesting but unexpected results, which allowed no significant correlation with the indicated changes within the lacustrine sediments.

Kurzfassung

Im Rahmen eines Projektes des Sonderforschungsbereiches 806 „Our Way to Europe“ wurde im März 2012 eine Geländekampagne mit dem Zweck der Erbohrung lakustriner Sedimente in Südspanien durchgeführt. Das Ziel dieses Projektes ist die Untersuchung der Geschichte des modernen Menschen und seiner Migration nach Europa anhand von sich ergänzenden geowissenschaftlichen und archäologischen Methoden. Der südwestliche Mediterranraum der Iberischen Halbinsel besitzt ein herausragendes Potential für die Erforschung des Paläoklimas, zusätzlich befinden sich dort archäologische Fundstätten von wesentlicher Bedeutung. Der Mediterranraum und der Süden Spaniens bieten somit beste Voraussetzungen für eine wissenschaftliche Untersuchung vergangener Umweltbedingungen und deren Bedeutung für den Menschen.

Im Rahmen dieser Forschungsarbeit wurden verschiedene Methoden an Sedimenten der Laguna de Salada, Laguna Dulce, Lagune del Gosque und Laguna de la Ratoša nahe der Stadt Campillos in der Provinz Andalusien, Südspanien, angewandt. Diese liegen in einem endorheischen und unter Naturschutz stehenden Komplex, dessen größtes Gewässer die Laguna de Fuente de Piedra darstellen. Da Seen Archive terrestrischer Sedimente sind eignen sie sich ganz speziell für eine wissenschaftlichen Paläoumwelt und – klimarekonstruktion. Es wurden sedimentologische, geochemische (Röntgenfluoreszenzanalyse) und geophysikalische Methoden (Magnetische Suszeptibilität) genutzt, als auch eine Pollenanalyse an den lakustrinen Sedimenten durchgeführt. Mit deren Hilfe konnten Schwankungen der Paläoumweltbedingungen in Südspanien festgestellt werden.

Content

Introduction.....	6
Regional setting.....	7
Climate in the Western Mediterranean region.....	9
Geological setting.....	11
Salt lakes.....	20
Lacustrine sediments.....	22
Methods	25
Coring	25
Sedimentological methods.....	27
X-ray fluorescence analysis (XRF).....	27
Magnetic Susceptibility (MS).....	30
Pollen analysis	31
Results	36
Core Dul-CO3.....	37
Core SAL1.....	41
Core SAL2.....	45
Core SAL3.....	49
Core Sal-CO5.....	53
Results of pollen analysis	57
Interpretation/Discussion	64
Outlook.....	72
List of figures	73
List of tables	75
References.....	75

Introduction

The south-western Mediterranean region on the Iberian Peninsula constitutes an excellent site for paleoclimate reconstruction (Giralt et al. 2011) due to its unique environmental conditions (Martín-Puertas et al. 2010). The reconstruction of climate in paleolimnology is based on the relationship between climate and lacustrine sediments (Battarbee 2000a) (Martín-Puertas et al. 2010). The climate has strong influence on life (IPCC (Intergovernmental Panel on Climate Change) 2001), more precisely it can stimulate changes in human culture and therefore influences the cultural development (Berglund, 2003).

This thesis contributes to the work of the Collaborative Research Centre 806 “Our way to Europe” which combines geoscientific and archaeological methods to study the history of mankind in terms of population dynamics and mobility from the African continent to Europe.

In this study, lakes have been chosen for a multi-proxy study because they show a rapid response to environmental variations like physically, chemically and biologically changes (Battarbee 2000a). The reconstruction has to be done very carefully because each lake is unique and controlled by various factors like the origin, the age, the climate, the water composition and chemistry as well as the geographic and geological setting (Cohen, 2003).

In order to make this investigation more effective, records of multiple lakes in the same region have been combined.

Regional setting



Fig. 1 Map of the Iberian Peninsula, the city Antequera is marked with a red point

The study site, named the Antequera region, lies within the southwestern Mediterranean, which includes the western part of the Alboran Sea as well as the northern part of Morocco and the southern part of the Iberian Peninsula (Martín-Puertas et al. 2010)(Fig.1). The Mediterranean region comprises the countries bordering the Mediterranean Sea (FAO 2013). The marginal and semi-enclosed Mediterranean Sea with an area of about 2.5 million km² (Black Sea is excluded) is surrounded by multiple countries on three continents. The Mediterranean Sea is linked to the Atlantic through the Gibraltar Strait (Lionello et al. 2006).

The semi-permanent salt lakes Laguna Salada (N37°02', W4°51'), Laguna Dulce (N37°03', W4°50'), Gosque (N37°7', W4°56'), Ratosa (N37°11', W4°42') and Laguna Fuente de Piedra (FDP), are located southwest, northwest and north of the town Fuente de Piedra (Fig.2). The FDP, a basin with a length of 6.8 km and a width of 2.5 km, constitutes the biggest of these endorheic basins and has a watershed area of about 150 km² (Reed 1996). The basins lie within a protected wetland and represents a part of the natural reserve in Andalusia, Southern Spain as well as an ideal nesting and breeding area for pink flamingos (Kohfahl et al. 2008).

Regional setting



Fig. 2 Map of the two cities Fuente de Piedra and Antequera (red points) and the location of the Laguna Salada, Dulce, del Gosque, Fuente de Piedra and de la Ratosa (blue points)



Fig. 3 Google earth map of the Lagunas with lake level charge from the 03/12/2013 (unfortunately the lake level is not visible at the Laguna Salada due to the seize)

The term Laguna (span. for lagoon) is mistakable. Murawski & Meyer (2010) state that a lagoon is a basin separated from the sea through coral reefs, dams or walls. This is apparently not the case for the salt lakes of the investigated area, but the term will be used as a name in this study.

Climate in the Western Mediterranean region

The climate of southern Spain is characterized by a Mediterranean Climate, which is highly variably at annual to centennial time scales due to global-scale climatic external and internal processes (Jalut et al. 2009) (Abrantes et al. 2012). Examples for these variable processes are solar radiation, land-sea distribution, concentrations of trace gas in the atmosphere, volcanic eruptions, migration of oceanic circulations and major atmospheric circulation cells (Cohen 2003) (Lionello et al. 2006) (IPCC (Intergovernmental Panel on Climate Change) 2001).

Köppen (1936) states that the term Mediterranean climate stands for areas where the precipitation in the winter is thrice as high as in the summer. This climate type with seasonal variation is typically found between the 30° and 40° latitude (or 45° after (Vanniere et al. 2011) and 35° after (Strahler & Strahler 1999)) at the west side of the continents (Bolle 2003) (Lionello et al. 2006). The term climate is used for the mean and the variability of the weather in a specific time and region (IPCC (Intergovernmental Panel on Climate Change) 2001).

Its geographical position and the orographic characteristics of the surrounding regions are factors outlining the complexity of the Mediterranean climate (Jalut et al. 2009), considered as one of the most sensitive regions to future climate change (Fletcher & Zielhofer 2013). As this region is located in a transition zone between the middle latitudes and affected to a huge extent by the semi-permanent North Atlantic Oscillation (NAO) and the seasonal migrating Intertropical Convergence Zone (ITCZ; narrow Zone where the equatorial directed trade winds get together (Strahler & Strahler 1999)) it is further influenced by the northern Africa subtropical Oscillation, the Eastern Atlantic pattern, the Scandinavian pattern and the Eastern Atlantic/Western Russia pattern (EA/WR) (Jalut et al. 2009)(Bolle 2003)(Vanniere et al. 2011). The North Atlantic Oscillation is declared as the atmospheric circulation over the North Atlantic (IPCC (Intergovernmental Panel on Climate Change) 2001). The climate of the countries bordering the Alborán Sea shows a strong season dependency (Jiménez-Moreno et al. 2013) with hot and dry summers and southern and southwestern winds. The humid and mild winter is affected by western and northwestern winds (Fletcher & Sánchez Goñi 2008).

As already mentioned, the salt lakes lie at the middle latitudes in the Antequera region in Andalusia, Southern Spain. This is located in the Western Mediterranean region, which is characterized by a semi-humid Mediterranean climate (Martín-Puertas et al. 2010). The semi-humid climate of the Mediterranean is characteristic for mild and wet winters due to the NAO (influences precipitation) and the EA/WR as well as long, warm and dry summers (Martín-Puertas et al. 2010) with a strong soil water deficit. Therefore the period of summer is affected by water shortage, evaporation processes and wild fires. A more decoupled zonal circulation system occurs within the western Mediterranean region during summer and early autumn with no relation to the NAO (Bolle 2003) (Lionello et al. 2006). Precipitation in the

Mediterranean is strongly seasonally (Lionello et al. 2006), position and altitude controlled; from arid to humid precipitation conditions (Strahler & Strahler 1999).

At the onset of the deglaciation in the Late Pleistocene the climate was marked by repeated warmer/cooler and wet/dry events alternating abruptly or on a decadal to century scale (Cohen 2003). Consequential a decrease of 6°C in the mean temperature on the northern hemisphere is reported for the time period between 15 and 10 000 years, mainly triggered by the NA processes (Wansard 1996) (Luterbacher et al. 2012). The latitudinal position of the Westerlies is closely related to the evolution of climate within this time period. The subtropical high pressure belt was alternating seasonally between 21°N and 33°N when it reached its northern optimum at 41°N around 5000 years BP due to the northward migration of the subpolar low pressure system (Bolle 2003).

Against the assumption of a more or less stable climate with only gradual temperature changes in the Holocene it was variable on short and long-term trends up to millennial time-scales (Jalut et al. 2009). The Holocene warming differs across the world, with the southern latitudes warming up thousands of years before the northern latitudes (IPCC (Intergovernmental Panel on Climate Change) 2001).

The Holocene climate of the Mediterranean can be divided into three episodes due to fluctuations of temperature (Jalut et al. 2009):

Between 11 500 and 7000 cal BP the climate was lower humid, only interrupted by several dry episodes in the western Mediterranean during 10 900 - 9700 and 8400 - 7600 cal BP. The lower humid episode was followed by a transition phase with a decrease in insolation and fire activity and the installation of the present circulation of the atmosphere (on this hemisphere) until 5500 cal BP (Jalut et al. 2009) (Harrison & Digerfeldt 1993) (Carrión et al. 2010). Harrison & Digerfeldt (1993) a peak of wetness occurred in the Mediterranean region at 6000 BP resulting in high lake water levels.

The last phase towards the present is characterized by a gradually increase of aridity (Jalut et al. 2009)(Harrison & Digerfeldt 1993). This aridification trend is topic of contradictory interpretation, probably as a result of the regional heterogeneity of geographic gradients or seasonality in the Mediterranean (Magny et al. 2003) (Vanniere et al. 2011). Especially dryer episodes occurred in this last episode in the western part of the region between 5300 - 4200, 4300 - 3400, 2850- 1730 and 1300- 750 cal BP (Jalut et al. 2009). Valero-Garcés and Moreno (2011) describe on the contrary the Iberian-Roman period (between 2600 and 1600 years) as the most humid phase in the last 4000 years in Southern Spain(Sousa et al. 2006). The warm and dry Medieval Climate Anomaly also called the Medieval Warm Period with decreased lake levels occurred in the period between 900 and 1300 years in the Mediterranean (Moreno et al. 2012). Especially humid periods occurred in the Little Ice Age (LIA; 1300-1850 years; timing varying geographically) in Andalusia between 1570 - 1630, 1780 - 1800, and 1830 to 1870 years. The LIA was a period of a very wet climate within Medieval times (Sousa et al. 2006).

Geological setting

The Iberian Peninsula constitutes a wedged microplate between the convergence zone of the European and African plates (Gutiérrez et al. 2008) with a continuing convergent movement from Late Cretaceous to present (Reicherter & Peters 2005). It is bordered by two orogens, the Pyrenees in the North and the Betics (Betic Cordillera) in the South (Fig.4). They nearly define the northern and southern margin of the microplate and were formed due to Alpine orogeny in Cenozoic times (Gibbons & Moreno 2002). The Pyrenees initially builded up when Pyrenean Iberia was partly subducted under the Eurasian plate (Gibbons & Moreno 2002).

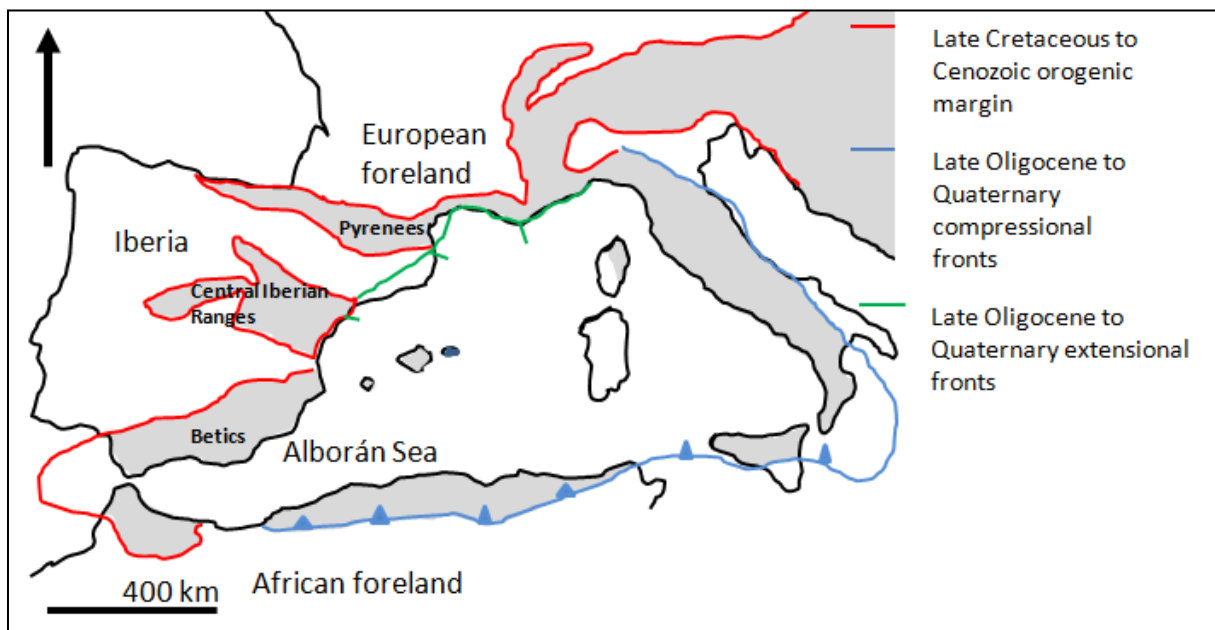


Fig. 4 Simplified Alpine tectonic setting of Iberia and the Alborán sea surrounding regions, modified after (Gibbons & Moreno 2002). The grey regions constitute the area where the Alpine orogen is exposed on land.

This was followed by the formation of the 600 km long and 200 km wide collisional mountain belt called the Betics (Betic Cordilleras) in the Tertiary (Paleogene to Pliocene) (Gibbons & Moreno 2002) (Ábalos et al. 2002) within the African-European Convergence zone (Reicherter & Peters 2005). They are composed of Palaeozoic to Quaternary rocks (Azanón et al. 2002) and represent the westernmost part of the Alpine orogen and the northern branch of the Gibraltar Arc (Reicherter 2001).¹

The Betics can be subdivided into the Alborán Domain, also called Internal zone, the Flysch zone, the External zone and the Neogene Basins (Reicherter & Peters 2005)(López-Gómez et al. 2002). The Alborán Domain displays the metamorphic overprinted core of the Betic orogen due to the collision of the Iberian and African plate (Reicherter & Peters 2005)(Reicherter 2001). The Flysch zone which is located in the western part of the Betic

¹ All geological periods are displayed in the International Chronostratigraphic chart from the International Commission of Stratigraphy in Fig.13 at the end of the chapter geological setting.

Cordillera was primarily build up along the passive margin of the African plate with a deposition of sediments of Cretaceous to Early Miocene age. The External zone contains sedimentary sequences of Triassic to Paleogene age, deposited at the further margin of Mesozoic south Iberia (Reicherter & Peters 2005).

The Betics in SE Iberia and the Rif cordilleras in North Africa are framing the Alborán Sea (which is the largest of the Neogene-Quaternary basins and still below sea level) in the north-western and southern part (Azanón et al. 2002). The Alborán Sea is part of the Mediterranean Sea and constitutes its westernmost basin (Fletcher & Sánchez Goñi 2008). It is further connected to the North Atlantic Ocean through the Strait of Gibraltar (Goñi et al. 2002)

The basin-and-range topography of the strongly deformed Betic Cordillera was created due to crustal extension in Neogene to Quaternary times (Gibbons & Moreno 2002) (Linares Girela & Rendón Martos 1998). The Neogene sedimentary basins are mainly filled with marine sediments becoming progressively continental in Quaternary times (Gutiérrez-Elorza et al. 2002) and were developed on and between the External and Internal zones since the Late Miocene in Tortonian times (Alonso-Zarza et al. 2002)(Azanón et al. 2002). They are covered with fluvial material of Quaternary age (Kohfahl et al. 2008). The sediments in the Neogene basins show faults and structures related to tectonic activity (Reicherter 2001). The Guadalquivir basin, a Neogene basin and located above the External Betics, takes up an area of almost 350 to 30 km and its sedimentary filling can reach a thickness up to 2000 m (Gutiérrez-Elorza et al. 2002) (Fig.5).

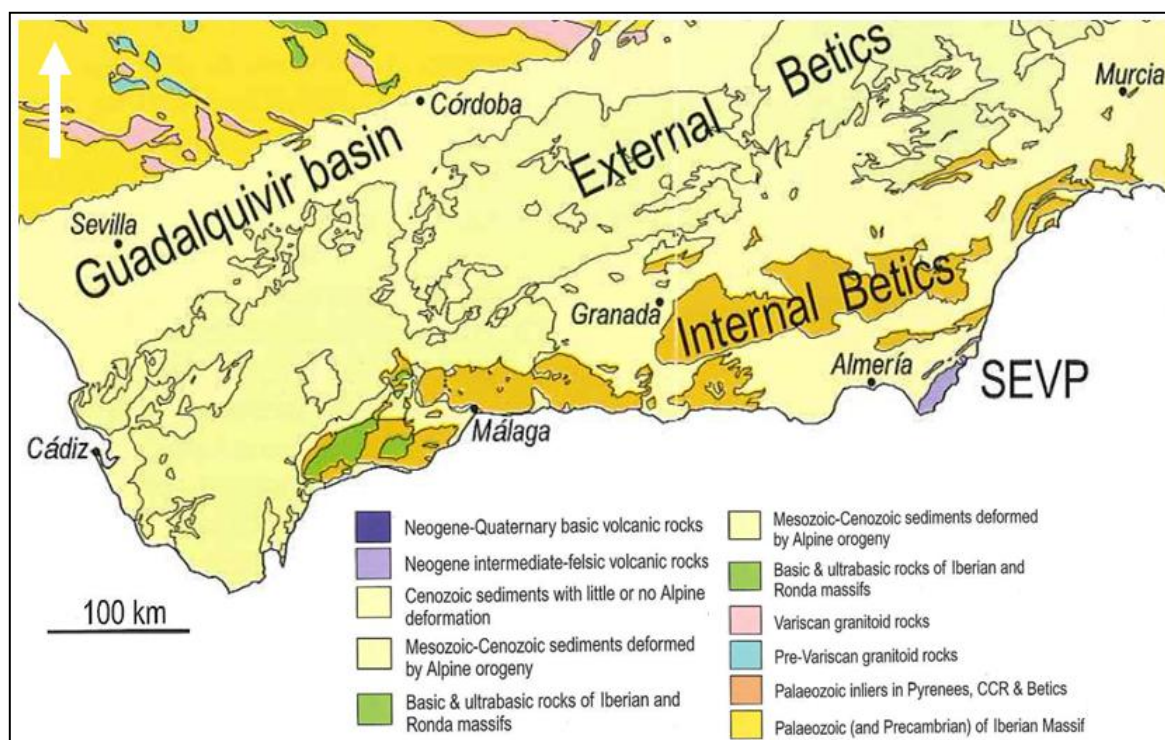


Fig. 5 Geological map of Southern Spain, modified after (Gibbons & Moreno 2002)

The Triassic sediments within this area are mainly composed of clays, sandstones and evaporates (Linares Girela & Rendón Martos 1998) (Kohfahl et al. 2008). The evaporates are made of reddish-green Triassic marls and evaporates and other types of rocks (Kohfahl et al. 2008).

In Triassic to present times large marine evaporite sedimentation in shallow-marine environments took place (Fig.6), frequently composed of Ca-sulfates like gypsum $[(CaSO_4) \cdot H_2O]^2$ and anhydrite $[CaSO_4]$ or halite $[NaCl]$. Some of the evaporitic rocks does also contain K-Mg chlorides and Na-sulfates like Glauberit $[Na_2Ca(SO_4)_2]$ and thenardite $[Na_2SO_4]$.

During Triassic and Lower Jurassic (Lias) the biggest sedimentation of evaporates took place. Continental evaporites were deposited in lakes during the Tertiary as a result of the dissolution and reprecipitation of older evaporite sequences (Gutiérrez et al. 2008).

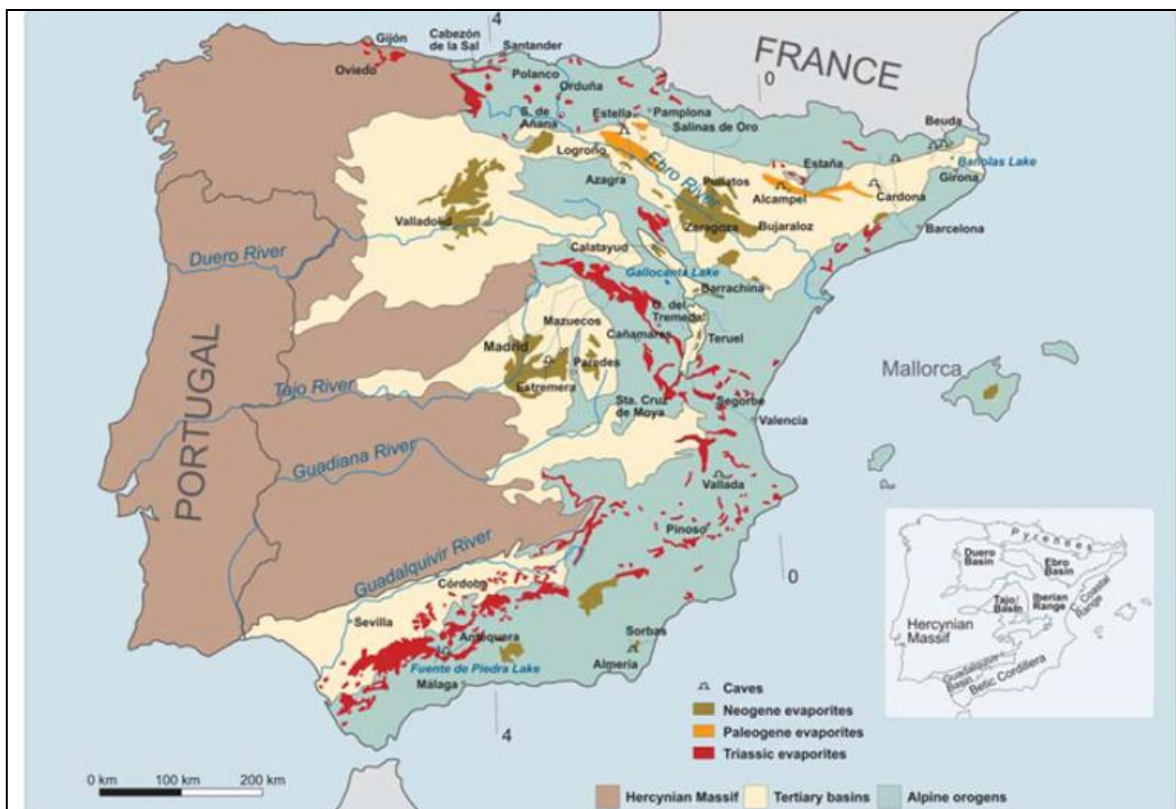


Fig. 6 Distribution of the main evaporate outcrops on the Iberian Peninsula (Gutiérrez et al. 2008)

Karstification of the impermeable Triassic and Tertiary evaporates lead to gravitational deformations and gradual subsidence (Gutiérrez et al. 2008), where a system can no longer support its own mass (Cohen 2003). Topographical depressions like basins and lake systems were formed due to the dissolution processes in evaporitic sequences (Gutiérrez et al. 2008).

² The chemical formulas are taken from (Okrusch & Matthes 2009)

The dissolution and karst formation is controlled by the reaction of CaCO_3 and CO_2 or other acids (Cohen 2003) or by gypsum dissolution through dedolomitization (Bischoff et al. 1994).

The karst massifs in Andalusia can be subdivided in the Sierra Morena, the Guadalquivir basin and the Betic Cordillera (Durán et al. 1998). Examples for these abundant topographical depressions are the endorheic salt lakes Laguna de Fuente de Piedra, Laguna Salada, Dulce, Ratosá and Gosque in the Antequera region and other ephemeral short-dated lakes (Gutiérrez et al. 2008) (Kohfahl et al. 2008).

These salt lakes lie within the Trias of Antequera (Alcalá-García et al. 2001). The Antequera Trias is a megabreccia in the western part of the Betic Cordillera composed of gypsum (at the surface) and halite and Ca-sulfates at depth, resedimented minerals from Triassic times in the Miocene. The Antequera karst was established out of these Triassic evaporates (Gutiérrez et al. 2008).

Geological setting

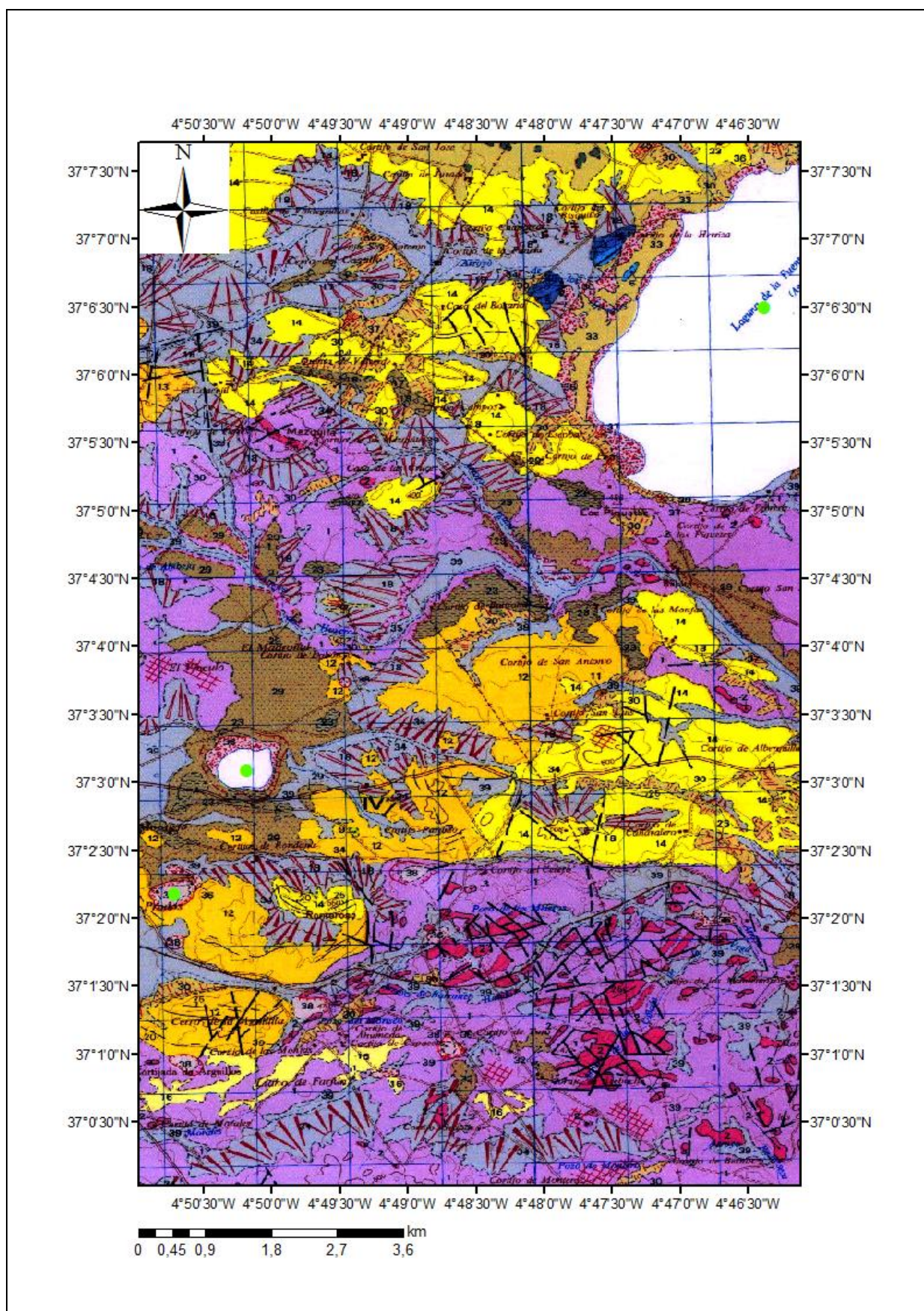


Fig. 7 Geological map with the three Lagunas Fuente de Piedra, Dulce & Salada (from North to South, indicated by the green points). This map was constructed with GIS on the basis of a geological map of the “SERVICIO DE PUBLICACIONES – MINISTERIO DE INDUSTRIA Y ENERGIA” of 1986.

Geological setting

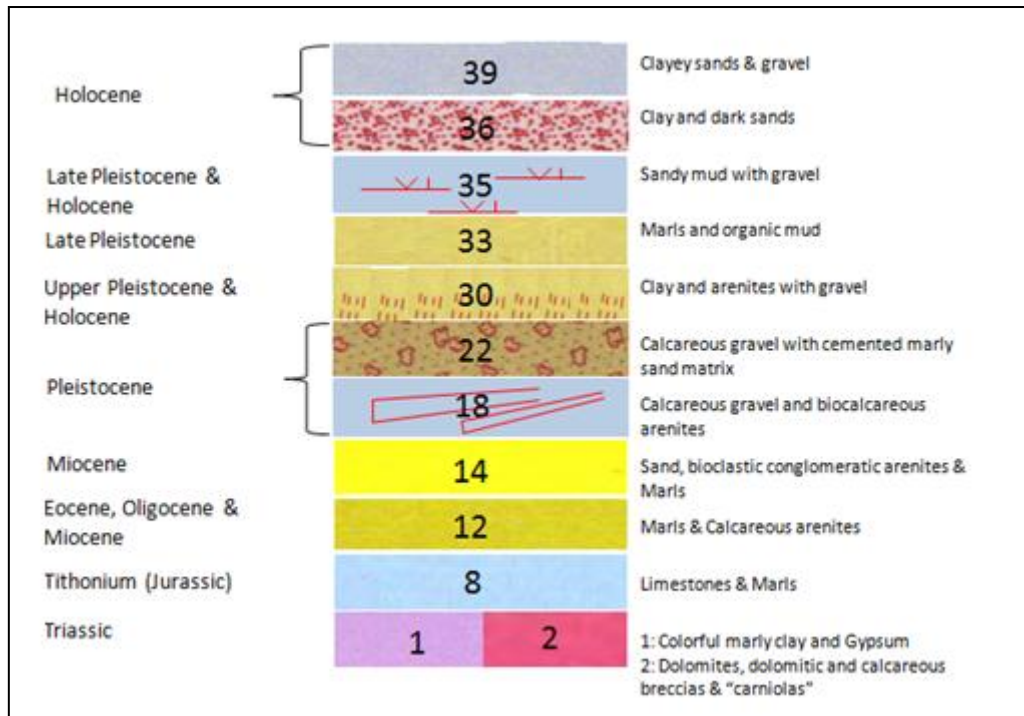


Fig. 8 Legend for the geological map in Fig.7

The geological maps in Fig. 7, 9 and 11 are done with Arc GIS on the basis of UTM maps. In the first map (Fig.7) the Laguna FDP and the Laguna Dulce as well as the Laguna Salada can be seen.

The area is dominated by Triassic clay, gypsum, dolomites and calcareous breccias. But there are also Palaeogene rocks outcropping as well as rocks and sediments of Neogene age. The area around all three lagunas is dominated by Holocene clay and sand, Triassic sediments, Palaeogene and Neogene sediments.

The second map (Fig.9) shows the location of the Laguna de la Ratosa, which is surrounded by mud, sand, clay and gravel of Holocene age. In wider distance, Miocene arenites, marls and conglomerates, Pleistocene sediments as well as Triassic sediments are deposited.

In the geological map (Fig.10), the location of the saline Laguna de Gosque can be seen. The lake is mainly surrounded by undifferentiated alluvium of Holocene age. Furthermore, Pleistocene and Pleistocene sediments and rocks are dominating the area. In addition, marls and limestones of Palaeogene and Mesozoic age exist.

Geological setting

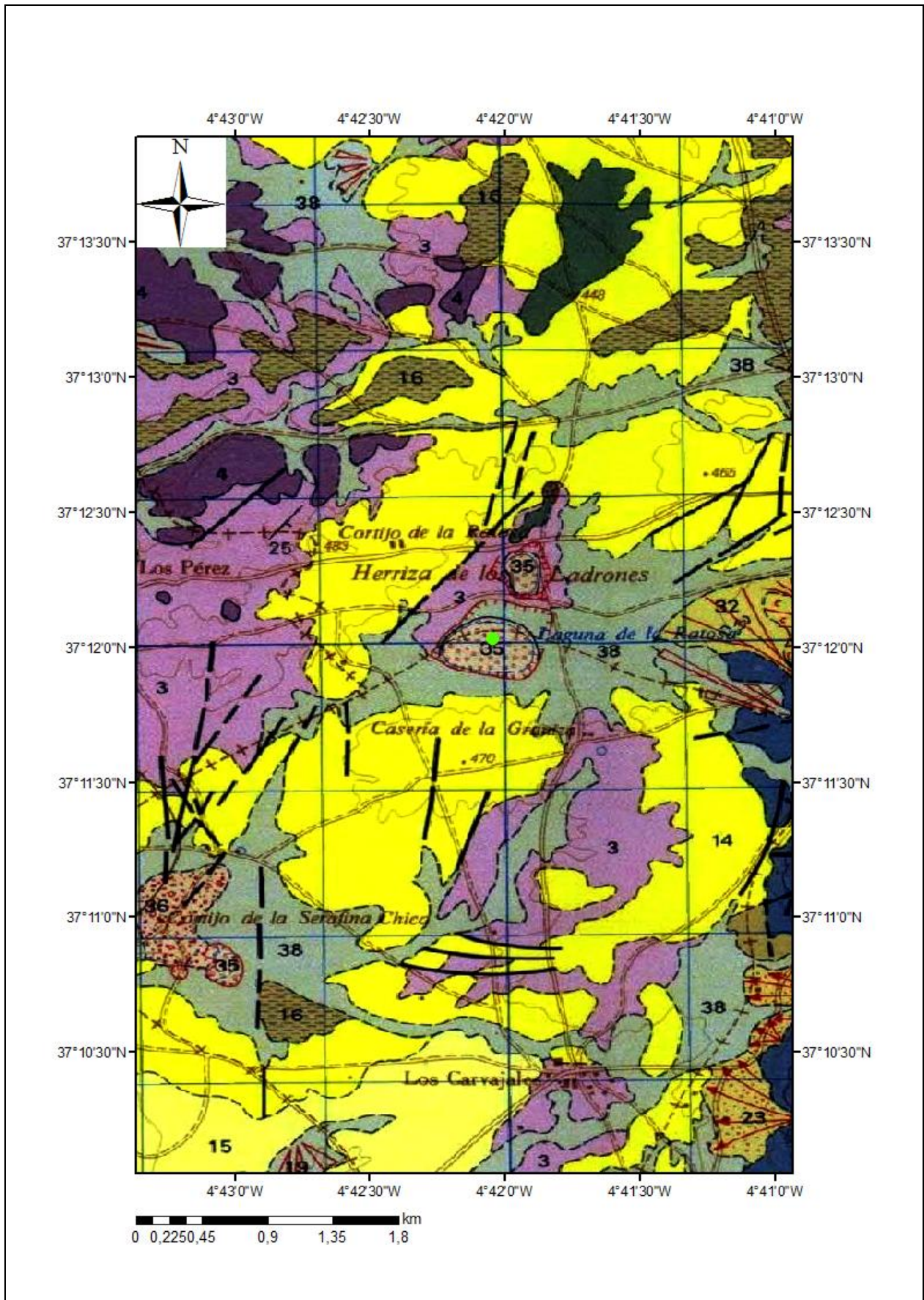


Fig. 9 Geological map of the Laguna de la Ratosa, indicated by the green point. This map was constructed with GIS on the basis of a geological map of the "SERVICIO DE PUBLICACIONES – MINISTERIO DE INDUSTRIA Y ENERGIA" of 1986.

Geological setting

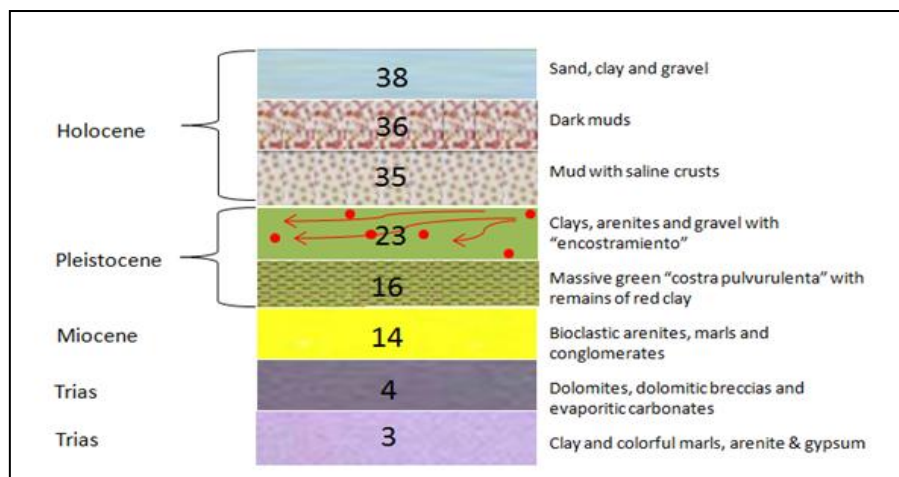


Fig. 10 Legend for the geological map with the Laguna de la Ratosa in Fig.9 (no translation available for words in quotation marks)

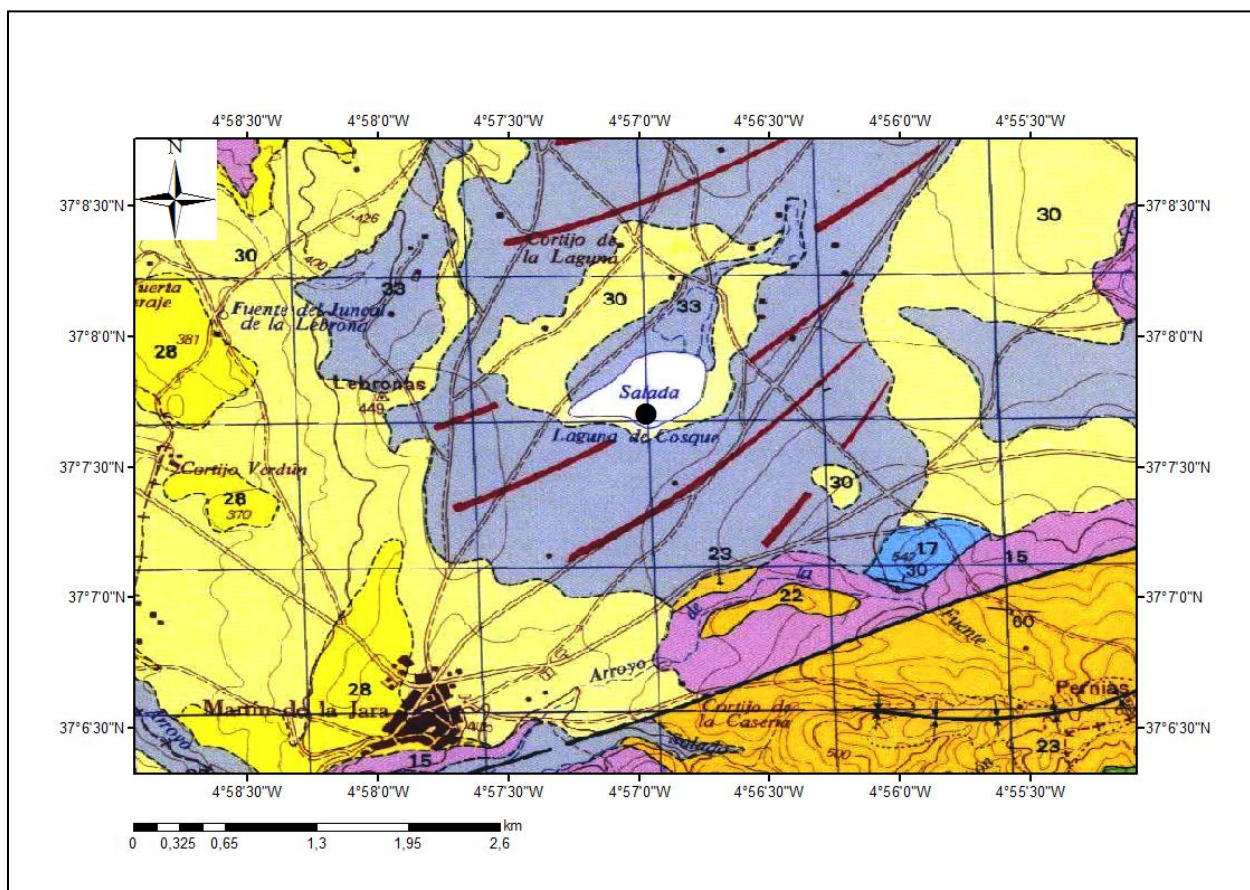


Fig. 11 Geological Map of the Laguna del Gosque, indicated by the black point. This map was constructed with GIS on the basis of a geological map of the "SERVICIO DE PUBLICACIONES – MINISTERIO DE INDUSTRIA Y ENERGIA" of 1986.

Geological setting

Holocene	33	Undifferentiated alluvium
Pliocene & Pleistocene	30	Clay, Mud and fluvial conglomerates
Messinian & Tortonian (Miocene)	28	Sand & bioclastic arenites
Eocene & Oligocene & Miocene	23	Marl & turbiditic and biotrititic limestone
Upper Cretaceous & Paleocene & Eocene	22	Marl & white and rosy marly-limestone
Jurassic (Dogger)	17	White calcareous marl with chert & Marl
Trias	15	Clay, Arenite & Gypsum

Fig. 12 Legend for the geological map with the Laguna del Gosque in Fig.11

Eonothem / Eon Erathem / Era System / Period		Series / Epoch	Stage / Age	GSSP	numerical age (Ma)	Eonothem / Eon Erathem / Era System / Period		Series / Epoch	Stage / Age	GSSP	numerical age (Ma)	
Phanerozoic		Cenozoic	Quaternary	Holocene	present	Mesozoic	Phanerozoic	Mesozoic	Jurassic	Upper	Tithonian	~ 145.0
				Upper	0.0117						Kimmeridgian	152.1 ± 0.9
				Middle	0.126					Oxfordian	157.3 ± 1.0	
				Pleistocene	0.781					Callovian	163.5 ± 1.0	
			Pliocene	Gelasian	1.806	Bathonian			166.1 ± 1.2			
				Piacenzian	2.588	Bajocian			168.3 ± 1.3			
				Zanclean	3.600	Aalenian			170.3 ± 1.4			
				Messinian	5.333	Toarcian			174.1 ± 1.0			
				Neogene	Tortonian	7.246			Lower	Pliensbachian	182.7 ± 0.7	
					Miocene	11.62				Sinemurian	190.8 ± 1.0	
		Serravallian	13.82		Hettangian	199.3 ± 0.3						
		Langhian	15.97		Rhaetian	201.3 ± 0.2						
		Paleogene	Oligocene	Chatthian	20.44	Triassic	Upper	Norian	~ 208.5			
				Rupelian	23.03			Carnian	~ 227			
			Eocene	Priabonian	28.1	Middle	Ladinian	~ 237				
				Bartonian	33.9		Anisian	~ 242				
				Lutetian	38.0	Lower	Olenekian	247.2				
				Ypresian	41.3		Induan	251.2				
			Paleocene	Thanetian	47.8	Paleozoic	Paleozoic	Permian	Cisuralian	Changhsingian	252.17 ± 0.06	
				Selandian	56.0					Lopingian	254.14 ± 0.07	
Danian	59.2			Wuchiapingian	259.8 ± 0.4							
Maastrichtian	61.6			Capitanian	265.1 ± 0.4							
Mesozoic	Cretaceous	Upper	66.0	Guadalupian	268.8 ± 0.5							
			66.0	Roadian	272.3 ± 0.5							
			72.1 ± 0.2	Kungurian	283.5 ± 0.6							
			Campanian	83.6 ± 0.2	Artinskian				290.1 ± 0.26			
			Santonian	86.3 ± 0.5	Sakmarian				295.0 ± 0.18			
			Coniacian	89.8 ± 0.3	Asselian				298.9 ± 0.15			
	Lower	Turonian	93.9	Carboniferous	Pennsylvanian	Upper	Gzhelian	303.7 ± 0.1				
		Cenomanian	100.5				Kasimovian	307.0 ± 0.1				
		Albian	~ 113.0			Middle	Moscovian	315.2 ± 0.2				
		Aptian	~ 125.0				Bashkirian	323.2 ± 0.4				
Barremian	~ 129.4	Lower	Serpukhovian	330.9 ± 0.2								
Hauterivian	~ 132.9		Visean	346.7 ± 0.4								
Valanginian	~ 139.8	Tournaian	358.9 ± 0.4									
Berriasian	~ 145.0											

Fig. 13 Essential part of the International chronostratigraphic chart from the International Commission of Stratigraphy (v2013/01) for the geological site description

Salt lakes

Lakes are enclosed basins of standing water in a terrestrial environment, which respond relatively quick (as a function to their size) to environmental change (Cohen 2003). In general they may be subdivided into hydrologically open or closed systems. Open systems have permanent run-off of water and they are strongly influenced by a river system (Tucker & Wright 1990).

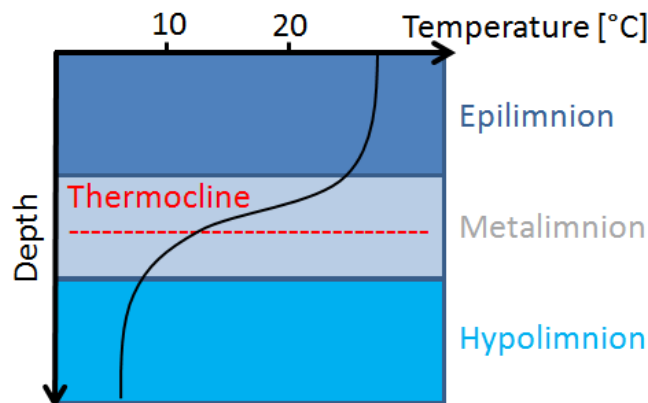


Fig. 14 Temperature distribution & zones in a thermally stratified lake;
Modified from Bayly & Williams, 1974

In the figure above the temperature distribution and zoning of a thermally stratified lake can be seen. The epilimnion represents the water surface layer separated by the metalimnion from the hypolimnion at the bottom of the lake. The metalimnion constitutes the water zone with the biggest change of temperature; it results out of the strong temperature and density difference of the epi- and hypolimnion. It further includes the thermocline, a layer of maximum rate of temperature change (Tucker & Wright 1990)(Cohen 2003).

The hypolimnion contains the least amount of oxygen and is the coolest water layer. The warming effect of solar radiation is decreasing with depths. The zoning of the water layers develops due to the density of the water (which depends on the temperature and the amount of suspended sediments within the water column) and depends on the shape and size of a lake. The density of water is at its greatest at 4° Celsius. An increasing or decreasing temperature as well as wind generates waves and sediment movement resulting in water movement and mixing (Tucker & Wright 1990).

Salt lakes may also be chemically stratified. The dense bottom layer is called the monimolimnion, overlain by the less saline and freely circulating mixolimnion and the chemocline, which defines the plane of the maximum rate of change of salinity. The composition of the brine evolution within salt lakes depends to a large amount on the nature of the surrounding bedrock and the weathering type (Tucker & Wright 1990).

Playas and saline lakes are characteristic in arid and semiarid environments (Cohen 2003). Salt or playa lakes can be divided because of the hydrogeological background into coastal and inland sabkhas (Kohfahl et al. 2008) (Rodríguez-Rodríguez et al. 2006). They are further defined as closed-basin lakes located in semi-arid warm and hot climates (Flügel 2010). They have a periodically little outflow by surface or groundwater (Battarbee 2000a) and can desiccate in the period of summer (Rodríguez-Rodríguez et al. 2006). Closed lakes are found in arheic and endorheic environments and can be of perennial and ephemeral type (Tucker & Wright 1990). Closed basin lakes do not have a surface outflow of water, which means that they can be described as endorheic lakes (Rodó et al. 2002).

The main property of hydrologically closed salt lakes is that moisture losses are dominated by evaporation which exceeds precipitation and inflow. This can result in lake-level variations and variations in the amount of soluble particles (causing salinity variations etc.) (Battarbee 2000a). Salt lakes and lakes in general are dynamic systems and react very sensitive to variations caused by climate change or human activities (Rodríguez-Rodríguez et al. 2006).

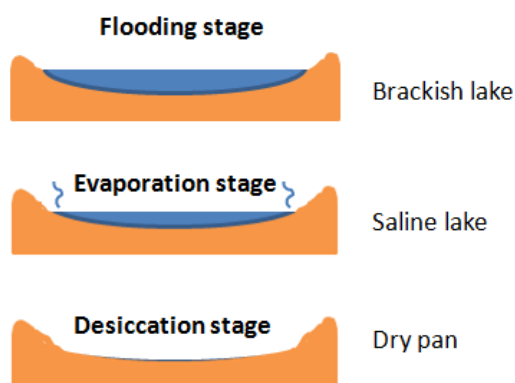


Fig. 15 Cycle development from a flooded brackish lake to a dry pan (modified after (Lowenstein & Hardie 2006))

Figure 8 shows a rough sketch of the evolution from a brackish lake to a waterless dry pan. In the first stage, there is suspended material in the water and at the lake bottom. The missing surface-, ground-water or precipitation input of water at high temperatures in periods basins leads in the next step to evaporation and retraction and at a final stage to the formation of a saline lake. Further desiccation produces a dry pan with the diagenetic growth of salts (Lowenstein & Hardie 2006) (Talbot & Allen, 1996).

Freshwater lakes contain under 1 g/l, brackish water lakes 1 to 5 g/l and salt lakes more than 5 g/l of dissolved constituents (Flügel 2010). The salinity of the water is expressed as milligrams or grams per liter and measures the total concentration of all dissolved ions, which becomes progressively enriched in closed lake waters (Cohen 2003). The salinity of a lake is closely linked to the precipitation and drainage and therefore a proxy for palaeoclimate (Cohen 2003).

The salt lakes of the Antequera region are related to the dissolution and the subsidence of the underlying evaporates at or beneath the surface of Tertiary or Triassic age (Reed 1998).

Lacustrine sediments

According to Cohen (2003) lakes are environments of relatively rapid accumulation of sediments in comparison to other environments like oceans. The sedimentary facies deposited in lakes are described as lacustrine sediments, differing from other environments due their properties, productivity as well as their kinetics (Flügel 2010). Their composition and characteristics are mainly influenced by the nature of the lake and the surroundings, internal lake processes, vegetation and the climate (Cohen 2003). Eventually this leads to variations in depositing sediments in the lake (Flügel 2010).

Lake sediments can be of chemical, biochemical or siliclastic origin, depending on an open or closed system. Most of the siliclastic material is transported to the open lakes by rivers, in suspension or as bedload; often seasonally controlled (Talbot & Allen, 1996).

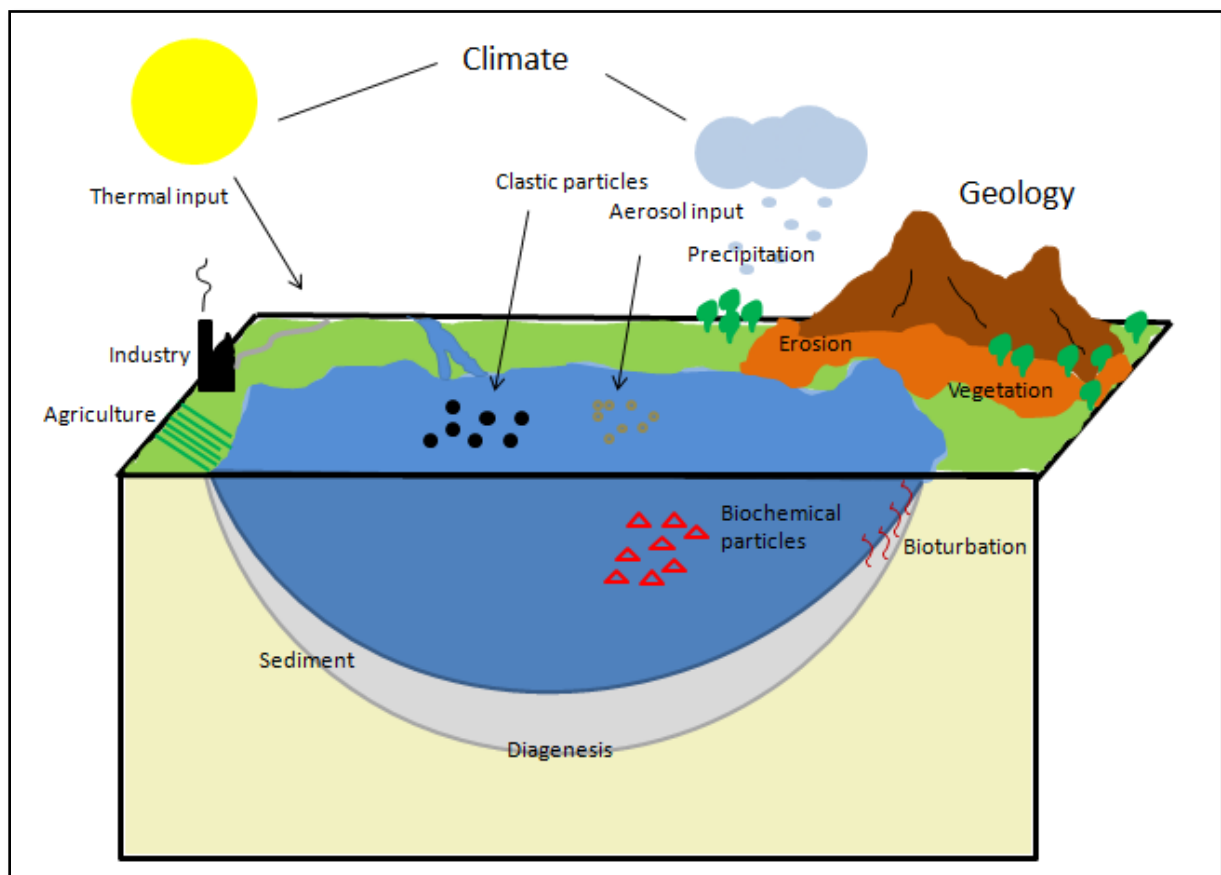


Fig. 16 Simplified model of factors affecting lake sediments modified after Cohen (2003)

Sediments of lacustrine origin include autochthonous material, produced by organisms within the lake or chemical particles, and allochthonous material. Allochthonous material are terrigenous particles originated from the lake surroundings (like pollen) or aerosol input of for example cosmogenic or volcanogenic origin (Anderson et al. 2007) (Cohen 2003).

A further division according to their amount of nutrients can be made. An eutrophic lake defines a lake with a high nutrient productivity resulting in green-brown and organic- and autochthonous rich lake sediments. On the contrary are oligotrophic lakes of low productivity with a deficit of nutrients, leading to the precipitation of mainly inorganic, clastic and lighter sediments (Anderson et al. 2007).

As the endorheic salt lakes in the investigated area of Southern Spain are closed systems, the lake is dominated by chemical or biochemical deposits like carbonates, evaporate and silicate minerals (Talbot & Allen, 1996). Carbonates in saltwater lakes designated by the precipitation of High- and Low-Mg calcite is mostly fine laminated (called laminate, if more than two sediment types are present (Warren, 2010)) with carbonates and intermediate layers of silicates like sand or siliciclastic clay, evaporate salts and organic components (Flügel, 2010) (Warren, 2010). The sediments deposited in salt lakes reflect climate changes because of lake expansion and contraction and seasonal change (Cohen 2003).

Some major evaporate minerals that are deposited as lake sediments can be seen in the following table (Warren, 2010).

Mineral	Formula
Anhydrite	CaSO ₄
Aragonite	CaCO ₃
Calcite	CaCO ₃
Dolomite	Ca _(1-x) Mg _(1-x) (CO ₃) ₂
Gypsum	CaSO ₄ 2H ₂ O
Halite	NaCl
Mg-Calcite	(Mg _x Ca _{1-x})CO ₃

table 1: some major evaporite minerals after Warren, 2010

Carbonates are the first precipitated minerals of an evaporitic sequence. Evaporates (in the case of salt lakes in form of primary salts) precipitates from saturated brines due to solar evaporation (Warren, 2006).

At the beginning of a drying process, relatively insoluble carbonate minerals like aragonite, low and high magnesium calcite will precipitate when their saturation coefficient is reached. This is followed by a later precipitation of more soluble minerals (Battarbee 2000b) (Rodó et al. 2002). Siliciclastic minerals are often deposited with the evaporitic carbonate minerals in times of lake water refilling (Rodó et al. 2002) or in more marginward facies at the shore zone (Warren, 2010). The carbonates can be of various origins. Detrital carbonates are derived by erosion from the surrounding environment, while the biogenic carbonate remains from skeletons of organisms like mollusks or phytoplankton. Furthermore the carbonates can also be of diagenetic origin, if primary deposited carbonate minerals were altered after the deposition inducing secondary deposition of diagenetic carbonate (Tucker & Wright 1990).

Gypsum does precipitate after the Ca-Mg-carbonate minerals, followed by the precipitation of saline minerals which is normally associated with hot and arid climate conditions. Towards this, salt minerals can also be formed by cooling of a salt brine, leading to supersaturation and precipitation as well. Salt minerals can be formed as cements, in perennial brine bodies or open saline lakes or in addition as crusts on and around ephemeral episodically water fed salt pans. The sources of salt are diverse. It can be derived from surface or groundwater, hydrothermal water, aeolian dust and older evaporate deposits (Talbot & Allen, 1996).

Most lakes in Southern Spain show human impact since the Neolithic because they have been exploited for water leading to an increase of the sedimentation rate and sediment deposition. An increased sedimentation rate from 3 mm/year in the last 2000 years to 10 mm/year in the last century was recorded in multiple lakes in this area (Valero-Garcés & Moreno 2011).

Methods

Coring

The drilling campaign took place in march 2012. The sediment cores were taken at the lake shore by a vibracorer (Fig.17a) (with sampling tubes or PVC-liner extraction) and with a Russian drilling device from a floating platform (Fig.17b). Coring is the suitable method to gain a one-dimensional column of lake sediment. The quantity of the sample is limited by the diameter of the core barrel. The vibra-corer is used to drive the barrel into the ground, powered by a vibrating motor. It is used to drill within coarse-grained, unconsolidated sediments (Cohen 2003).

The locations of the drill holes are shown in a table in the chapter results and on the map in Fig.18 (Dulce & Salda).

The stratigraphy of the open drill probes (Fig.17c) was described in the field, the liner tubes were cut in halves in the laboratory before applying the next steps of procedure (Fig.17d).



Fig. 17 Pictures of coring with a vibracorer (a), of the floating platform (b), the open drill probes (c) & halves of liner tubes (d)

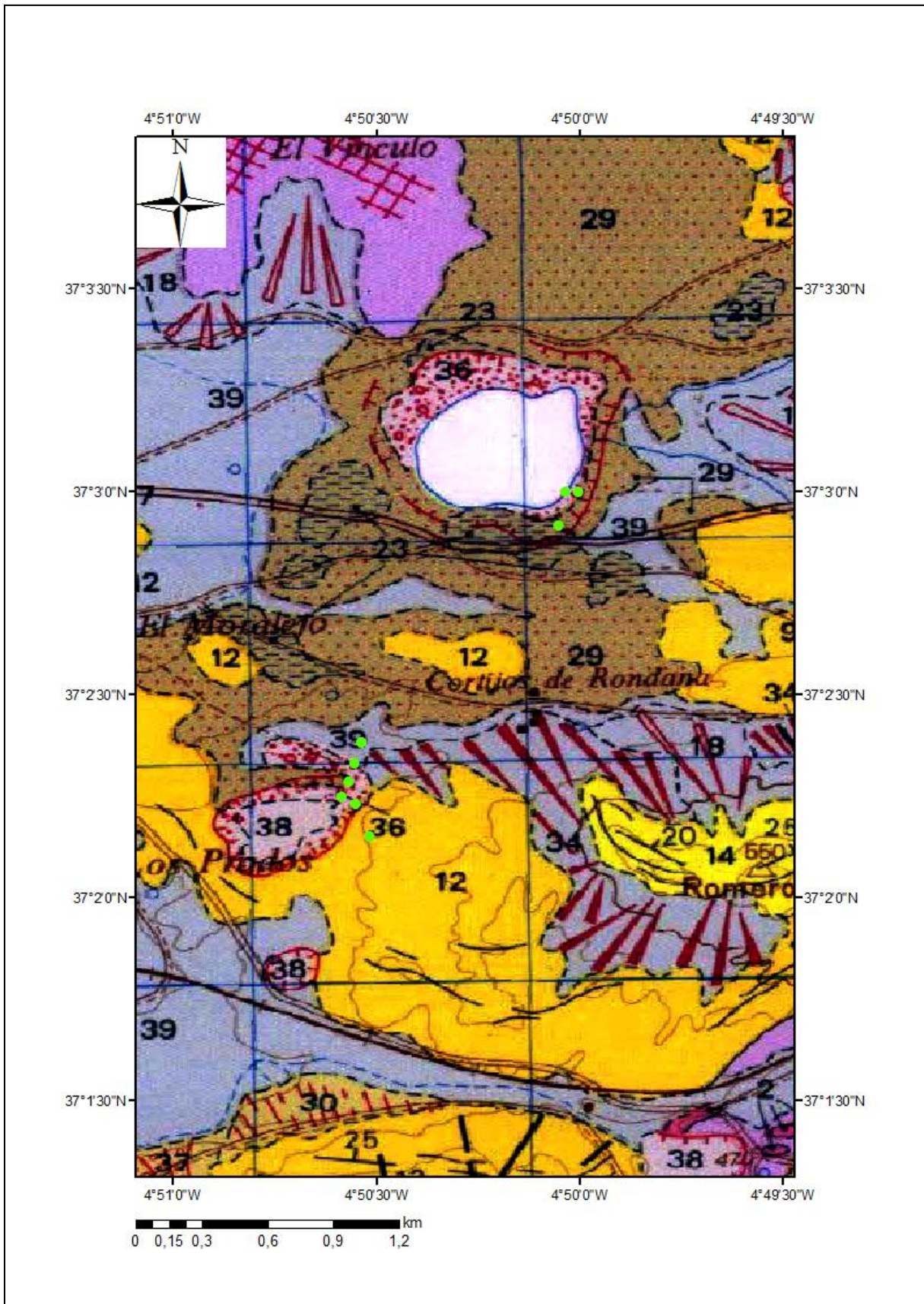


Fig. 18 Geological map of the Laguna Salada & the Laguna Dulce with drilling points

Sedimentological methods

The sedimentological method was applied by describing the sediment cores. This basic description is essential for the study of lacustrine sediments because of the possible amount of information that can be received, like major changes of the depositional environment and water depth (Cohen 2003).

A very important indicator is the change of the sediment itself like changes of the grain size, which can be explained in various ways. Therefore the sediment descriptions should be combined with other information and methods (Harrison & Digerfeldt 1993). The focus is on the color, grain size, layer boundaries (contact relationships), composition and sedimentary structures, content of carbonate and the existence of concretions and concentration of minerals as well as the existence of macrofossils within the sediment core.

X-ray fluorescence analysis (XRF)

The radioisotope source X-ray fluorescence method is a rapid, non-destructive and sufficiently accurate technique used in analytical chemistry, environmental and palaeolimnological research. With this method the geochemical distributions of the sample is measured in a short time period (Boyle 2000) (Rothwell et al. 2006), leading to a valuable information about the geochemistry of the sediment as well as the evolution of the lake system (Engstrom & Wright, 1984) without the use of additional techniques. Advantages of the XRF are that there is no need for a big amount of sediment and no necessary extraction or preparation of the sample (Boyle 2000).



Fig. 19 Picture from the Itrax XRF Core scanner (www.coxsys.se)

The continuous down-core XRF measurements were carried out with the ITRAX core scanner (Cox Analytical, Sweden) of the University of Cologne, with a spatial distribution of 5 mm (Fig.19). The sediment cores were cut in half (from top to bottom), carefully flattened and covered with a special film. The tube voltage was set on 30kV and a Cr X-ray tube and a current setting of 30 mA is used. The scanning time constituted on 10 seconds.

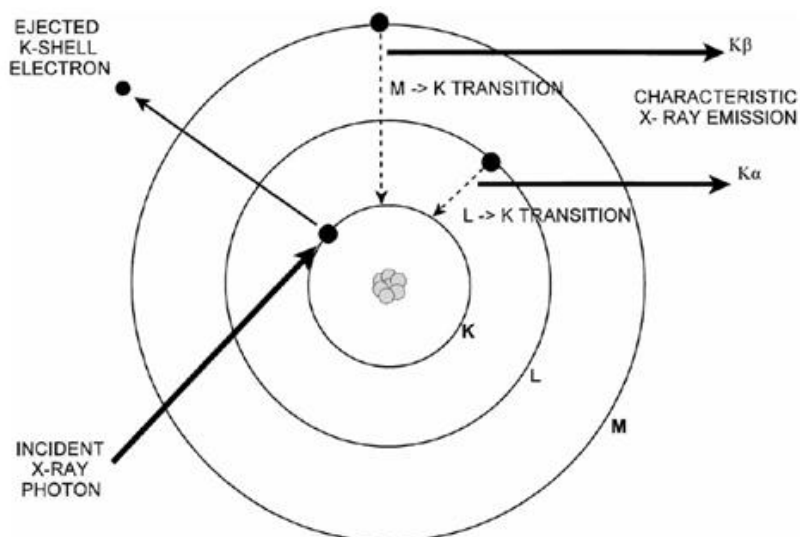


Fig. 20 Mechanism for X-ray fluorescence of an atom (Kalnicky & Singhvi, 2001)

The mode of operation is based on the characteristic photoelectric fluorescence (specific energies in form of specific fluorescent photons characteristic for the source atom) of elements, stimulated and excited by the irradiating X-rays (Boyle 2000) (Kalnicky & Singhvi 2001) (Fig.20 & 21). This allows to perform a qualitative and quantitative analysis (of most elements) (Kalnicky & Singhvi 2001).

As illustrated in the figure above, a vacancy within the inner shell, an electron hole, is created. This leads to an electronic transition, a falling of an electron from an outer shell into this electron hole. This process is accompanied by the characteristic emission of detectable X-rays because of energy equalization (qualitative identification). The intensities of X-rays is compared to standard intensities for a quantitative analysis (Kalnicky & Singhvi 2001). Standards in terms of reference material is used to calibrate the XRF analyzer (Boyle 2000).

The K X-rays are the emitted x-rays after the replacement from an electron from shell K ("L-shell transition produces L X-rays). As a sample consists of various elements, a spectrum of X-rays is created (Fig.21). The penetration of X-rays within the sample is approximately 2mm (Kalnicky & Singhvi 2001).

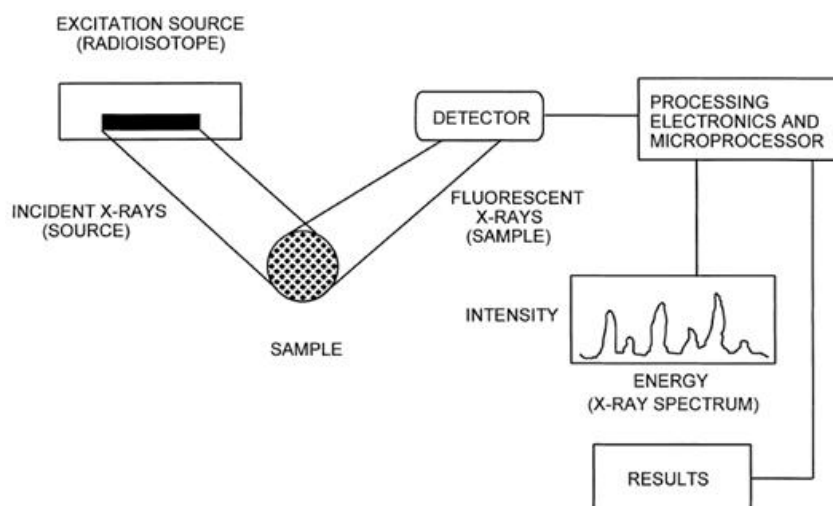


Fig. 21 Block diagram for a typical energy dispersive XRF spectrometer (Kalnicky & Singhvi 2001)

The result of measurement is depending on the number of samples and denoted by the measurement precision. On the other hand, major elements are measured with a greater precision (which typically improves with atomic number and concentration) than minor elements. The precision for elements is depending on the detector type and the excitation of the radioisotope source (Boyle 2000).

The uncertainty of XRF analysis is depending on the element, the matrix, the analysis time and the moisture content (Kalnicky & Singhvi 2001). Matrix effects and errors can occur when the composition has extreme characteristics; because of very coarse sediments with a weakened signal for light elements or if the concentration of Fe is greater than 100mg/g. A Ca concentration above 150 mg/g dominates the signal at the disadvantage of the elements S, K and Ti (Boyle 2000). Moisture content greater than 20 % causes an increased error of analysis. Therefore, sediment samples containing more than 20% moisture content should be dried (Kalnicky & Singhvi 2001). Furthermore, a poor peak discrimination in the X-ray spectra, changes of the porosity of the samples, artifacts like compaction and an uneven surface for measurement can lead to even more errors (Rothwell et al. 2006).

Magnetic Susceptibility (MS)

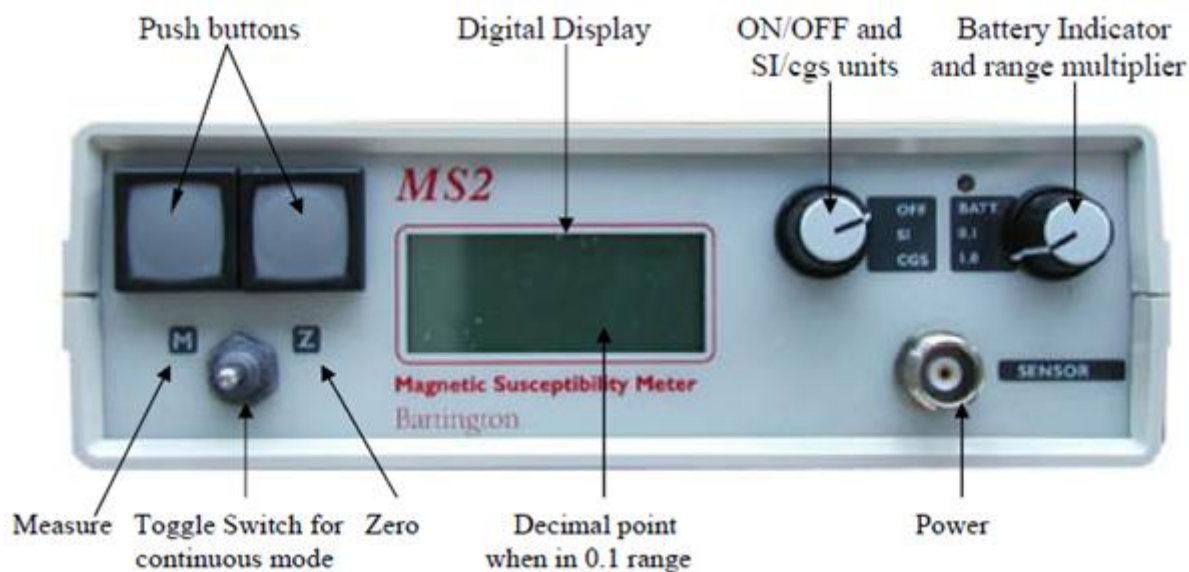


Fig. 22 Display panel of the Bartington MS2 (Dearing 1999)

The MS is a rapid, extremely simple and non-destructive analysis, which complements other types of environmental analytical measurements (Stockhausen & Zolitschka 1999) (Dearing 1999) (Fig.22).

Magnetic susceptibility data has been generated with a Bartington MS2K measurement device in 5 mm intervals. The sensor was zeroed after each fifth measurement with pushing the Z button. The Bartington MS2K sensor is “designed to provide highly repeatable surface measurements on moderately smooth surfaces. It is used for magnetic stratigraphy, identifying horizons, characterizing outcrops and logging plastic film covered split cores”³. Measurements are taken in SI or cgs units.

The Cgs value multiplied by 0.4 gives the SI value [dimensionless]. The SI value can be further used to calculate the mass specific frequency dependent susceptibility (MSFDS) by dividing by mass and by 10, resulting in values of unit $10^{-9} \text{ m}^3\text{kg}^{-1}$ ($0.1 \text{ [SI; dimensionless]}$ is equal to $0,001 * 10^{-6} \text{ m}^3\text{kg}^{-1}$). The MSFDS is used for comparison of samples different in weight (Dearing 1999).

The rockmagnetic property constituted as magnetic susceptibility is measured by detecting the magnetisability of a sample as a response to an applied magnetic field (Borradaile 1988)(Dearing 1999) . The MS is measured as a sum of values of the magnetized elements or minerals (Dearing 1999).

³ Dearing, J. (1999) Environmental Magnetic Susceptibility. Using the Bartington MS2 System. 2nd Edition. Chi Publishing, England.

Ferromagnetism is a term used for the magnetic behavior of a material (for example iron) with highly ordered magnetic moments showing the same trend. Ferrimagnetism is referred to strongly aligned but opposing and unequal magnetic moments. An example for a ferromagnetic mineral is magnetite which is about 1000 times more magnetic than a material with an antiferromagnetic or paramagnetic behavior. Haematite obtains a canted antiferromagnetic behavior with opposing magnetic moments showing the same orientation canceling each other out. Many Fe-containing minerals like biotite or olivine and salts have a paramagnetic behavior. This weak magnetic susceptibility only arises when a magnetic field is induced (Dearing 1999). Local or regional variations of the magnetic susceptibility within an environment can be detected. An increased magnetic susceptibility can be the result of landscape erosion, which can be stronger in cold periods due to absent vegetation (Stockhausen & Zolitschka 1999). Furthermore it can result out of rising anthropogenic soil erosion (Dreßler et al. 2010).

The magnetic minerals can be altered due to diagenesis. Hematite with a low susceptibility can evolve from magnetite with a high magnetic susceptibility, affecting a decreased MS. Furthermore the MS is depending of the concentration, the mineralogy, the grain shape and size of the magnetic minerals. (Cohen 2003)(Borradaile 1988). A table of some minerals with magnetic susceptibility and their chemical formula can be seen in the following table:

Element/Mineral	Formula
Iron	αFe
Cobalt	Co
Nickel	Ni
Magnetite	Fe_3O_4
Hematite	$\alpha\text{Fe}_2\text{O}_3$
Goethite	αFeOOH
Olivine	$4[(\text{Mg},\text{Fe})_2\text{SiO}_4]$
Biotite	Mg,Fe, Al silicate

table 2 Table of some minerals with magnetic susceptibility (Dearing 1999)

Pollen analysis

Pollen analysis is an important tool used for Quaternary science giving delivering insights into terrestrial and aquatic regional palaeoenvironments (Seppä & Bennett 2003)(Fletcher et al. 2007). Pollen are biotic proxies, which reflect vegetation and vegetation changes as well as climatic history on a local, regional and global scale (Birks & Birks 2006)(Fletcher et al. 2007). They can be transported over long distances by various mechanisms like wind and water into the catchment area (Birks & Birks 2006) in dependence of their transport efficiency (Cohen 2003).

The transport mechanism of pollen in arid areas seems to be controlled by wind (Cohen 2003).

Pollen can be derived from aquatic plants within the lake, but also from vegetation from the proximal lake margin and more distant sources by the mentioned mechanisms. Larger pollen grains mostly come from proximal areas of the catchment (Cohen 2003). Furthermore, the pollen source area is depending on the size of the basin. The smaller the basin, the smaller the source area (Seppä & Bennett 2003). The amount of pollen transported into an area is also depends on various factors like the climate, the pollen productivity and deposition (Seppä & Bennett 2003), the proximity of plants to the lake, the size and shape of the pollen grains and the transport mechanism.

Pollen remains of Holocene or Late Pleistocene age are often still extant in lake deposits. They require evidence for the palaeoenvironment (Cohen 2003), but the biological response to climate is indirect (Battarbee 2000a).

Protocol for Preparation:

The pollen preparation was done applying the following method:

The sample volume is determined with the addition of distilled water. Then the sample will be centrifugated for 5 minutes and the water is removed. Lycopodium spores (2 tablets) as well as distilled water are added to the sample and heated in a water bath for 9 minutes (Fig.23A). The vortex mixer (Fig.23C) is used every time when a mixing of the sample is necessary. After centrifugalizing, the water has to be removed (Fig.23B).

The HCl treatment serves the purpose of the removal of carbonates and sulphates as well as the dissolution of the Lycopodium tablets. HCl (10%) is added to the sample and heated in the waterbath (at 96°C) for 10 min. In the following steps the sample should be centrifugalized, the HCl removed and washed with distilled water, centrifugated again and the water is removed.

The KOH treatment is done to destroy aggregates of clay and humus and to dissolve the humic substances. KOH (10%) is added, the sample heated in the waterbath for 10 min and sieved. In this preparation procedure only the fraction smaller than 112 µm was separated from macroremains. In the following, the HF-Treatment is done to destroy the silicates within the sample (Fig.23E&F). Five times 2 ml of HF (40%) are added to the sample and stirred after every addition. At last the sample should be left 24 h in closed sample tubes. Then the HF should be removed and the sample is washed two times with water, followed by centrifugating and removing of the water.

The acetolysis is the last step of chemical treatment, cellulose will be destroyed and the pollen will be colored. Acetic acid is added to the sample and removed after centrifugation. 4.5 ml acetic anhydride and 0.5 ml sulfuric acid are added to the sample, heated in waterbath for 10 min and the mixture removed after centrifugation. Then the sample should be cleaned with distilled water and the water is removed.

Methods



Fig. 23 (A) Picture of waterbath (middle right side of the picture), (B) centrifugal, (C) Vortex Mixer, (D) safety equipment for HF-treatment, (E) HF-treatment & (F) ultrasonic bath with preparation equipment

With the ultrasonic treatment the sample is cleaned from dissolved particles smaller than $10\ \mu\text{m}$ (Fig.23F). The sample will be poured back into the sample tube.

If the sample is stored with water, the sample should be centrifugated, the water is removed with a pipette and the sample covered with Glycerin (4-5 drops usually but less in this preparation because of the small amount of sample).

The slides are prepared by putting warm wax on object plates as frame (Fig.24A), followed by the transfer of the sample on the object plate (Fig.24B) and finally by covering the sample with a thin glass plate. This is heated up until the wax closes and protects the sample (Fig.24C). The remaining sample is transferred in Eppendorf caps.

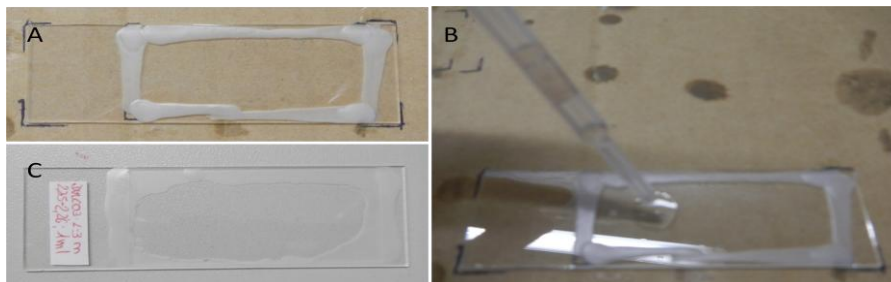


Fig. 24 Last steps of pollen and pollen slide preparation



Pollenanalysis Protocol for Preparation



Name: Selma Tala

Start of preparation: 22.03.2013

Sample name	Depth [cm]	Volume [ml]		Remarks
		read	sample-vol.	
✓ SALCOS	0-1m 80-81cm	8,4	1,6	
✓ SALCOS	2-4m 3,29-3,3	8,1	1,9	
✓ SALCOS	1-3m 8,7-2,71	8,1	1,9	
✓ SALCOS	1-2m 1,26-1,27	7,8	2,2	

- **determination of the sample volume** in the sample tubes (make **immediately** a note of the values!)
- centrifugate 5 min, then remove H₂O
- add 2 tablet of **lycopodium spores** to each sample

Specifications:
Lycopodium tablets
20848 Spores/Tab.
1031 Batch No.

HCL - Treatment

- add HCL (10%) and heat in waterbath (96°C) for 10 min
- centrifugate 5 min, then remove HCL
- add H₂O dest.
- centrifugate 5 min, then remove H₂O dest.

KOH - Treatment

- add KOH (10%) and heat in waterbath (96°C) for 10 min
- sieve (112 µm sieve) into a beaker
- new tube for remaining fraction
- pour the liquid sample into big glass sample tubes
- pour the liquid sample back into the sample tubes
- centrifugate 5 min, then remove H₂O

Special sieving and storage of the fractions:

Remarks:

2 mm _____

250 µm _____

125 µm _____

112 µm _____

Additional fraction: _____ _____

HF - Treatment

- add 5 x 2 ml HF (40%) carefully and stir after every addition
- leave at least for 24h in closed sample tubes
- centrifugate 5 min (sample tubes closed!), then remove HF
- add H₂O dest.
- centrifugate for 5 min, then remove H₂O dest.

HF-Treatment
start date: 23.07
end date: 26.07

if necessary
Second Treatment
start date: _____
end date: _____

Fig. 25 Protocol for pollen preparation (part1)

Density Separation		<i>Alternative to HF-Treatment</i>										
<ul style="list-style-type: none"> • ___ time density separation with zinc chloride <input type="checkbox"/> • wash with H₂O dest. twice <input type="checkbox"/> 												
Acetolysis												
<ul style="list-style-type: none"> • add acetic acid <input checked="" type="checkbox"/> • centrifugate for 5 min, then remove the acetic acid <input checked="" type="checkbox"/> • add 4,5 ml acetic anhydride and 0,5 ml sulfuric acid (9 : 1) <input checked="" type="checkbox"/> • heat in waterbath (96°C) for not more than 10 min <input checked="" type="checkbox"/> • centrifugate 5 min, then remove the mixture <input type="checkbox"/> • wash with H₂O dest. <input type="checkbox"/> 												
Ultrasonic Treatment												
<ul style="list-style-type: none"> • clean the sample in a ultrasonic waterbath <input checked="" type="checkbox"/> • pour the sample back into the sample tube <input checked="" type="checkbox"/> 												
Storage		End of preparation: <u>26.07.13</u>										
<ul style="list-style-type: none"> • centrifugate for 5 min <input checked="" type="checkbox"/> • remove H₂O dest. with a pipette <input checked="" type="checkbox"/> • cover the sample with Glycerin (4-5 drops) <input checked="" type="checkbox"/> 												
Preparation of Slides		Date of slide preparation: <u>29.07.13</u>										
<ul style="list-style-type: none"> • prepare pollen slides <input checked="" type="checkbox"/> • note any problems during the preparation of the slides <input checked="" type="checkbox"/> • transfer the remaining sample in Eppendorf cap <input checked="" type="checkbox"/> 												
<table border="1" style="width: 100%; border-collapse: collapse;"> <thead> <tr> <th style="width: 30%;">Sample name</th> <th>Remarks</th> </tr> </thead> <tbody> <tr><td> </td><td> </td></tr> <tr><td> </td><td> </td></tr> <tr><td> </td><td> </td></tr> <tr><td> </td><td> </td></tr> </tbody> </table>	Sample name	Remarks										
Sample name	Remarks											

Fig. 26 Protocol for pollen preparation (part2)

Results

Location of drilling points at the Laguna Salada, drilling type and depth [m]

Bore hole	Drilling type	Coordinates	Drilling depth [m]
SAL 1	Russian drilling device	Unknown	1
SAL 2	Russian drilling device	37°02'15,2"N 4°50'35,8"W	2
SAL 3	Russian drilling device	37°02'14,1"N 4°50'33,3"W	1,5
SAL-CO1	Vibracorer/sampling tubes	37°02'9,09"N 4°50'30,55"W	5
SAL-CO2	Vibracorer/sampling tubes	37°02'17,7"N 4°50'34,6"W	5
SAL-CO3	Vibracorer/sampling tubes	37°02'20,0"N 4°50'33,9"W	6
SAL-CO4	Vibracorer/sampling tubes	37°2'23,1"N 4°50'32,7"W	5
SAL-CO5	Vibracorer/PVC-liner extraction	37°2'23,1"N 4°50'32,7"W	4

Location of drilling points at the Laguna Dulce, drilling type and depth [m]

Bore hole	Drilling type	Coordinates	Drilling depth [m]
DUL-PL1	Russian drilling device	37°3'0,0"N 4°50'0,7"W	1?
DUL-CO1	Vibracorer/sampling tubes	37°03'19,4"N 4°50'2,0"W	5
DUL-CO2	Vibracorer/sampling tubes	37°02'55,4"N 4°50'3,2"W	7
DUL-CO3	Vibracorer/PVC-liner extraction	37°02'55,4"N 4°50'3,2"W	4

Location of drilling points at the Laguna del Gosque, drilling type and depth [m]

Bore hole	Drilling type	Coordinates	Drilling depth [m]
GOS-CO1	Vibracorer/sampling tubes	37°7'47,3"N 4°56'37,8"W	4

Location of drilling points at the Laguna de la Ratosa, drilling type and depth [m]

Bore hole	Drilling type	Coordinates	Drilling depth [m]
RAT-CO1	Vibracorer/sampling tubes	37°12'09,6"N 4°41'50,7"W	5

The cores SAL1, SAL2, SAL3, SAL-CO5 and DUL-CO3 have been chosen for measurement and interpretation because of their suitability. In the following, the cores will be examined in detail; starting with the stratigraphy, followed by the results of the magnetic susceptibility as well as the X-ray fluorescence measurements. Not all elements measured with XRF are diagrammed, only the elements and ratios that were chosen for interpretation. All results will be presented on the enclosed CD. The description of the results is done with round figures for convenience. The unit that is used for the content is ppm. The ratios and values of the magnetic susceptibility are dimensionless (x-axis) and the depth is displayed in meter (y-axis). If necessary in XRF examination, the x-axis was adapted for several elements because of a better display. This is the reason for double figures with the same elements.

Core Dul-CO3

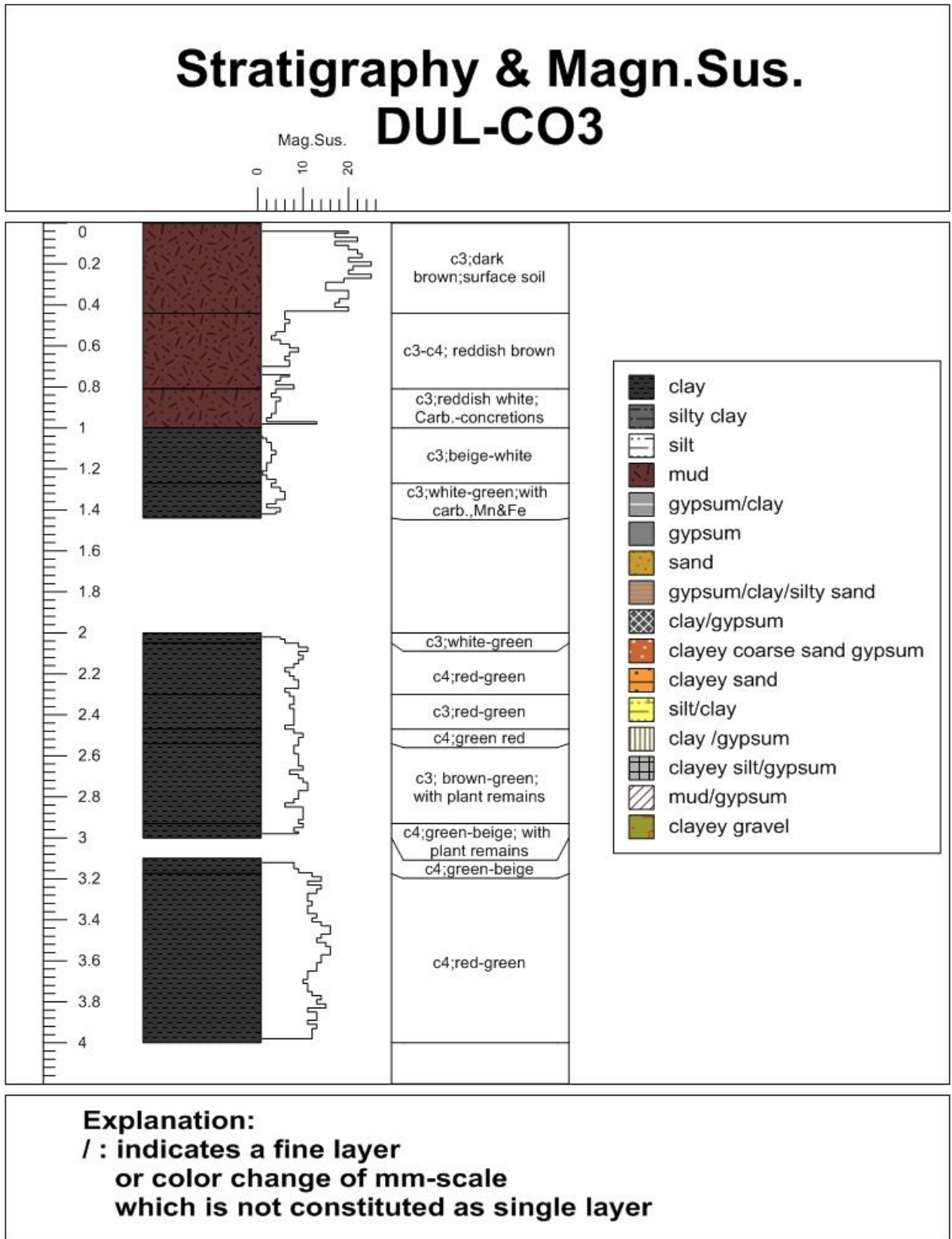


Fig. 27 Stratigraphy, further description and magnetic susceptibility of DUL-CO3

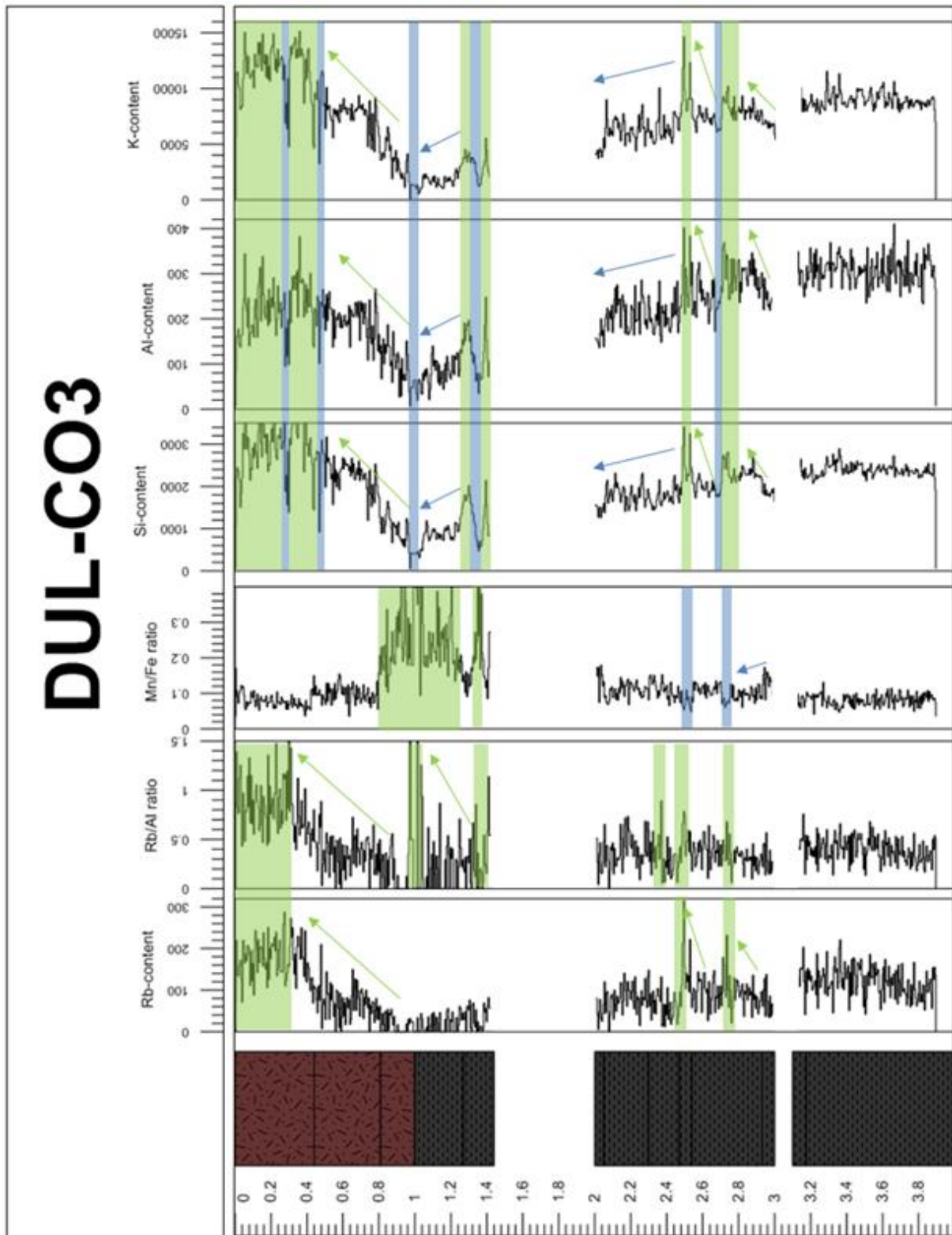


Fig. 28 Plot of the stratigraphy, Rb-, Si-, Al- and K-content as well as the Rb/Al and Mn/Fe ratio of DUL-CO3, the Rb/Al and Mn/Fe ratio is presented at higher resolution. Highs and increases are illustrated in green, lows and decreases are illustrated with the blue boxes and arrows

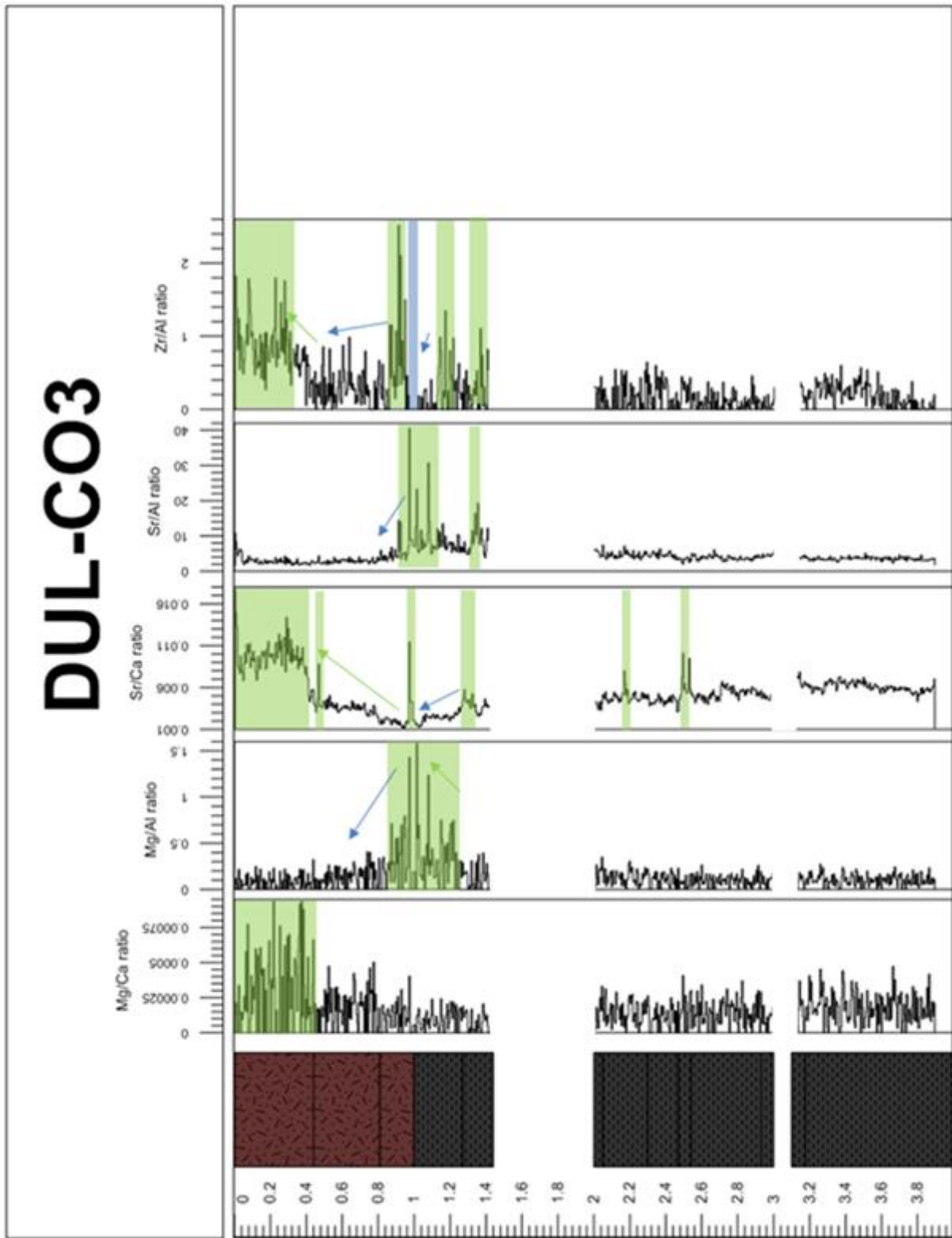


Fig. 29 Plot of the stratigraphy as well of the Mg/Ca, Mg/Al, Sr/Ca, Sr/Al and Zr/Al Fe ratio in a higher resolution as in the previous figure of DUL-CO3. Highs and increases are illustrated in green, lows and decreases are illustrated with the blue boxes and arrows

Results

The core has been divided into four intervals for a simplified description of the variation of elements.

The first interval from 4 m to 3 m depth shows medium to high, steadily fluctuating values of the K-, Al- and Si-content. The Mn-Fe ratio also fluctuates but on a low level. The Rb-content as well as the Rb/Al ratio fluctuate on a low to medium level. The Mg/Ca, Mg/Al, Sr/Ca, Sr/Al and Zr/Al ratios fluctuate on low to medium-low values.

In the section from 3 m to 2 m depth, the elements and element ratios show more variety. The values of the Rb-, Si-, Al- and K-content increase, reaching a high between 2,8 m and 2,7 m depth. The Mn/Fe ratio shows an oppositional trend at this depth and between 2,5 m and 2,4 m it shows a sudden but not very strong drop. A slight drop of the Si-, Al- and K-content can be observed between 2,7 m and 2,65 m depth before the contents increase at a depth of 2,5 m. The Sr/Ca ratio has a high at 2,5 m and also at 2,2 m depth, too. This high of the Si-, Al- and K-content can be observed in the Rb-content and the Rb/Al-ratio as well. At a depth between 2,5 m and 2 m, the Si-, Al- and K content decrease more or less steadily. This trend cannot be observed for the fluctuating Rb-content and Rb/Al ratio between low to medium values. In this core section, a very obvious correlating trend of the elements Si and Al can be seen. The K-content shows the same trend, but not with the same accurateness. The Mg/Ca, Mg/Al, Sr/Ca, Sr/Al and Zr/Al ratios fluctuate again, but the Mg/Ca as well as the Sr/Ca ratio undulate on a slightly lower level as in the first interval.

Between ~1,40 m and 1 m depth the values for contents and ratios show big discrepancies. At the beginning, the Si-, Al- and K content show a high, followed by a drop and a high at a depth around 1,3. The low can be observed in the Rb-content and the Rb/Al ratio as well. While values of the Rb-, Si-, Al- and K content declines up to a depth of 1 m, the Rb/Al ratio increases and the Mn/Fe ratio fluctuates on a high level. In the case of the Mn/Fe ratio, this fluctuation on a high level can be observed up to 0,8 m depth. The Mg/Ca ratio has a similar trend as in the interval before while the Mg/Al ratio goes up and reaches a high at 1 m depth. The Sr/Ca ratio declines between a depth of ~2,3 m and 1 m, where it shows a high. The Sr/Al ratio has a little peak at about 1,4 m, then the values decrease and gently fluctuate up to 1,2 m, where they suddenly rise and dramatically fluctuate between high and low values. The Zr/Al ratio decreases from a gently high at around 1,4 m depth, rises again at a depth at around 1,2 m and gradually declines to the top at 1 m.

At a depth between 1 and 0 m, the values of the Rb-, Si-, Al- and content rise and show a drop at nearly 0,5 m and 0,3 m depth. This fall is more gently for the Rb- content and the Rb/Al ratio. In between 0,3 m and 0 m depth, the Rb-, Si-, Al- and K-content as well as the Rb/Al ratio zig-zag on a high level. The Mn/Fe ratio flutters on a low level between ~0,8 m and ~0,5 m depth, followed by an undulated trend on a lower level up to 0 m depth. The Mg/Ca ratio flutters on a higher level than before and steeply climbs and fluctuates between 0,4 m depth and the surface as well as the magnetic susceptibility, the Si-,Al- and K-content and the Mg/Ca ratio. The Mg/Al ratio declines from the peak at around 1 m up to 0 m depth. The Sr/Ca ratio increases and shows high values between 0,4 m depth and the surface, while the Sr/Al ratio slightly fluctuates on a low level. The Zr/Al ratio shows a little decrease up to around 0,5 m depth, where it increases again to high values between 0,4 m and 0,2 m depth. The magnetic susceptibility of the entire core DUL-CO3 seems to show the same trend as the Si-, Al- and K content and do also show similarities with the Sr/Al ratio.

Core SAL1

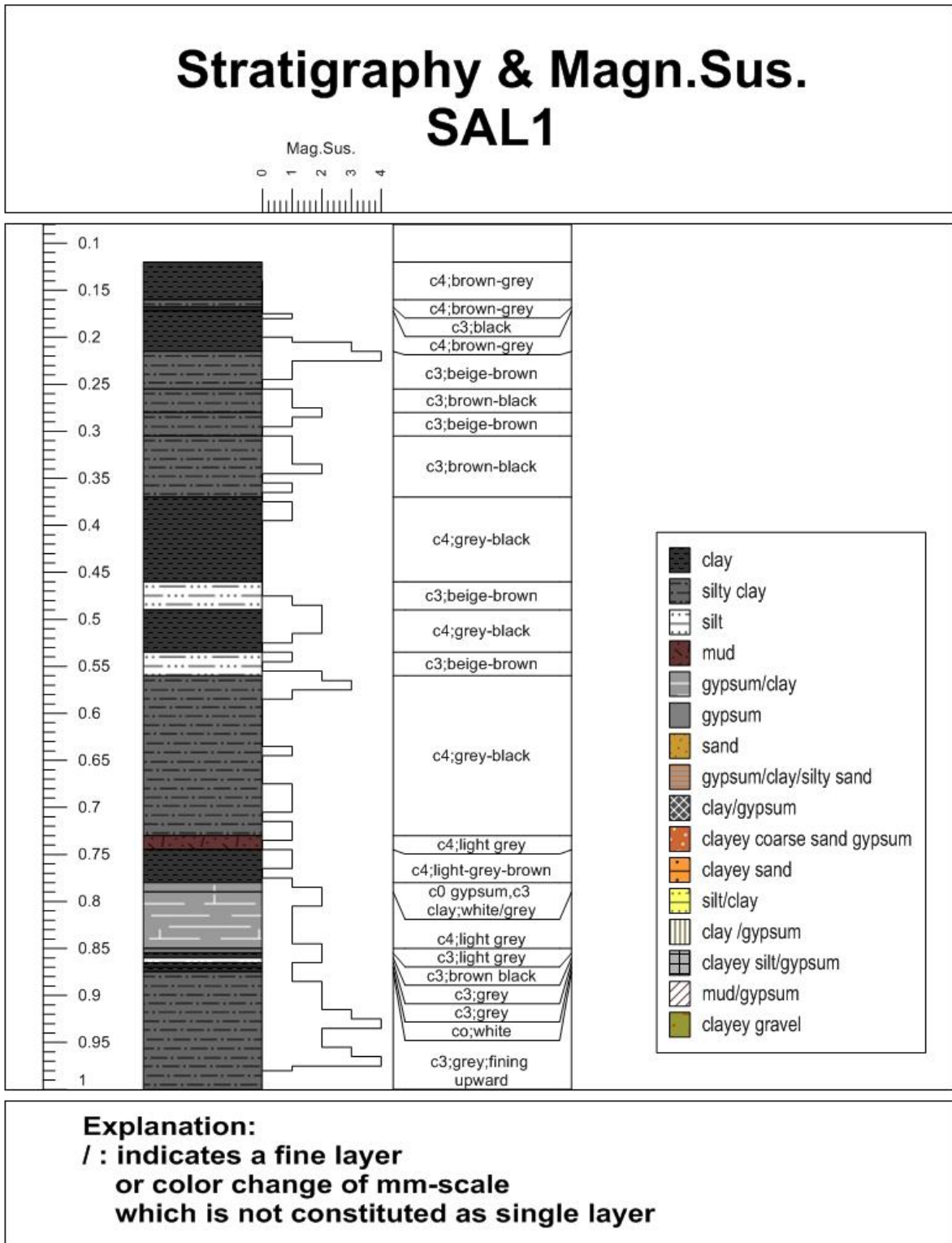


Fig. 30 Stratigraphy, further description and magnetic susceptibility of SAL1

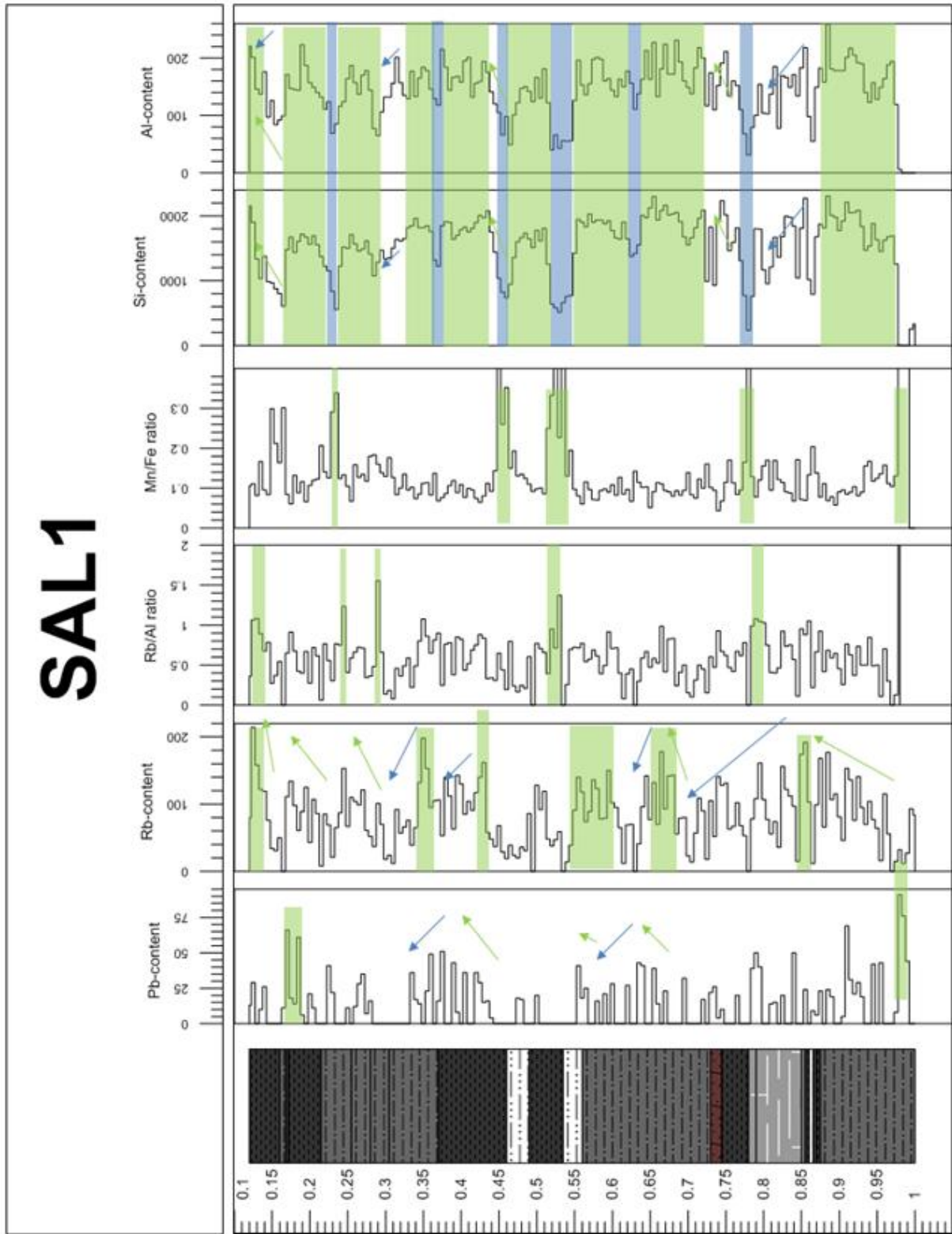


Fig. 31 Next plot of the stratigraphy as well of the Pb-, Rb-, Si- and Al content as well as the Rb/Al and Mn/Fe ratio in a higher resolution as in the previous figure. Highs and increases are illustrated in green, lows and decreases are illustrated with the blue boxes and arrows

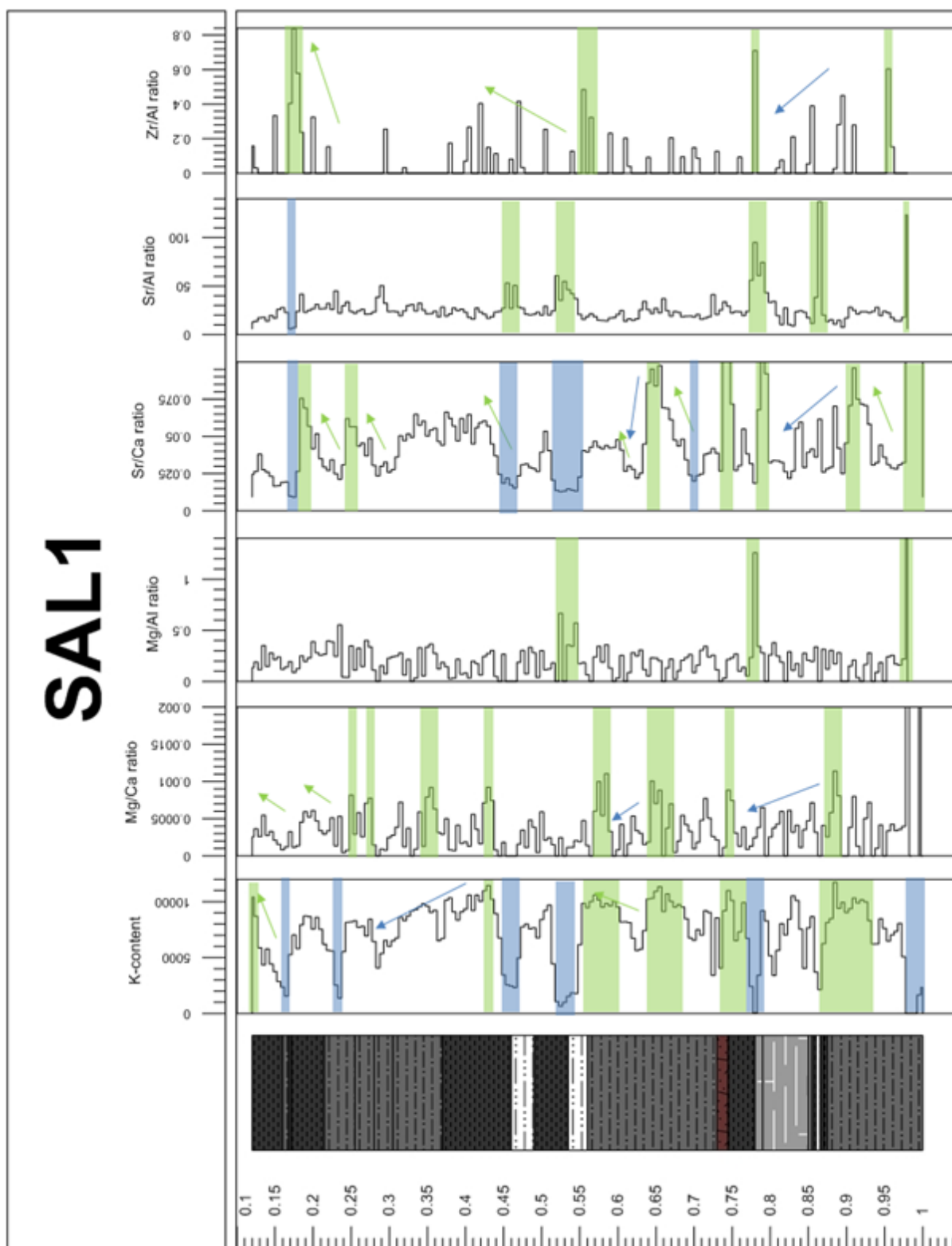


Fig. 32 Plot of the stratigraphy as well of the K- content and the Mg/Ca, Mg/Al, Sr/Ca, Sr/Al and Zr/Al ratio in a high resolution. Highs and increases are illustrated in green, lows and decreases are illustrated with the blue boxes and arrows

The core has been divided into two intervals for simplified description of the variation of elements.

Results

The interval between 1 m and 0,5 m depth contains mostly silty clay, but also gypsum, silt, mud and pure clay layers. The Pb-content highly fluctuates with several highs, overall decreases up to a depth of nearly 0,7 m. Then it rises and falls again with a peak at 0,55 m depth and is not present and measured until 0,5 m depth. The Rb-content zig-zags and collectively grows up to 0,85 m depth, where it drops. This is followed by a further increase up to nearly 0,65 m depth, a second fall and a next high between 0,62 m and 0,55 m depth. The Rb/Al ratio slightly increases up to 0,8 m depth, followed by an undulating trend up to 0,5 m depth. The Mn/Fe ratio shows peaks at 1 m and 0,8 m depth, while overall the values gently decrease but highly flutter. The trend of the Si- and Al-content is similar; shows high values in greater depth, drops after 0,87 m to a very low level, and increases overall with a little low at nearly 0,65 depth. The potassic content highly fluctuates and shows various peaks and lows up to the end of the interval. At first, it increases up to its highest peak at 0,9 m depth, then it sharply declines, rises and falls to its lowest value at 0,8 m depth. Thereafter, it shows high but also highly zig-zagging values until 0,5 m depth. The Mg/Ca ratio shows a very high value in the beginning, as well as the Mg/Al, Sr/Ca and Sr/Al ratio. A high peak of the Zr/Al ratio comes shortly afterwards. Overall, the Mg/Ca ratio is low up to values of ~0,5, with the mentioned peak in the beginning and further highs at 0,8 m and 0,55 m depth. The Sr/Ca ratio sharply undulates with very high values at first and moderate values at 0,5 m depth. The Sr/Al ratio is low and displays highs at 0,87 m and 0,85 m depth. The first peak is as mentioned at odds with the other ratios. This is followed by a decrease of the values and a high at 0,78 m and 0,56 m depth.

The division between 0,5 m depth and the surface mostly contains clay, but also silty clay and silt. In comparison to the deeper core section, the overall grain size gets smaller from the deeper to the upper part of the core. The Pb-content is lesser as in part 1 and increases from low values up to nearly 50 ppm at 0,37 depth. Then it drops again, climbs up at 0,2 m depth and decreases again. The Rb content has a high in the beginning and fluctuates with drops and rises up to the surface. The Rb/Al ratio is similar to the deeper part of the core and shows highs at 0,55 m, 0,3 m, 0,26 m and between 0,1 and 0,15 m depth. The Mn/Fe ratio overall in this section slightly grows, with peaks at 0,47 m, 0,25 m and 0,17 m depth. The Si- and Al-content are similar again, the trend of this values first decreases, then grows until a little low at 0,47 m depth, when it goes up again until 0,35 m depth; only interrupted of a little low at 0,37 m depth. This is followed by a steady decrease up to 0,3 m depth, when it grows again, falls and ends up with high values at the surface. The K-content fluctuates again, but not that sharply as in the lower part of the core. In general, the values decrease with a little high in the end. The Mg/Ca ratio is low with lower peaks in comparison to the deeper section at 0,45 m, 0,35 m, 0,28 m and 0,25 m depth. This is followed by a slight increase, a drop and a second increase. The Mg/Al ratio is not very conspicuous and zig-zags from low values to slightly higher values (up to ~ 0,5). The Sr/Ca ratio slightly correlates with the K-content but does not show these sharp increases, the values rise more slowly but are generally high in the same depth. The Sr/Al ratio in general gets lower with fewer peaks. Nevertheless, the peaks at the bottom occur when the Sr/Ca ratio is low, but the ratios both show the same low at 0,17 m depth. The Zr/Al ratio increases in the beginning, then drops and is non-existent up 0,25 m depth, only interrupted by two little occurrences at 0,33 m and 0,3 m depth. Then it shows a high at 0,17 m depth with a preceding increase and an oncoming decrease up to the surface.

Within all the cores of the Laguna de Salada, the element Pb was measured. This is not the case for the core DUL-CO3 of the Laguna Dulce.

Core SAL2

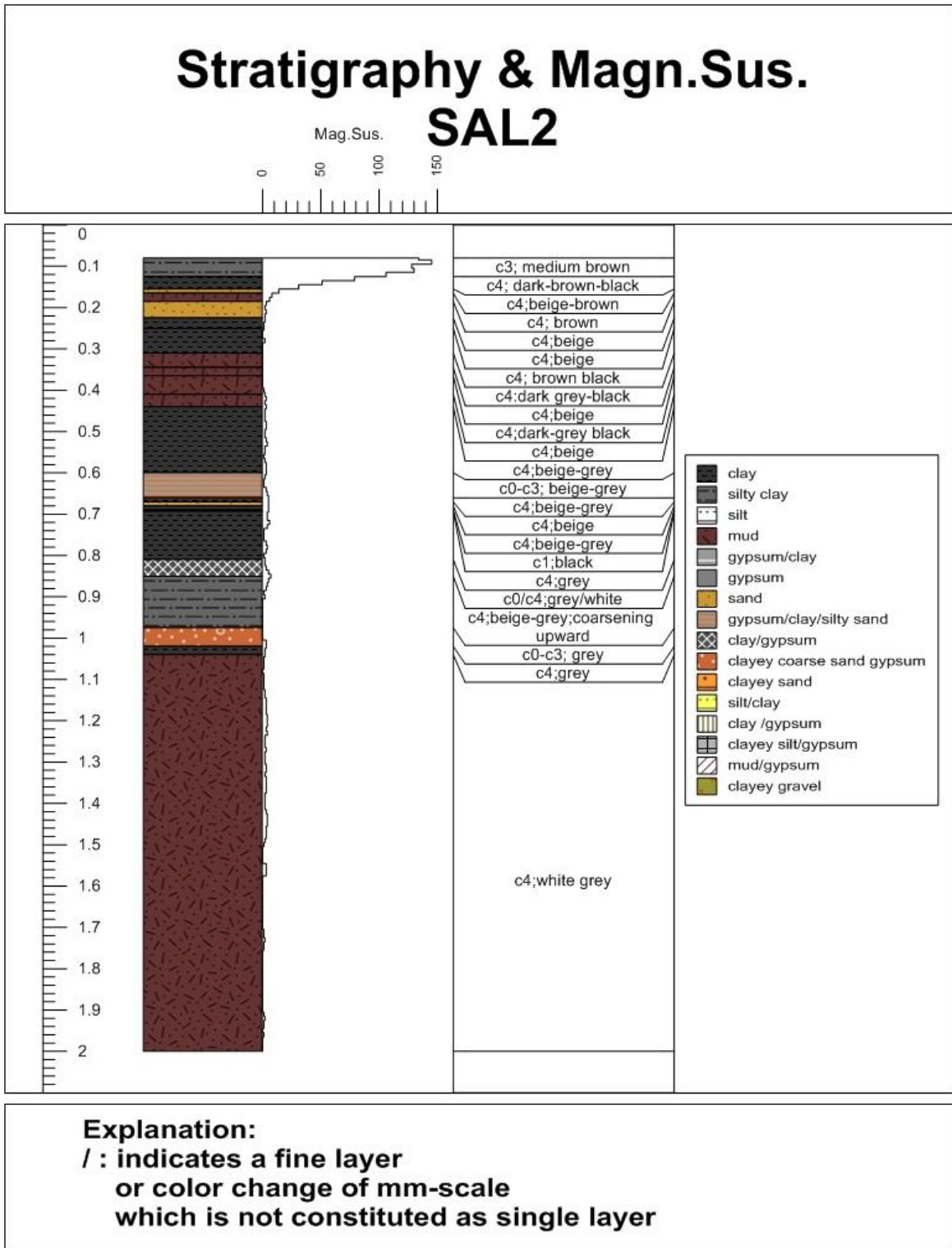


Fig. 33 Stratigraphy, further description and magnetic susceptibility of SAL2

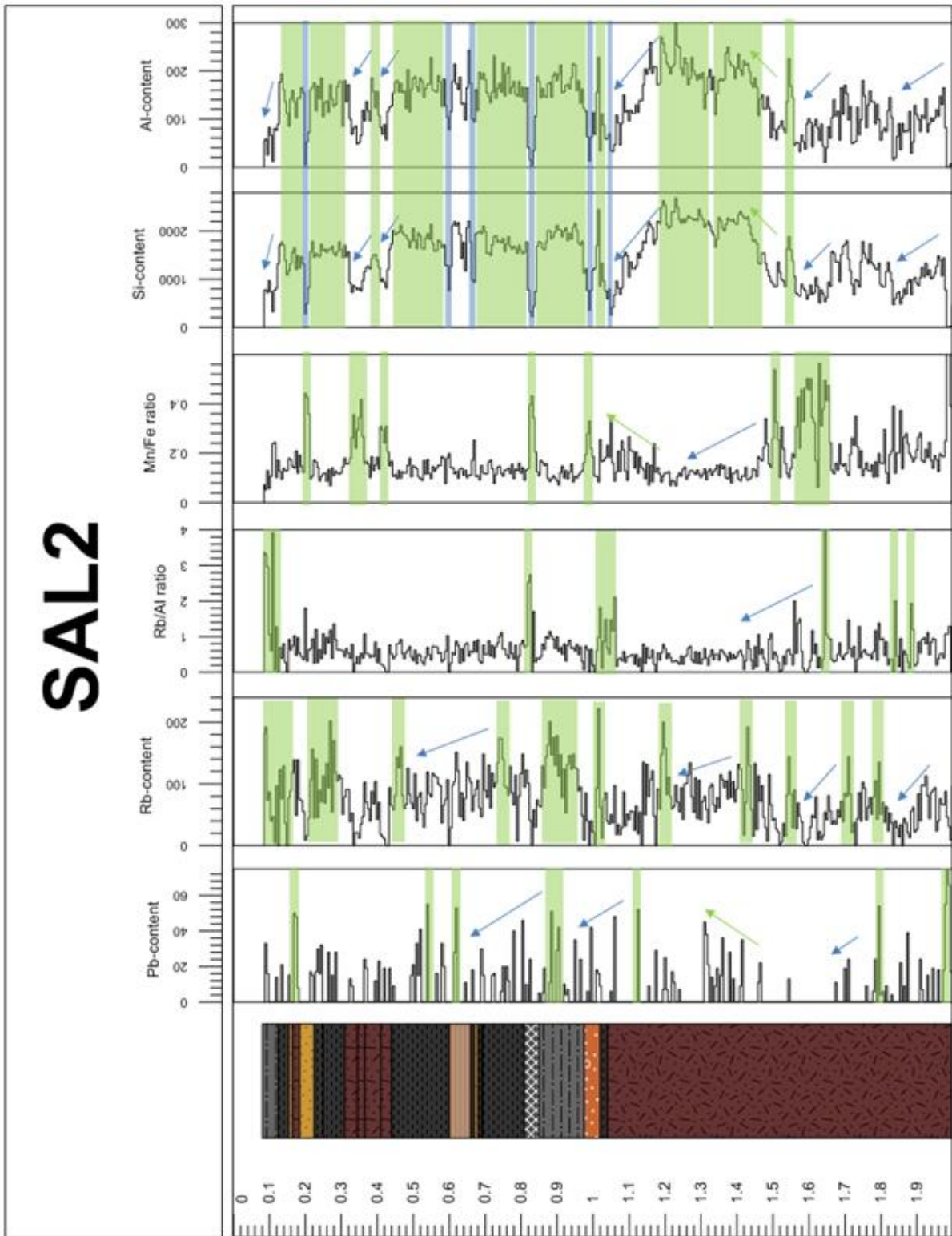


Fig. 34 Next plot of the stratigraphy, Rb-, Si-, Al- and K-content as well as the Rb/Al and Mn/Fe ratio of SAL2, the Rb/Al and Mn/Fe ratio is presented at higher resolution. Highs and increases are illustrated in green, lows and decreases are illustrated with the blue boxes and arrows

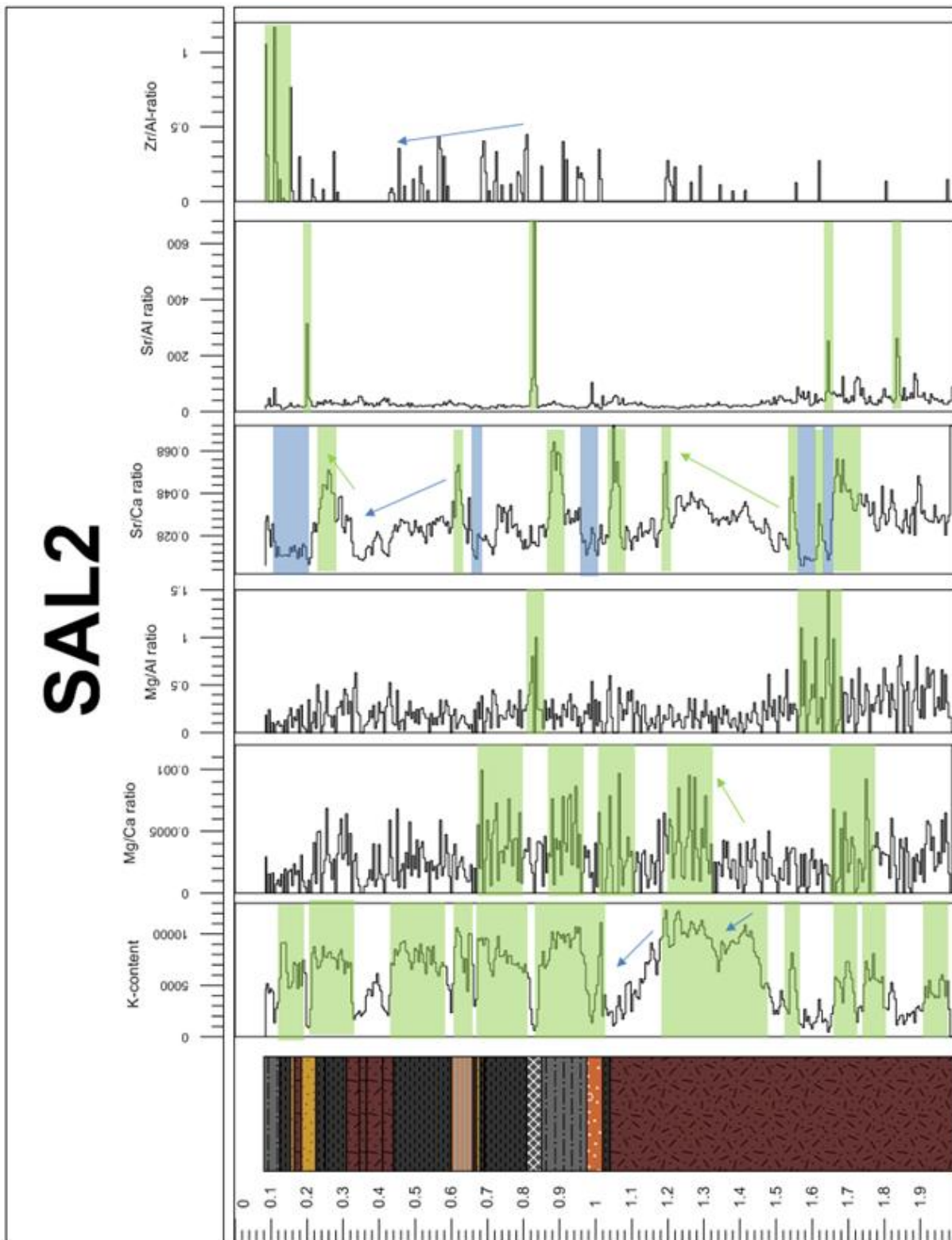


Fig. 35 Plot of the stratigraphy as well of the K- content and the Mg/Ca, Mg/Al, Sr/Ca, Sr/Al and Zr/Al ratio in a high resolution. Highs and increases are illustrated in green, lows and decreases are illustrated with the blue boxes and arrows

The core SAL 2 has been divided into two intervals for a simplified description of the variation of elements.

Results

The lower section between 2 m and 1 m depth contains mainly mud, followed by a clay layer and some alternating clayey coarse sand/gypsum layers. The Pb-content has the highest peak in the greatest depth, fluctuates with little peaks and decreases up to 1,65 m depth. Little values exist in the upper part of this interval, but overall the Pb peaks rises between 1,45 m and 1,1 m depth. A lower peak occurs at around 1 m depth. The Rb-content first drops from medium high values around 100 ppm, then it grows to higher values and two highs at 1,8 m and 1,7 m depth. The peak at 1,8 m depth occurs at the same time as a high of the Pb-content. Then it declines again and has two more peaks at 1, m and 1 m depth. The Rb/Al ratio zig-zags very strong, has to medium high peaks at 1,9 m and 1,8 m depth and undulates again with the highest peak at 1,6 m depth. This is followed by a gradual decrease and more or less stabilized values until a depth of 1,05 m, where values increase up to 2 ppm. The Mn/Fe ratio shows in both sections more or less the opposite trend as the content of Si and Al. The Fe-content is high at 2 m, between 1,7 m and 1,6 m and at 1,5 m depth. This is followed by a gradually decrease and a medium high peak at the end of the interval. The Si- and the Al-content shows firstly two slight drops, followed by a high and further increase, at the same depth where the Mn/Fe ratio decreases. The potassium content is very high within these sediments, but also highly fluctuates with lows between 1,9 m-1,8 m, at 1,72 m, between 1,65 m and 1,55 m and at around 1,5 m depth. This trend does not fit at all with the Mg/Ca ratio, which increases between 1,8 m and 1,65 m depth. The entire trend of this ratio is low. The Mg/Al ratio is low too, except between a depth of 1,7 m and 1,6 m. The Sr/Ca ratio is medium high with ~ 0,048 in a depth between 1,95 and 1,7 m, but the start value of the beginning of the core is very high. It further shows decreases, where the Mg/Al ratio is high and shows an increase up to 1,2 m depth, where it has a high. This is followed by a drop and a next peak. The Sr/Al ratio is low and has peaks at around 1,8 m and 1,65 m depth, the trend declines. The Zr/Al ratio does not give many results and is overall below values of 0,5.

The upper part between 1 m and 0,11 m depth consists of clay, sand, mud and silty clay layer and alternating clay/gypsum and clayey coarse sand/gypsum layer. This more distinct separation of layers is of limited visibility within the XRF results: The Pb-content is higher and flutters more in this section. Peaks occur at around 0,9 m, 0,6 m 0,55 m and 0,2 m depth, between them the trend more or less decline. The magnetic susceptibility is going to increase from very low values up to values around 140 near the surface. The Rb-content first increases, drops and has a next peak up to ~ 180 ppm at 0,75 m depth. This is followed by a gradual decrease and further peaks at 0,5 m and between 0,3 m-0,2 m and 0,18 m-0,11 m depth. The Rb/Al ratio is low with highs at 0,8 m depth and near the surface. The Mn/Fe ratio shows as mentioned peaks, where the Si- and Al-content has lows. The K-content is high again and seems to correlate in a positive way with clay and silty clay layers. The Mg/Ca ratio has high values between 0,98 m- 0,85 m, 0,8 m-0,7 m depth, followed by highly fluctuating values up to the surface. The Sr/Ca ratio also zig-zags, it is first low, sharply increases in the following to medium high up to high values, drops again until 0,7 m depth, followed by a gentle low and high. From the last peak, it decreases up to 0,35 m depth, where the values increase again and drops from 0,2 m to 0,11 m depth. The Sr/Al ratio is lower than in the lower section but contains higher peaks; more than 600 at 0,85 m depth (where the K-content is low) and up to 300 at 0,25 m depth. The Zr/Al ratio could be calculated more often, shows a declining trend from medium high values around 0,5 and a increase to more than 1 next to the surface.

Core SAL3

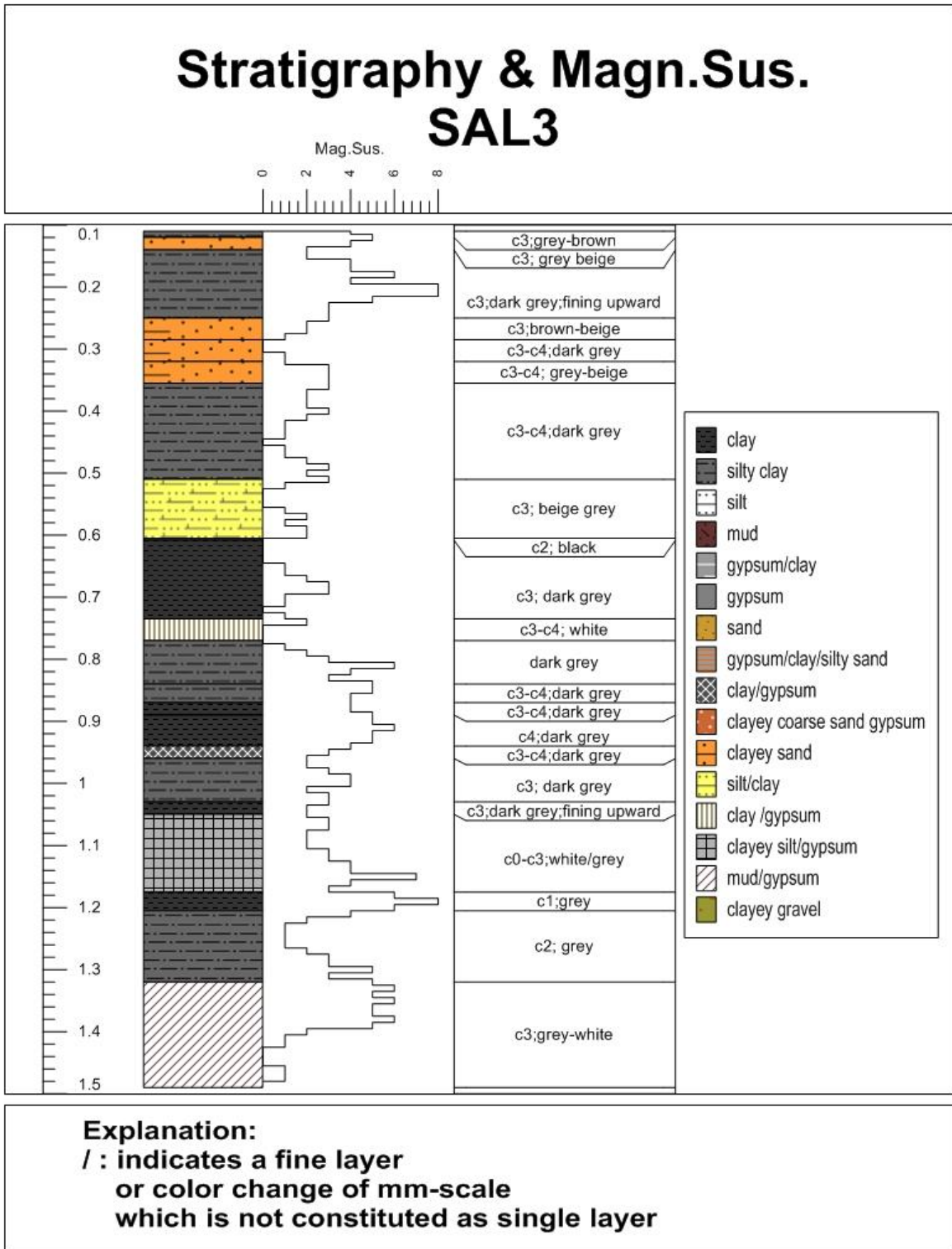


Fig. 36 Stratigraphy, further description and magnetic susceptibility of SAL3

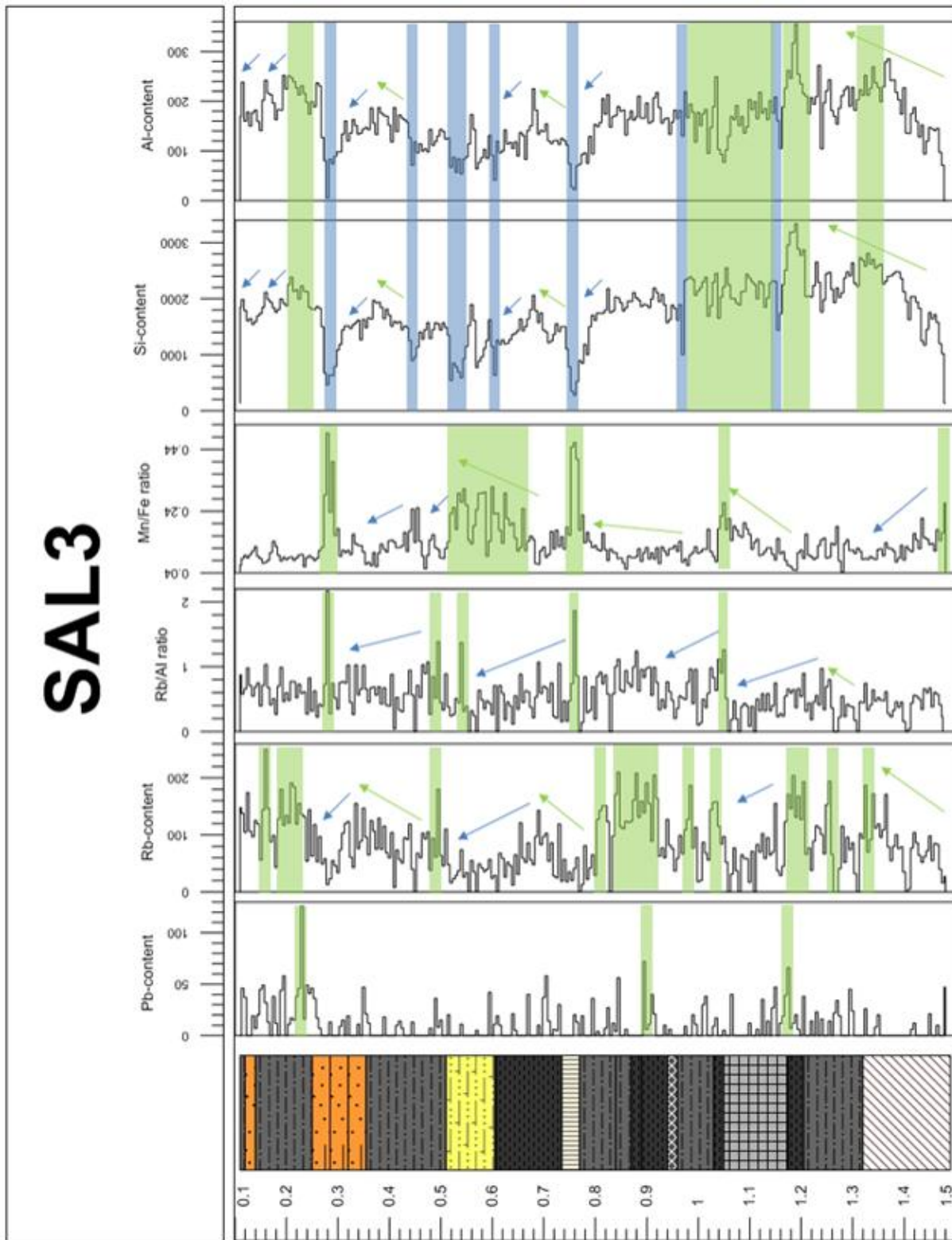


Fig. 37 Plot of the stratigraphy as well as the Pb-, Rb-, Si- and Al content as well as the Rb/Al and Mn/Fe ratio of SAL3

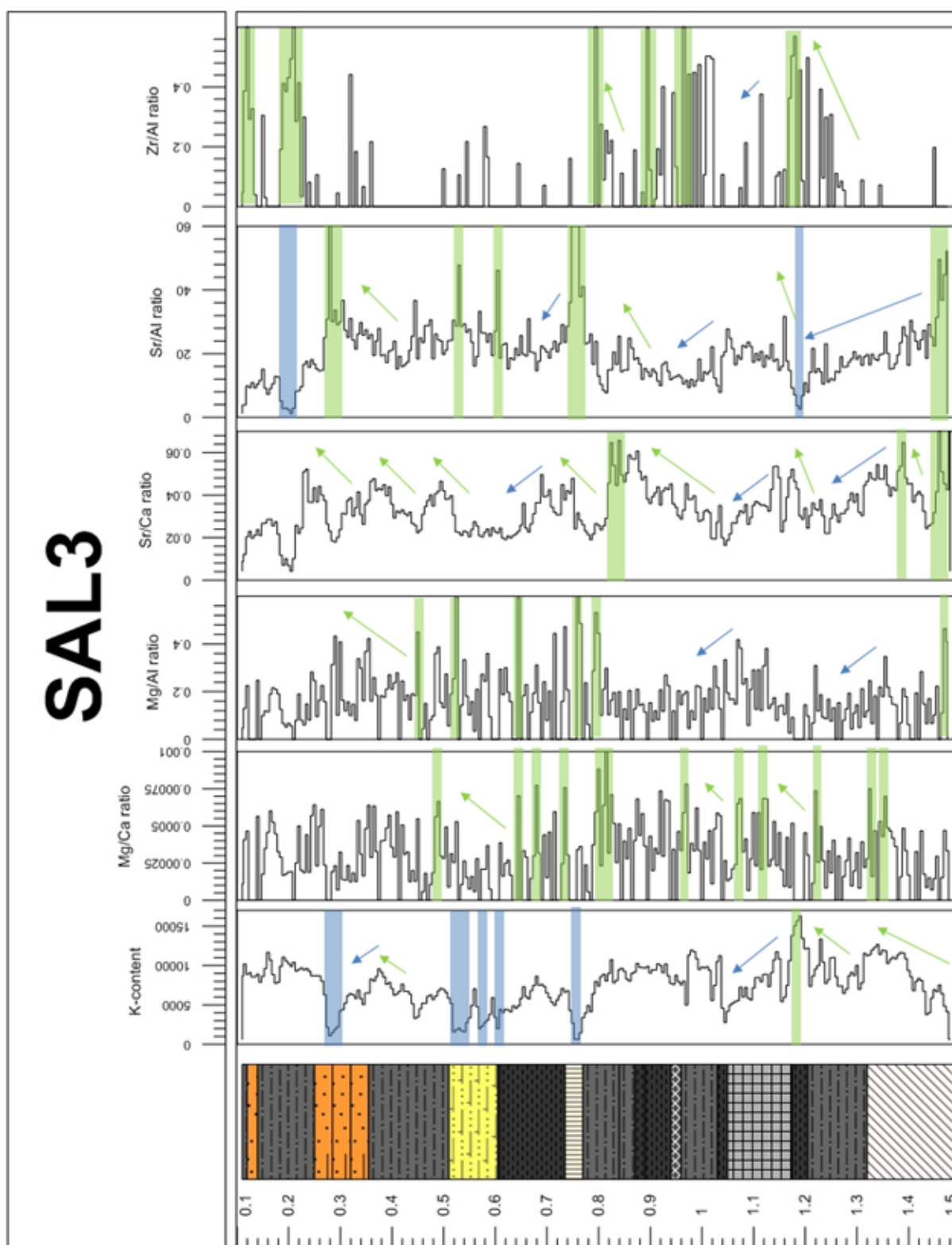


Fig. 38 Plot of the stratigraphy as well of the K- content and the Mg/Ca, Mg/Al, Sr/Ca, Sr/Al and Zr/Al ratio in a high resolution. Highs and increases are illustrated in green, lows and decreases are illustrated with the blue boxes and arrows

The core SAL 3 has been divided into two intervals for a simplified description of the variation of the element content.

Results

The section between 1,5 m and 0,8 m depth mostly contains alternating mud/gypsum layers and clayey silt/gypsum layers, but also clay, silty clay and alternating clay/gypsum layers. The carbonate content as well as the color differs a lot. The magnetic susceptibility shows values up to 8. Higher values occur between 1,4 m-1,3 m, at 1,2 m up to 1,1 m and between 0,95 m-0,8 m depth. The Pb-content attains values up to ~ 80, highs occur at 1,18 m and 0,9 m depth. The Rb-content is higher, grows at the beginning, has some peaks at 1,3 m, 1,25 m and around 1,2 m depth, declines gradually up to 1,05 m depth and fluctuates in the following between very high and low values. The Rb/Al ratio shows low values up to 1 with a gentle increase and decrease until 1,05 m depth, when it goes up and falls again. The Mn/Fe ratio shows a high in the same depth at 1,05 m depth, after decrease and climb. This is followed by a sudden drop and a very gentle rise. The Si- and the Al-content shows again the same trend, which increases up to a high at around 1,2 m depth, a slight drop and high values interrupted by to lightly lows at 1,5 m and 0,95 m depth. This is followed by a fluctuation at values around 2000 for Si and 150 for Al. The values drop up to 0,8 m depth. The K-content is high and shows two rises up to 1,2 m depth, decreases up to 1,05 m depth to values around 2500 and ends up highly zig-zagging with values around 10 000 until 0,8 m depth. The Mg/Ca ratio undulates at very low values around 0 and 0,0015 up to a depth of 0,8 m. A lot of small increases, drops and highs can be seen. The Mg/Al ratio has a start value around 0,5 in 1,5 m depth, fluctuates with obvious decreases and ends with a high value of ~0,45 in a depth of 0,8 m. The Sr/Ca ratio exhibits a high at 1,5 m depth, followed by a steeply drop and a gentle increase up to a value of 0,06. Then it drops up until 1,2 m depth to around 0,03; increases, drops and rises again and ends at a high at 0,8 m depth. The Sr/Al ratio indicates a high value at 1,5 m depth, a gradual drop until 1,2 m depth, increases to moderate values and fluctuates on a lower level until 0,8 m depth. The Zr/Al ratio represents a high in the same depth as the K-content at 1,2 m; before it rises strongly up to this high. Then the values decrease again up to 1,05 m depth and evidence a higher ratio up to 0,5 at a depth between 1,05 m and 0,8 m.

In the interval between 0,8 m and the surface, there are less gypsum layers and it mostly contains of clay, alternating silt/clay, silty clay and clayey sand layers. The carbonate content not alternates as in the deeper section. The magnetic susceptibility fluctuates slightly within this part and shows a high at 0,2 m depth. The Pb-content overall gets lower in this section, but there is a very high peak around 150 at 0,25 m depth. The Rb-content starts with an increase, decreases again and shows a gentle high at 0,5 m depth. Proximate, the values increase, drops and ends up fluctuating on a high level. The Rb/Al ratio first drops until 0,55 m depth, has to highs at 0,55 m and 0,5 m depth, falls again and has its highest peak in 0,3 m depth. Up to the surface, the values of the Rb/Al ratio are low. The K-content starts with a low at 0,8 m depth, increases then to moderate values up to 0,6 m depth, fluctuates then on a very low level and ends up with moderate values around 10 000 at the surface. The Mg/Ca ratio overall is lower in this section, but it zig-zags at the same time. The Mg/Al ratio is higher in comparison to the deeper part of the core, it starts with highs up to 0,5 in 0,8 m, 0,62 m and 0,5 m depth, shows a rising trend up to 0,3 m depth, where it drops and flutters up to the surface on low to moderate values. The Sr/Ca ratio firstly rises, followed by a drop until 0,6 m depth and remains nearly constant up to 0,5 m depth. This is followed by highs and lows and low values near the surface. The Sr/Al ratio shows gentle highs at 0,6 m and 0,5 m, fluctuates and increases up to a high in 0,3 m depth and drops again to very low values near the top. The Zr/Al ratio indicates fewer values than in the deeper core section, but has highs at 0,35 m, around 0,2 m and at the top.

Core Sal-CO5

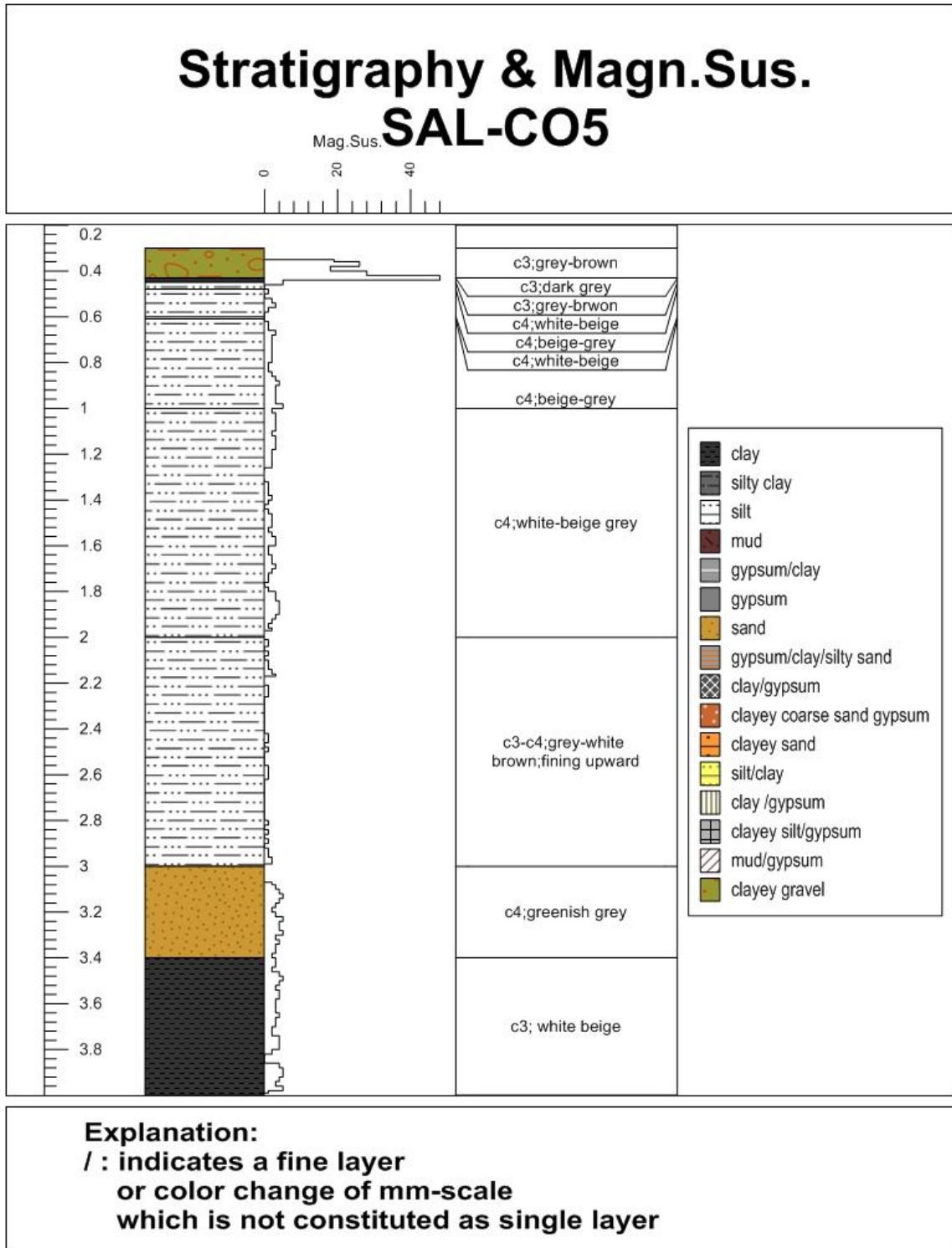


Fig. 39 Stratigraphy, further description and magnetic susceptibility of SAL-CO5

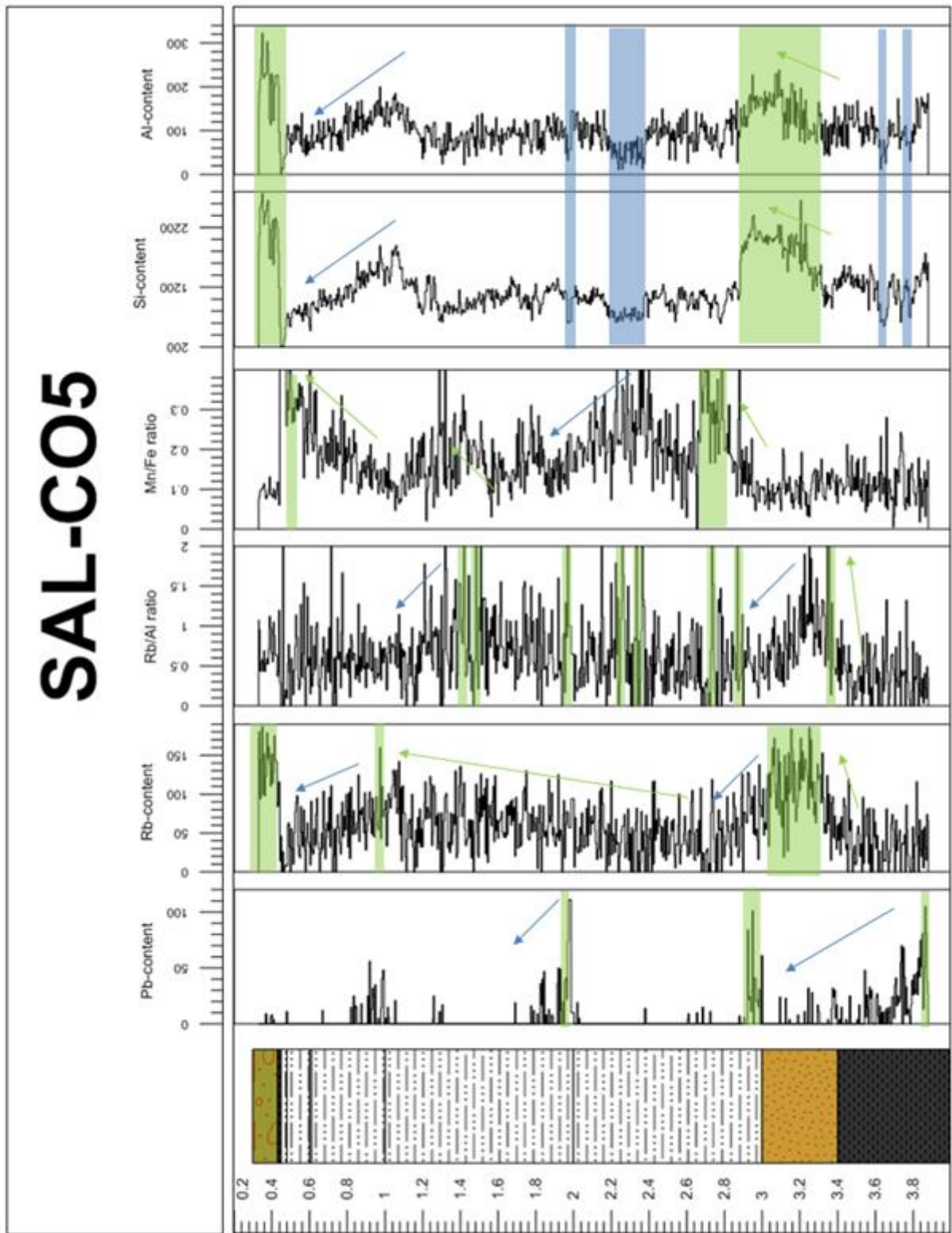


Fig. 40 Plot of the stratigraphy as well of the Pb-, Rb-, Si- and Al content and the Rb/AI and Mn/Fe ratio in a high resolution. Highs and increases are illustrated in green, lows and decreases are illustrated with the blue boxes and arrows

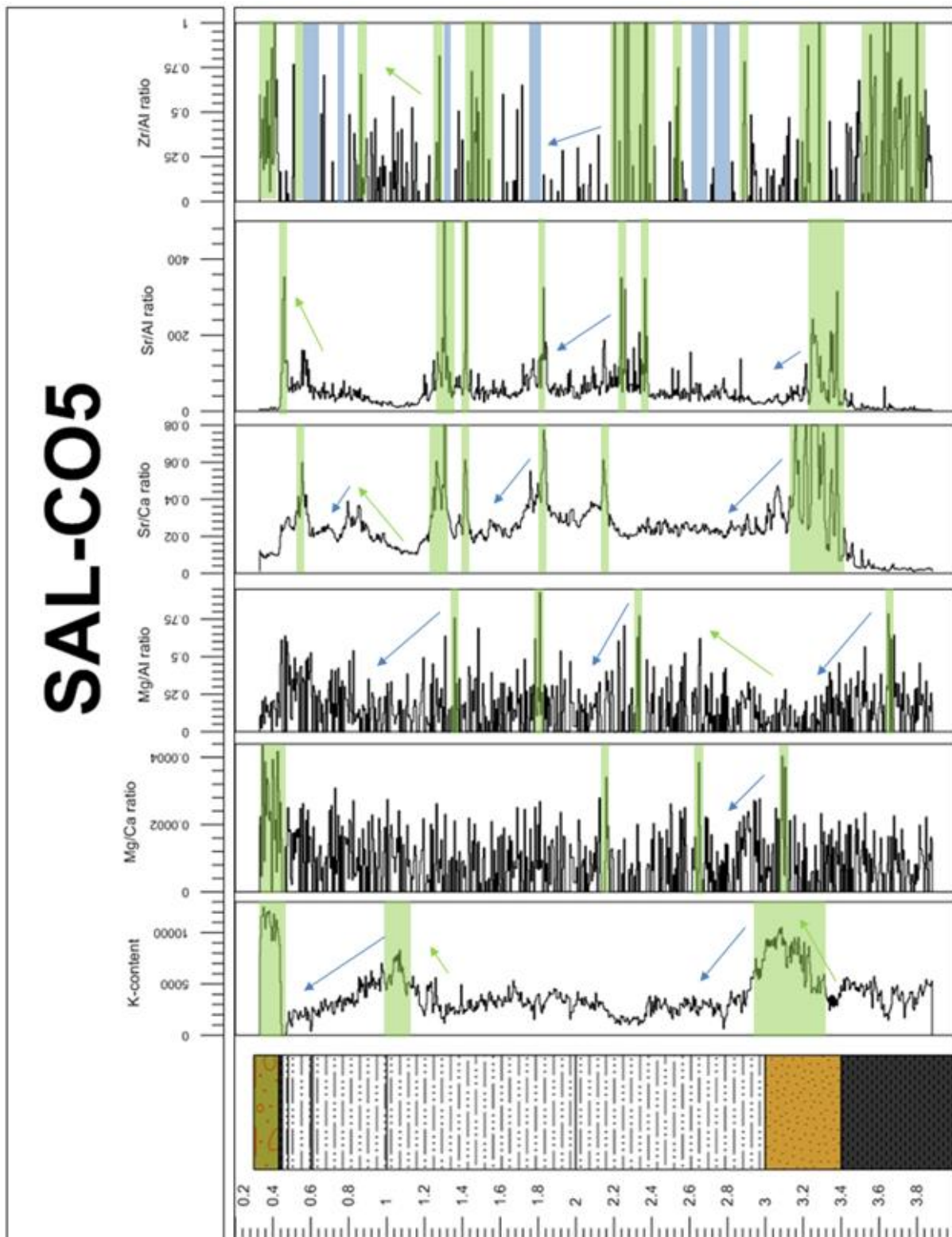


Fig. 41 Plot of the stratigraphy as well of the K- content and the Mg/Ca, Mg/Al, Sr/Ca, Sr/Al and Zr/Al ratio in a high resolution. Highs and increases are illustrated in green, lows and decreases are illustrated with the blue boxes and arrows

The core SAL-CO5 has been divided into two intervals for a simplified description of the variation of the element content.

Results

The first interval is located between 4 m and 2 m depth and dominated by silt, sand and clay layers and a high carbonate content. The magnetic susceptibility within this section is low (around 2), nevertheless it is higher in the lower section at the sand and clay layers. The Pb-content decreases from high values within the clay and sand layer, shows at the layer boundary in 3 m depth again high values and only a few isolated values up to 20 in five zones. The Rb-content highly fluctuates with a peak around 3,2 m depth, falls afterwards and shows a gradual increasing trend up to 2 m depth. The Rb/Al ratio shows a high in the region, followed by a gradual decrease and further highs at around 2,98 m and 2,8 m depth. Between 2,8 m and 2,4 m the values are more or less staying the same, followed by two highs at 2,4 m and 2,2 m depth. A slight decrease can be observed up to 2 m depth, where a next peak is located. The Mn/Fe ratio zig-zags on a low level until 3 m depth, increases in the silt layer, falls and slightly rises and falls again. The trend of the Si- and Al-content is similar, shows moderate values in greatest depth, two lows at 3,8 m and 3,6 m depth, an increase within the sand layer and a sharp drop at 3 m depth where the silt layer begins. Within this 3 m and 2 m depth the values fluctuate on a low level with two lows between 2,4 m-2,2 m and at 2 m depth.

The section between 2 m depth and the surface is dominated by silt layers which differ in color and other properties with high carbonate content. The magnetic susceptibility is very low except near the surface where values up to 50 are reached within a clayey gravel layer. The Pb-content is indicated with a high value near 2 m depth, drops and occurs only scattered towards the top near 1,3 m, between 1,05 and 0,8 m, at 0,7 m depth and near the surface. The Rb-content still increases from the section below, shows at high at 1 m depth and falls up to a final high at the top. The Rb/Al ratio again highly fluctuates, shows several highs in 2 m, around 1,5 m, 0,8 m and 0,4 m depth. The Mn/Fe ratio is low, increases and falls again two times until it ends up with very high values in 0,5 m depth. The ratios near the surface are low. The Si- and Al-content undulates on a low to medium low level, increases at around 1 m depth and drops gradually until 0,4 m depth. Furthermore, both element contents show a peak in the clayey gravel layer on top. The K-content fluctuates on a level around 5000 until 1,1 m depth, increases a little bit until it drops again to very low values. In the upper layer, the K-content is very high. The Mg/Ca ratio again dramatically flutters and shows as well a peak next to the surface. The Mg/Al ratio has a high at 1,8 m and 1,4 m depth, overall the ratio undulates and declines up to the surface, where the values are low. The Sr/Ca ratio shows more peaks as in the first section, but they are smaller and more isolated, like at 1,8 m, 1,4 m, around 1,25 m and 0,45 m depth. The Sr/Al ratio shows similar peaks at 1,8 m, 1,4 m and around 1,25 m depth. The upper peak does occur later near the layer boundary between silt and clayey gravel. The Zr/Al ratio is very high and highly undulates and shows several lows and highs, decreases and increases until the surface is reached.

Results of pollen analysis

The samples were taken by choosing layers and areas within the cores which seem to show a potential for pollen preservation, like organic rich layers. Areas with visible fungi as well as dry areas at the surface were avoided. In the following table, an overview of the samples as well as their availability of pollen is given. A quantity of pollen that is not representative and is therefore described as no pollen (x). Pollen grains were investigated after Beug (2004).

Name	Core [m]	Depth [m]	Pollen
DUL-CO3	0-1	0,3-0,31	x
DUL-CO3	0-1	0,75-0,76	x
DUL-CO3	1-2	1,08-1,09	x
DUL-CO3	1-2	1,26-1,27	x
DUL-CO3	1-2	1,42-1,43	x
DUL-CO3	2-3	2,1-2,11	x
DUL-CO3	2-3	2,25-2,26	x
DUL-CO3	2-3	2,45-2,46	x
DUL-CO3	2-3	2,51-2,52	x
DUL-CO3	2-3	2,72-2,73	x
DUL-CO3	2-3	2,95-2,96	x
DUL-CO3	3-4	3,14-3,15	x
DUL-CO3	3-4	3,34-3,35	x
DUL-CO3	3-4	3,54-3,55	x
DUL-CO3	3-4	3,74-3,75	x
DUL-CO3	3-4	3,94-3,95	x
SAL-CO5	0-1	0,42-0,43	✓
SAL-CO5	0-1	0,8-0,81	x
SAL-CO5	0-1	0,98-0,99	x
SAL-CO5	1-2	1,26-1,27	x
SAL-CO5	1-2	1,69-1,70	x
SAL-CO5	2-3	2,38-2,39	x
SAL-CO5	2-3	2,7-2,71	x
SAL-CO5	3-4	3,29-3,3	x
SAL-CO5	3-4	3,7-3,71	x
SAL2	0-1	0,19-0,2	✓
SAL2	0-1	0,39-0,4	✓
SAL2	0-1	0,59-0,6	✓
SAL2	0-1	0,6-0,62	✓
SAL2	0-1	0,79-0,8	✓
SAL2	1-2	0,19-0,2	x
SAL2	1-2	1,39-1,4	x
SAL2	1-2	1,55-1,6	x
SAL2	1-2	1,59-1,6	x
SAL2	1-2	1,79-1,8	x
SAL2	1-2	1,99-2	x

table 3 overview of the samples as well as their availability of pollen

Summing up, the uppermost sample of the core SAL-CO5 as well as the five uppermost samples of the core SAL2 contain pollen grains. An overview of the most representative pollen grains as well as some explanations will be given in the following.

SAL2; 0-1 m; 0,19-0,20 m

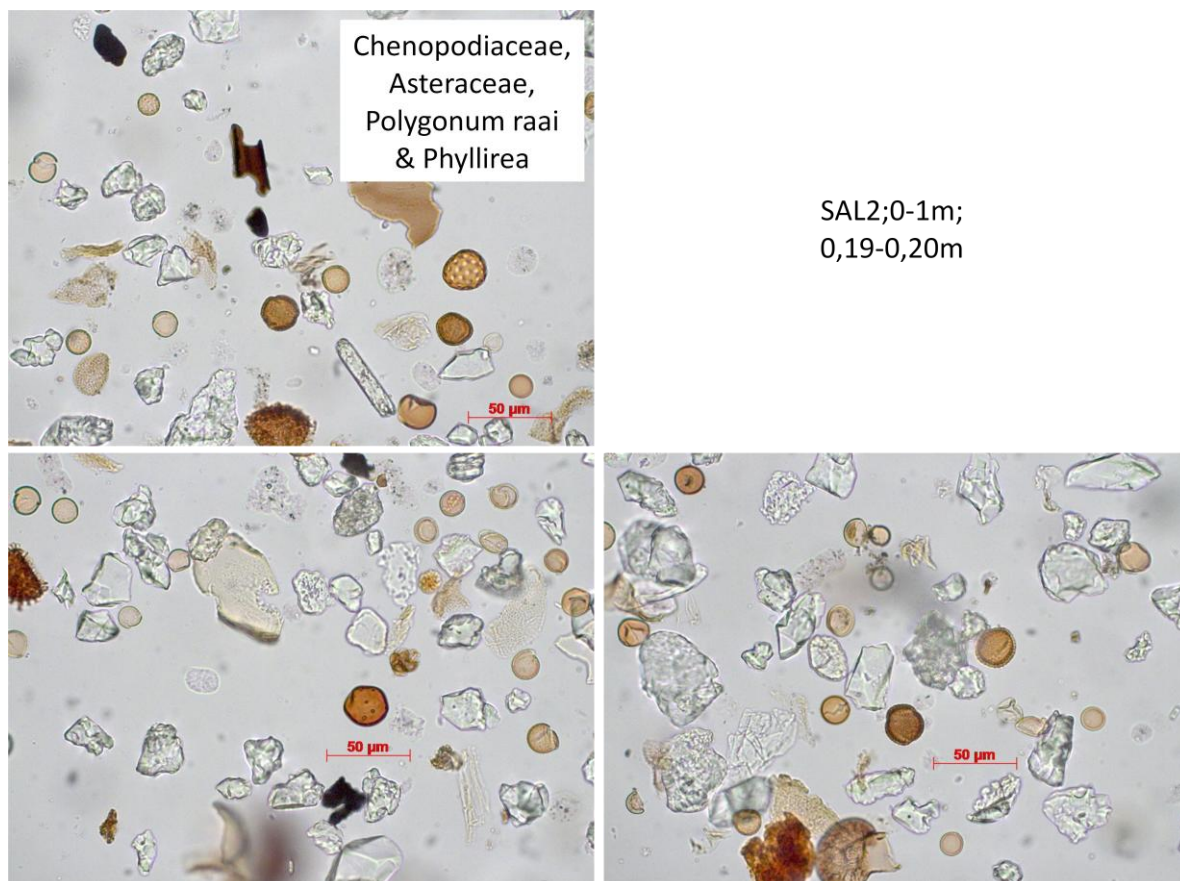


Fig. 42 Pictures of the sample SAL2; 19-20 cm with the most representative pollen grains within this sample: Chenopodiaceae, Asteraceaea, Polygonum raai & Phyllirea

The family of the Chenopodiaceae is characterized by a big amount of small pores and many other properties (Beug 2004). There exists a variety of Chenopodiaceae, some pictures are given below in Fig. 43. They are also called the Goosefoot family (plantsystematics.org) and can be produced in very dry periods (Giralt et al. 1999).

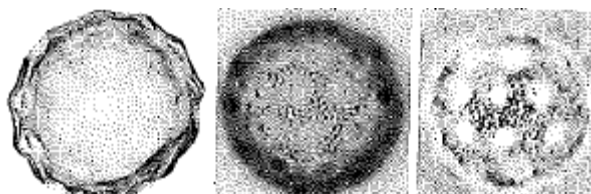


Fig. 43 From left to right: Salsola kali & Atriplex littoralis (2 times) (Beug 2004)



Fig. 44 Pictures of Chenopodiaceae, right: *Allenrolfea occidentalis*, left: *Maireana pyramidata* (www.plantsystematics.org)

SAL 2; 0-1m; 0,39-0,4 m

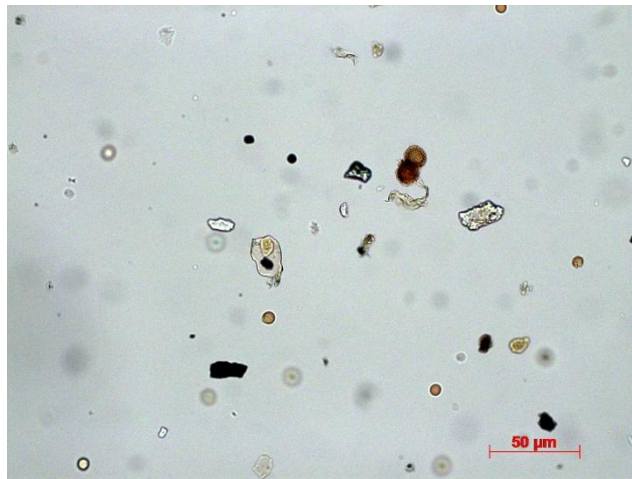


Fig. 45 Mineral remains, fungi & Lycopodium spores

Contains not a lot of pollen grains but the little that are existent are mainly Asteraceae, Chenopodiaceae and Poaceae. The Poaceae is a very large plant family and also called grasses (Beug 2004)(Fig.46).



Fig. 46 Picture of the Poaceae *Merostachys neesii* (www.plantsystematics.org)

SAL2; 0-1m; 0,59-0,60 m

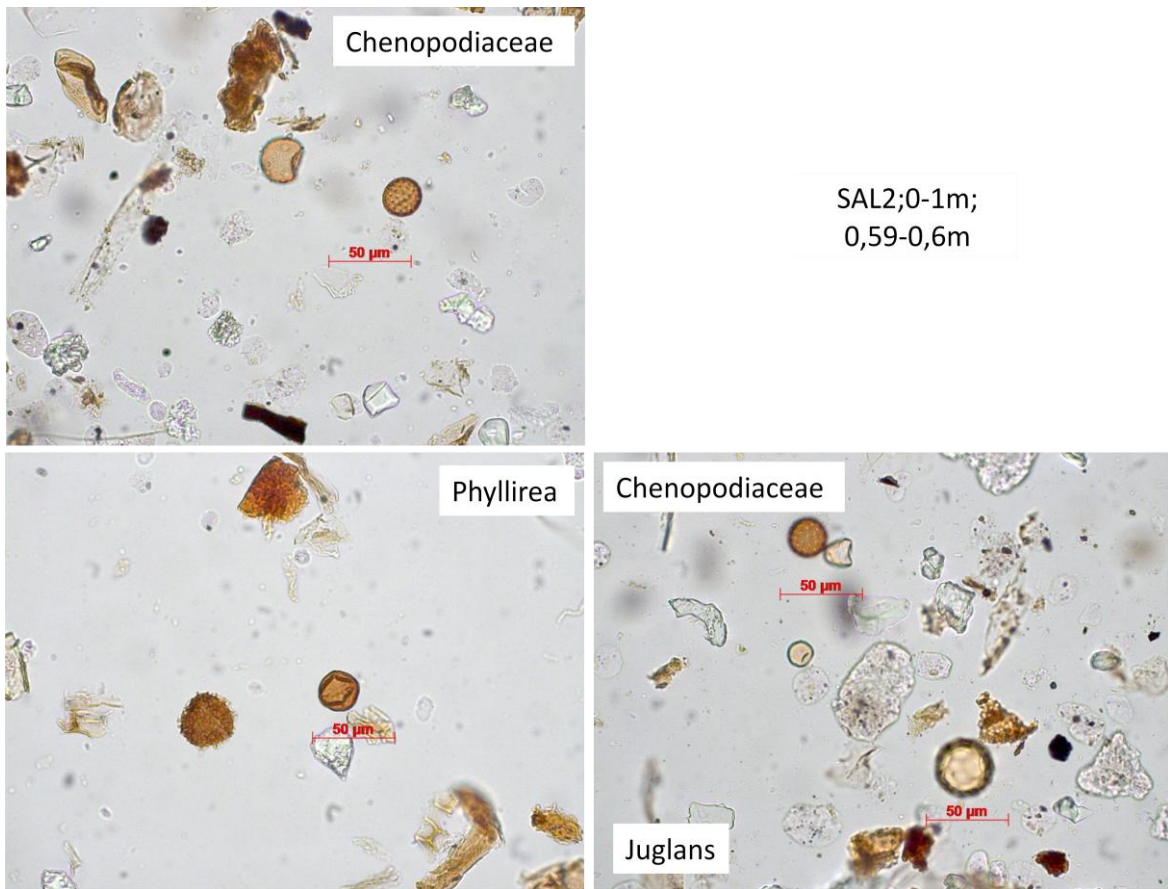


Fig. 47 Pictures of the sample SAL2; 0-1m; 0,59-0,60 m with the most representative pollen grains within this sample: Chenopodiaceae, Phyllirea

Juglans pollen grains were scarce and not representative for the whole sample. The most occurring pollen were Chenopodiaceae, Phyllirea and Asteraceae.

The group of the Phyllirea shows an orbicular pollen grain and medium large to large polar fields. They are often similar to another pollen type, the *Fraxinus excelsior* type (Beug 2004). Some pictures are given below in Fig. 46.

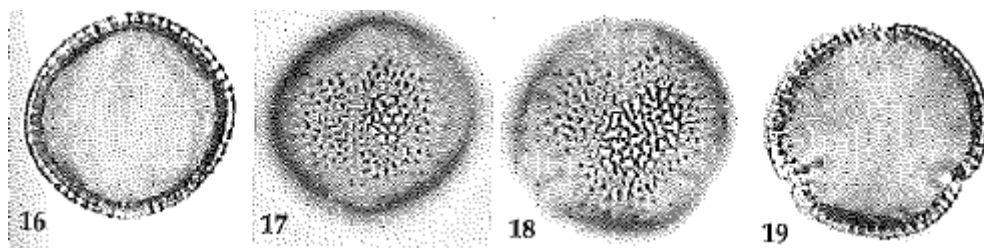


Fig. 48 Pictures of *Phyllirea media* (Beug 2004)

SAL2; 0-1m; 0,6-0,62m

There are not a lot of pollen grains, but if they could be identified they turned out to be mostly Asteraceae and Chenopodiaceae.

All middle European Asteraceae without the Artemisia belongs to the family of the Asteraceae. They do have an inner or an outer columella or the inner columella is so much reduced that there is a hollow space within the outer columella stratum (Beug 2004). It is furthermore with more than 15 000 species one of the largest families of flowering plants (Cronquist 1980).

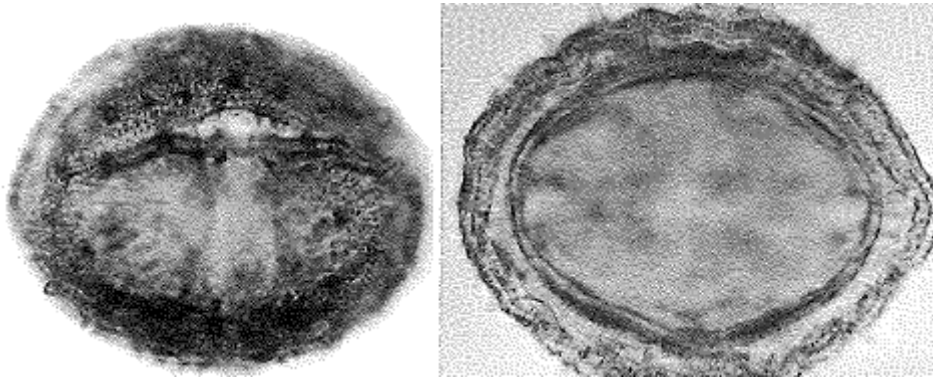
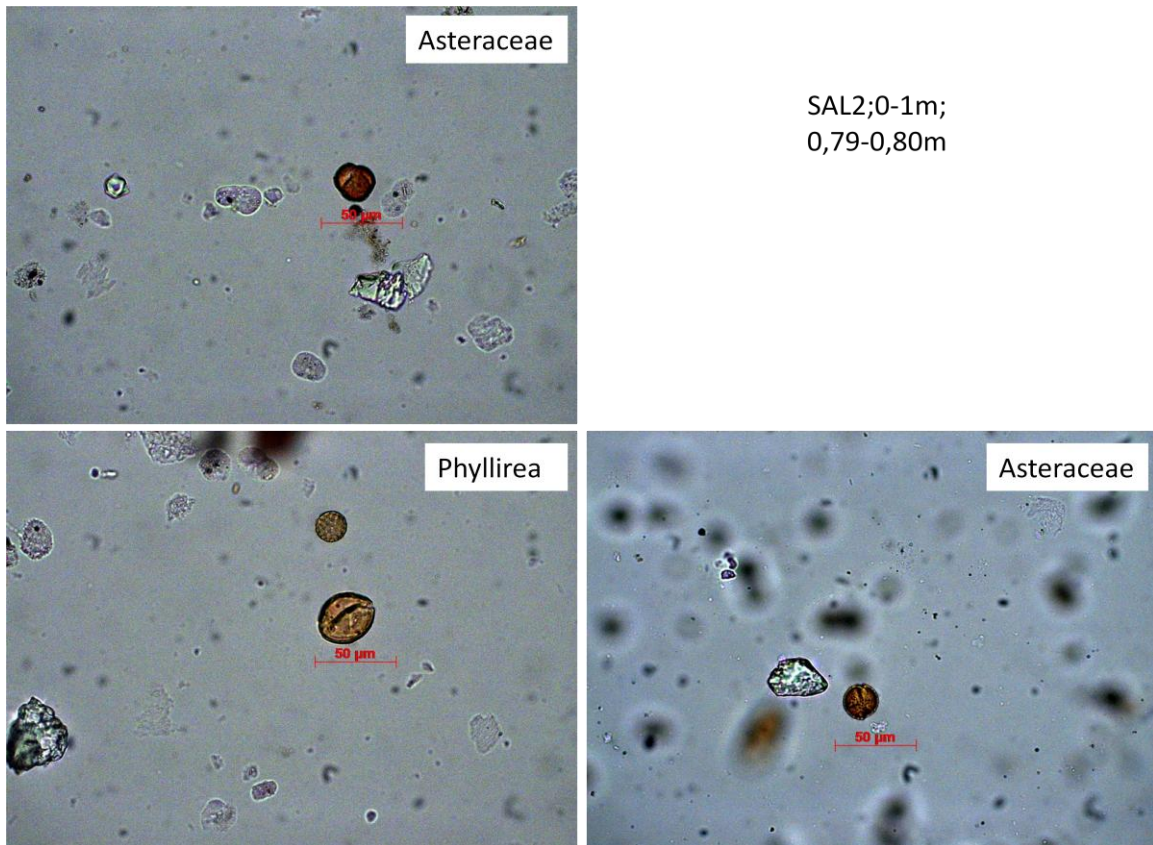


Fig. 49 Pictures of the *Crupina vulgaris* of the group of the Asteraceae (Beug 2004)



Fig. 50 Pictures of the Asteraceae *Aster novae-angliae* (left) and *Bellis perennis* (right) (www.plantsystematics.org)

SAL2; 0-1m; 0,79-0,80m



SAL2;0-1m;
0,79-0,80m

Fig. 51 Pictures of the sample SAL2; 0-1m; 0,79-0,8 m with the most representative pollen grains within this sample: Asteraceaea & Phyllirea (family of the Oleaceae)



Fig. 52 Picture of the *Phyllirea angustifolia* (www.plantsystematics.org)

SAL-CO5; 0-1m; 0,42-43m

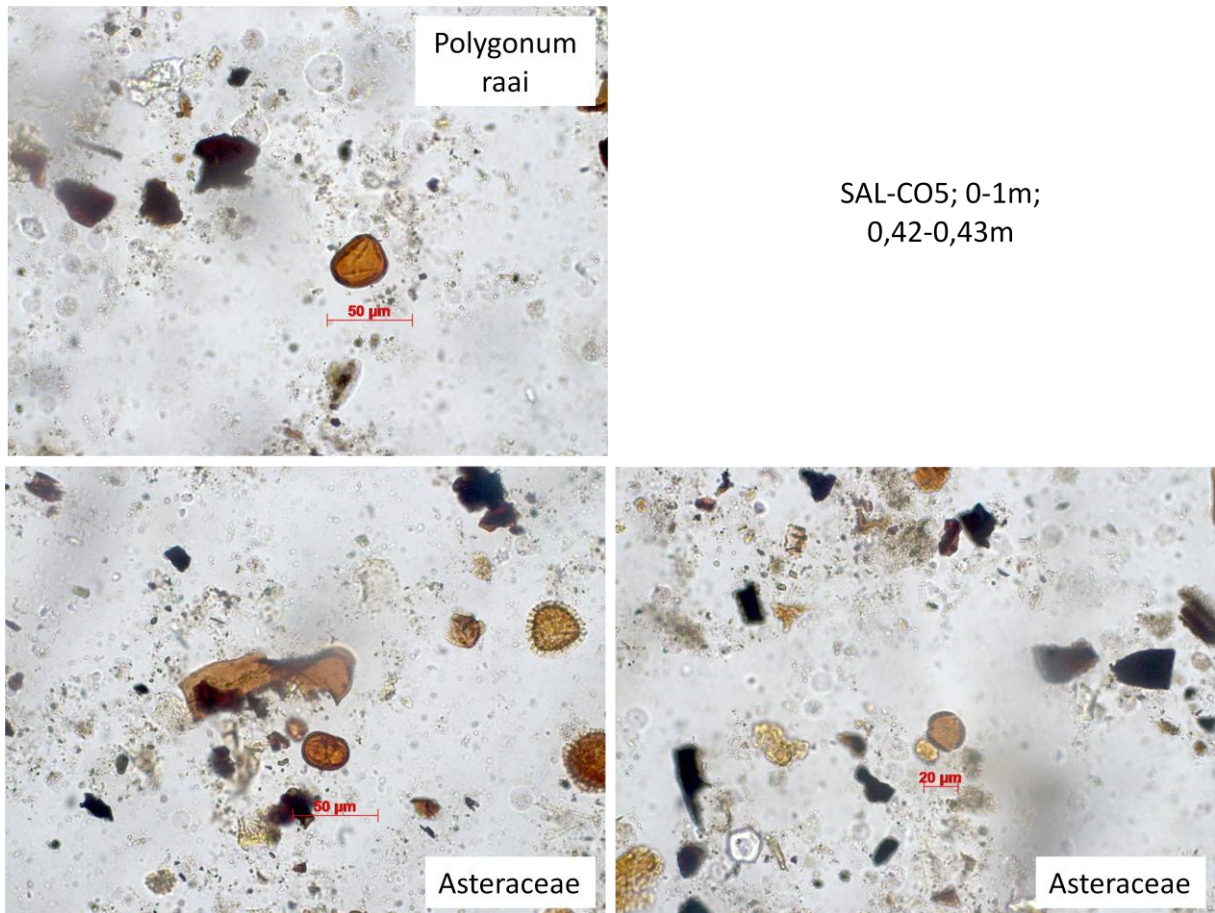


Fig. 53 Pictures of the sample SAL-CO5; 0-1m; 0,42-0,43m with the most representative pollen grains within this sample: Asteraceae, Polygonum rai (Polygonaceae)



Fig. 54 Pictures of Polygonum rai, left: pollen grains (Beug 2004), right: Eriogonum arborescens (www.plantsystematics.org)

Interpretation/Discussion

The interpretation is done using the different proxies which provide the potential for indicating changes of the palaeoenvironment. The interpretation will be done in sections for the core as well as in the presented results.

The sedimentological interpretation is done by comparing the different layers and cores and their properties with each other. Differences in conditions of sedimentation are visible in changes of sediment layers. If the water column is not very high, bioturbation and resuspension of sediments through waves or bottom currents can destroy the lamination of the sediments (Cohen 2003).

The evaluation of the magnetic susceptibility (MS) is done on the basis of Dearing (1999), who states that the MS indicates a specific mineralogy and geochemistry of a material. Furthermore, it provides a statement about the abundance of magnetic minerals or elements, like pure iron, magnetite and hematite. If no MS was measured, it does not necessarily mean that there are no magnetic minerals present. The magnetic susceptibility can be so weak, that it could not be measured.

In the following, the elements and element ratios presented within the chapter results are explained in an overview according to the possibility of interpretation after various authors. The results of the XRF-analysis are interpreted after their abundance of elements, trends, increases, decreases, peaks and lows. However, it has to be mentioned that the elemental distribution normally cannot be read as a direct indicator for a climate signal because of time effects, hiatus, the mentioned bioturbation and diagenetic effects (Boyle 2000) (Cohen 2003). Nevertheless, it is linked to climatic processes (Cohen 2003).

The interpretation of pollen data is done in a simplistic way because there is no expert knowledge of biological processes available author-side. The samples of DUL-CO3 contain no pollen, the samples of SAL-CO5 only show some pollen in the sample which has been taken out of the lowest centimeter of the uppermost clayey gravel layer. This could be due to the fact that these cores are taken at the shore lines of the salt lakes and that the pollen are probably oxidized and disappeared.

Furthermore, only five samples of the core SAL2 contain pollen grains, mainly Chenopodiaceae, Asteraceae, Polygonum raai and Phyllirea. The availability of pollen could be explained by the minor influence of air on these samples because it can be expected that the sediments containing these pollen grains were overlain by water. Why the samples from the deeper part of SAL2 do not contain any pollen remains unclear.

Element or ratio	Possible interpretation
Si	<ul style="list-style-type: none"> - The relatively nonreactive Quartz is transported mechanically into a lake (Cohen 2003) and is an important indicator for a terrigenous input (Rothwell et al. 2006). - Derives from weathering of silicate minerals like quartz, feldspars and micas; increasing weathering results in increasing Si-content (Cohen 2003). - Proxy for redissolved diatoms or siliceous algae (indicator for variation of productivity within a lake) (Cohen 2003).
Al	<ul style="list-style-type: none"> - Can derive from weathering of silicate minerals and indicates therefore changes in weather conditions (Cohen 2003) and detrital input (Eusterhues et al. 2005).
K	<ul style="list-style-type: none"> - Potassium salts accumulates under very arid conditions with little groundwater flow or surface flow (Cohen 2003). - Can indicate increases in salinity in closed-basins. Furthermore it is authigenic and an indicator for detrital input; the potassium content increases in times of erosion (Cohen 2003).
Pb	<ul style="list-style-type: none"> - Can be correlated to changes in the concentration of the silicate fraction (quartz and clay) (Koinig et al. 2003). - Possible indicator for pollution or soil dust, the latter increased during very cold periods or an increase in dust transportation (Koinig et al. 2003). In contrast, higher erosion rates also occur due to deforestation and therefore due to anthropogenic influence (García-Alix et al. 2013). - Indicates climate change, more detailed changes of humid and arid conditions (Kylander et al. 2007). - The pollution with lead in Southern Spain is increasing since around 3900 cal yr BP because of anthropogenic influence (García-Alix et al. 2013). - Is affected by redox conditions (Cohen 2003).
Rb	<ul style="list-style-type: none"> -Can be correlated to changes in the concentration of the silicate fraction (quartz and clay) (Koinig et al. 2003). - Indicator for watershed erosion and detrital input (Martín-Puertas et al. 2010) (Eusterhues et al. 2005).
Rb/Al	<ul style="list-style-type: none"> - Precipitation proxy (Martín-Puertas et al. 2010)
Ca, Sr	<ul style="list-style-type: none"> - Indicator for changes of silt, sand and calcite (Koinig et al. 2003).
Sr/Ca	<ul style="list-style-type: none"> - Gives information about the evaporation (Martín-Puertas et al. 2010)
Sr/Al	<ul style="list-style-type: none"> - Gives information about the evaporation, peaks indicate increases of evaporation (Martín-Puertas et al. 2010)
Mn/Fe	<ul style="list-style-type: none"> - Proxy for redox conditions (Koinig et al. 2003),
Mg/Ca	<ul style="list-style-type: none"> - Increases of the Mg/Ca ratio indicate an increase of salinity (Cohen 2003).
Mg/Al	<ul style="list-style-type: none"> - Precipitation proxy for Southern Spain (Martín-Puertas et al. 2010). - High Mg/Al and low Zr/Al can indicate river input (Martín-Puertas et al. 2010)
Zr/Al	<ul style="list-style-type: none"> - Coherent with the Mg/Al ratio used as precipitation proxy (Martín-Puertas et al. 2010). - Indicator for Sahara dust in the western Mediterranean basin, which are stronger in arid periods (Martín-Puertas et al. 2010)

table 4: Overview of elements and ratios used for interpretation

DUL-CO3

In the deeper part of the core, between 4 m and 3 m depth, the magnetic susceptibility is medium high which could mean that there could be some iron-bearing minerals present like magnetite according to Dearing (1999). The salinity, indicated by the Mg/Ca ratio (Cohen 2003), seems to fluctuate on a low level compared to other parts of the core and therefore times of deposition. This could indicate a more humid time period. The Mg/Al ratio stands for the variation of precipitation (Martín-Puertas et al. 2010) and is low within this section. The Sr/Ca ratio as well as the Sr/Al ratio indicate evaporation changes (Martín-Puertas et al. 2010), are low. This matches with low salinity indicated by the Mg/Ca ratio as well as the Zr/Al ratio which indicate possibly a higher precipitation (Martín-Puertas et al. 2010) at this time. The detrital input, indicated by the Rb-content (Eusterhues et al. 2005), the Si- (Rothwell et al. 2006)(Cohen 2003), Al- (Eusterhues et al. 2005) and K-content (Cohen 2003) seems to be moderate.

In the next core section between three and two meters depth, the magnetic susceptibility, as well as the potassium, aluminum and silica content decrease and indicate a possible decline of detrital input (Rothwell et al. 2006), (Cohen 2003)(Eusterhues et al. 2005), only interrupted by a peak of the K-, Al-, Si- and Rb-content as well as the Sr/Ca ratio, which gives indication of the evaporation (Martín-Puertas et al. 2010) and potentially indicates a short change to more arid conditions. This could not be correlated to the stratigraphy of Dul-CO3 which is not showing for example a change of the grain size. This is possibly followed again by more humid conditions (indicated with a high Mn/Fe ratio and interpreted after Koinig et al. (2003)). Up to the top of this core section at 2 m depth, the K-, Al- and Si-, contents decrease and this a possible indication of a decrease of the detrital input (Rothwell et al. 2006), (Eusterhues et al. 2005), (Cohen 2003).

In the upper part of the core, the low values of the K-, Al- and Si-content continue, followed by an increase of the element contents as well as the Sr/Al and Sr/Ca ratio. This does fit for the possible explanation of a high Sr/Al and Sr/Ca ratio which can indicate a higher evaporation (Martín-Puertas et al. (2010)) and therefore a higher temperature. Afterwards, up to 1 m depth, these values decrease. This could be an evidence for more humid conditions, also indicated by the higher Mn/Fe ratio which shows changes of the redox conditions (Koinig et al. (2003)). Up to the surface, proxies for more and more arid conditions, detrital input and the influence of Sahara dust can be observed (K-content (Cohen 2003), Al-content (Eusterhues et al. 2005), Si-content (Cohen 2003), Zr/Al ratio (Martín-Puertas et al. 2010), Sr/Ca (Martín-Puertas et al. 2010), Mg/Ca (Cohen 2003) and MS (Dearing 1999)). This is correlating with a low Mn/Fe and Mg/Al ratio as well as the mud content including various grain sizes in comparison to the clay layers below.

In this core, no lead has been measured. The reason for this error is unknown.

SAL1, 2&3

For better visualization, a map with the evaluated drilling points (without SAL1, because the coordinates are unknown) is inserted (Fig.55). The cores taken within the Laguna de Salada have been compared to each other, the core SAL-CO5, taken at the shore, is separate. The cores SAL1, 2 und 3 offer different depths, which is the reason for successiveness of the following interpretation.



Fig. 55 Map of the drilling locations of SAL,3 and SAL-CO5

Sal2 constitutes the longest core and the interpretation therefore starts with it, because the interpretation is done from the bottom to the top of the core.

SAL2 and SAL3 are nearly 70 m away from each other. Sal 2 shows moderate K, Al and Si values at a depth between 2 m and 1,8 m. This could be interpreted as moderate, terrigenous input to the lake. The detrital input derives from weathering of silicate minerals originated from erosion (Cohen 2003)(Eusterhues et al. 2005)(Rothwell et al. 2006). There occurs a peak of the Mg/Al at a depth of 1,8 m, which stands for the precipitation (Martín-Puertas et al. 2010), followed by a lower terrigenous input and again a period with more precipitation (the Mn/Fe ratio as well as the Rb/Al ratio is high at the same depth where the terrigenous input seems to be low; the Mn/Fe ratio is interpreted after Koinig. et al. (2003), the Rb/Al after Martín-Puertas et al. (2010)).

This decreasing trend is non-continuous and the terrigenous input is increasing again in the further part of the core, which could be resulted out of a more arid period. At the same time, the Rb-content decreases and possibly also indicates a less detrital input (Martín-Puertas et al. 2010)(Eusterhues et al. 2005). The core Sal3 is more or less comparable to SAL2 and shows the same trend in the element contents and ratios but with lower values.

SAL2 exhibits a decrease of Pb, Rb, Si, Al and K between 1,25 m and 1 m depth, interrupted by a high of Rb, Si, Al and K and coeval low of Mn/Fe at around 1,1 m depth. This could stand for a decrease and a short opposing trend of the weathering of silicates and the terrigenous input to the Laguna de Salada (Martín-Puertas et al. 2010)(Eusterhues et al. 2005)(Cohen 2003). The core SAL3 shows this trend as well, but for example the content of the element Pb increases up to 1 m depth. This can be evaluated as a higher pollution or soil dust deriving into the salt lake (Koinig et al. 2003) or as anthropogenic influence (García-Alix et al. 2013). At a depth of 1,25 m the high of the element ratio Zr/Al has to be mentioned. As it is not coeval with a high Mg/Al peak which would stand for a higher precipitation, this can be possibly an indication for Sahara dust (Martín-Puertas et al. 2010).

In the core SAL2 at a depth below 1 m, the contents of K, Si, Al, Rb, as well as the ratios Mg/Ca and Sr/Ca increase. Mn/Fe indicates an opposite trend. An explanation for this could be a change in conditions with higher terrigenous input (Cohen 2003)(Rothwell et al. 2006)(Eusterhues et al. 2005) and lower redox conditions (Koinig et al. 2003). This assumption could be reinforced by the peak of the ratio of Sr/Al, which stands for a high evaporation at this time (Martín-Puertas et al. 2010). These conditions seem to fluctuate with more humid conditions to greater highs and are also visible in the results of the XRF analysis of SAL3. In the same depth, the Mg/Ca ratio is lower and does not show this decreasing trend. The Sr/Al peak, indicator for a high evaporation (Martín-Puertas et al. 2010), is also visible in the results of SAL1, inevitably with a lower value.

The core SAL2 shows in the direction to the top lower values of the Sr/Al ratio, which could be an evidence for a change to more humid conditions again (Martín-Puertas et al. 2010). The terrigenous input represented by the magnetic susceptibility values increase to the top as well as the Pb-content and eventually indicate a period of more soil dust and erosion (Dearing 1999)(Koinig et al. 2003). However, the Mg/Ca ratio decreases and indicates slight decreases of salinity (Cohen 2003). Furthermore, the increase of the Zr/Al ratio to the top could be explained by a rise of Sahara dust (Martín-Puertas et al. 2010). SAL1 shows higher but comparable values as SAL2, but more abrupt changes, for example of Si, Al and potassium. By trend SAL1 shows considerably lower values of the magnetic susceptibility and on no account this dramatic increase to the top. Nevertheless the similar trend of the elements and ratios has to be mentioned.

SAL-CO5

This core is approximately 100 m-120 m away from the cores SAL2 and SAL3.

Between 4 m up to 3,4 m depth, the core SAL-CO5 contains homogenous clay and a low magnetic susceptibility. In addition with the high Zr/Al ratio, which stands for precipitation or Sahara dust (Martín-Puertas et al. 2010) as well as the low to medium values of Al, Si and K this can be an evidence for a low to medium high erosion at the time of deposition (Cohen 2003)(Rothwell et al. 2006)(Eusterhues et al. 2005). This is supported by the low Sr/CA and Sr/Al ratio.

The section between 3,4 m and 3 m depth is composed of sand, the magnetic susceptibility is approximately similar. On the contrary, the terrestrial influence is expected to grow at this time; the Rb-content is higher and probably indicating increased terrestrial input (Eusterhues et al. 2005); the Si-, Al-, and K-contents are higher, as well as the Sr/Ca ratio, standing for an increase of evaporation (Martín-Puertas et al. (2010)). There is no direct response observed for this thesis; the Mn/Fe ratio as well as the Zr/Al ratio only lower a little bit.

The interval from 3 m to around 0,4 m depth is build up of various silt layers which differ in color and carbonate content. The magnetic susceptibility is considerably lower as in the sections before. As this part consists of various layers, the element contents and ratios are also fluctuating a lot. They indicate several changes from humid to arid conditions. The proportions of these changes cannot be estimated. The changes can only be indicated and named by the comparison of the differing values. There seem to be at least three phases of low terrestrial input and weathering of silicate minerals (Rothwell et al. 2006)(Cohen 2003)(Eusterhues et al. 2005)(Kylander et al. 2007) (Koinig et al. 2003) (indicated by peaks of the proxies Si, Al, K and Pb and an opposite trend of the Mn/Fe ratio). On the other hand several high peaks of the Sr/Ca as well as the Sr/Al ratio have to be mentioned, suggesting a high evaporation (Martín-Puertas et al. (2010)).

The upper layer is made of clayey gravel, underlain by alternating clay/gypsum and mud layers and has a high magnetic susceptibility in comparison to the other three sections of the core. The Zr/Al ratio is high at this time and indicates precipitation or Sahara dust. Meanwhile, the evaporation seems to be low, reported by low Sr/Ca and Sr/Al ratios (Martín-Puertas et al. 2010). A high amount of silicate minerals is registered in this upper section, indicated by high Si and Al values. This fits with the high potassium content, which is also an indicator for detrital input into the lake and increases during times of erosion (Cohen 2003).

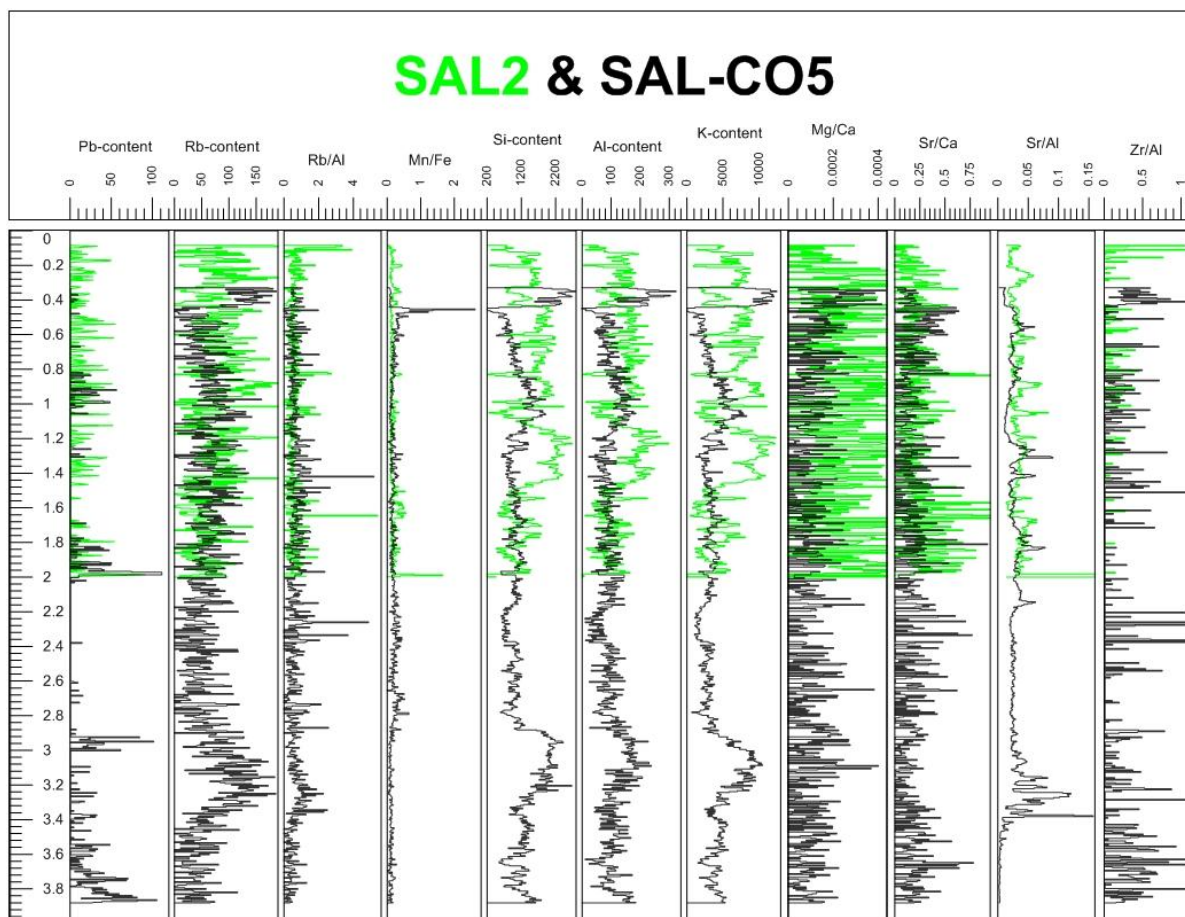


Fig. 56 Comparison of the cores SAL2 and SAL-CO3 respective the Pb-, Rb-, Si-, Al— and K-content and the Rb/Al, Mn/Fe, Mg/Ca, Sr/Ca, Sr/Al and Zr/Al ratio

In general, the core SAL-CO5 contains higher values of the magnetic susceptibility, less potassium, a lower Mg/Ca, Sr/Ca and Sr/Al ratios in comparison to the cores taken out of the lake floor (Fig.56). The Pb-, Rb-, Si-Al- content is lower as well. The Zr/Al ratio is higher. The peak of various elements in the SAL-CO5 core has to be mentioned as well, which does not occur in the SAL2 core. The interpretation of Fig. 56 let assume that the deposition of soil dust or pollution particles, reported with the Pb-content (Koinig et al. 2003), within the lake sediments are higher. Why the detrital input, probably reported with Rb (Eusterhues et al. 2005) Si (Rothwell et al. 2006), Al (Eusterhues et al. 2005) and K (Cohen 2003) is lower at the shore line is unresolved. The higher Mg/Ca ratio, indicating higher salinity (Cohen 2003) as well as the higher Sr/Ca ratio, representing a proxy of evaporation (Moreno et al. 2012) of SAL2 could be expected because of the location affected by lake water. As visible within the figure above, the Zr/Al ratio could be calculated more often for the core SAL-CO5. There are some peaks of the Sr/Al ratio in both cores, but the sediments taken directly out of the lake bottom show in general in the section between the surface and 2 m depth more high. One can assume that these sediments are probably more sensitive to changes in the environment or climate.

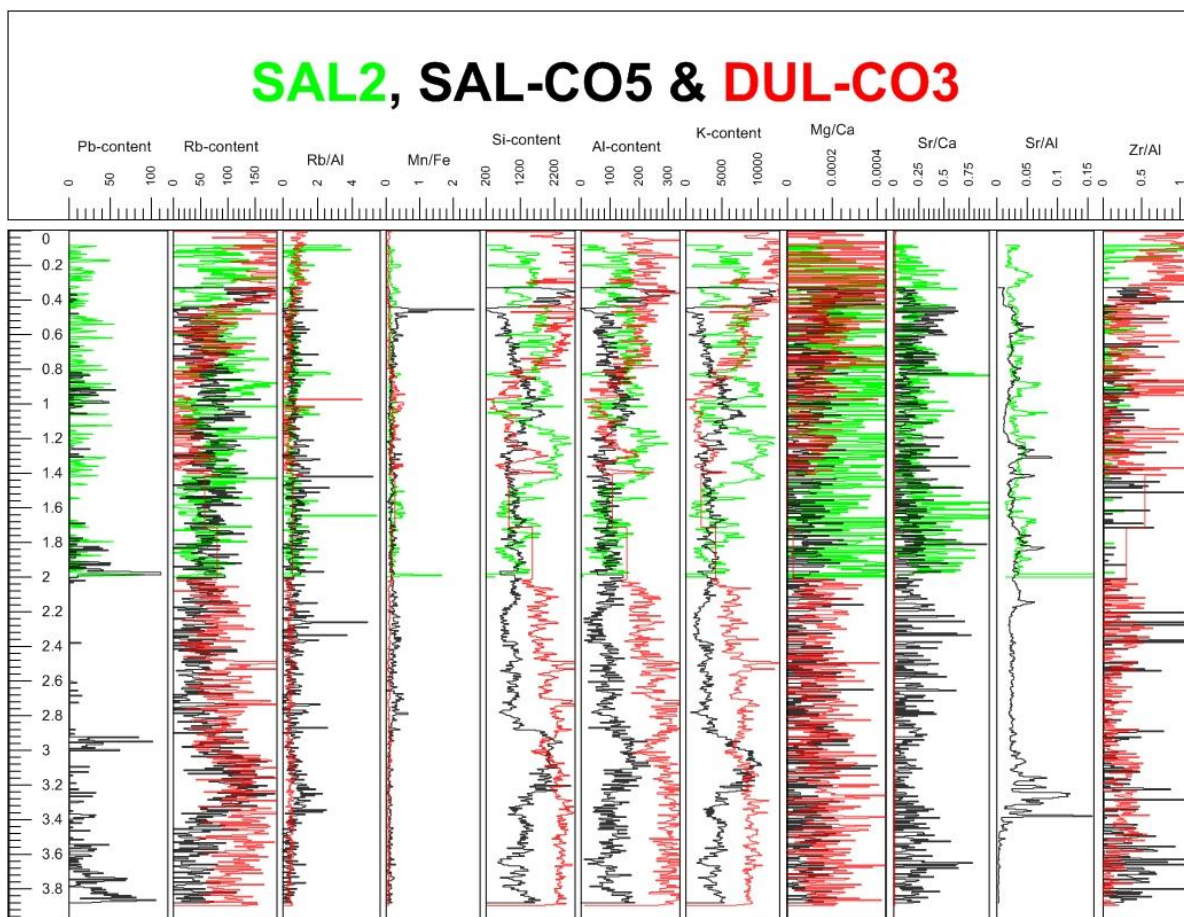


Fig. 57 Comparison of the same elements and ratios as in the picture before but in addition of DUL-CO3

As visible in Fig.57, the cores taken from the Laguna de Salada and the Laguna Dulce do not seem to be comparable. Lead was not measured within DUL-CO3. The Rb content is lower, higher, similar or showing a slight opposite trend at different depths. The Rb/Al ratio of DUL-CO3 in general is lower, but shows a high where there are no peaks at the other two cores reported. Though the comparison of the Al-, Si- and K-content is interesting and show that these elements are deposited within the DUL-CO3 core in a higher amount and furthermore an increasing or decreasing trend, while the SAL-CO5 core shows the opposite.

The absence of pollen probably can be explained by oxidation, leading to no preservation, or different reasons like only a few plants, too young plants or no flowering plants are present within the landscape (Hicks 2006). Additionally, there are differences in pollen transport, production or deposition of the different plants (Cohen 2003) and as Fletcher et al. (2007) has stated, the abundance of pollen grains within the sediments varies a lot between different areas in Spain.

The samples that did contain pollen did not show a clear change of the ecosystem, neither a lot of quercus pollen, which as Goñi et al. (2002) stated have been derived from evergreen oak forests and dominate the Mediterranean region. As the samples do not show a high difference of the ecosystem, they are not used for a palaeoclimate reconstruction.

Outlook

This multi-proxy study was done to contribute to the work of the SFB 806 “Our way to Europe” concerning the history of mankind, which is strongly influenced by the climate. Changes of environmental conditions leading to variability of sedimentation could be scientifically proven in this research work. The non possible correlation between the results of the Laguna Salada and Dulce has to be investigated in future work, nevertheless it has been stated by Battarbee (2000) that even lakes located close to each other are not always responding in the same way to the climate and its variations. It has to be mentioned that some methods applied could be reassessed; this concerns the pollen analysis which was not as successful as intended, probably as a result of the drying and shrinking of the lakes resulting in no conservation of pollen grains.

In order to extend the impact on the humankind and the expressiveness of this thesis, further work concerning the investigation on the sediment cores could be done. This may be done with diatom, ostracod or charcoal analysis as well as by comparing the investigated salt lakes with the Laguna de Fuente de Piedra, the biggest salt lake in the endorheic complex located close to the Laguna Salada and Dulce. This would improve the significance of this work as well as discover the dimensions of the detected variations. Furthermore, dating methods have to be applied to correlate the climate oscillations with exact time dates or periods.

List of figures

Fig. 1 Map of the Iberian Peninsula, the city Antequera is marked with a red point	7
Fig. 2 Map of the two cities Fuente de Piedra and Antequera (red points) and the location of the Laguna Salada, Dulce, del Gosque, Fuente de Piedra and de la Ratosa (blue points)	8
Fig. 3 Google earth map of the Lagunas with lake level change from the 03/12/2013 (unfortunately the lake level is not visible at the Laguna Salada due to the seize)	8
Fig. 4 Simplified Alpine tectonic setting of Iberia and the Alborán sea surrounding regions, modified after (Gibbons & Moreno 2002). The grey regions constitute the area where the Alpine orogen is exposed on land.	11
Fig. 5 Geological map of Southern Spain, modified after (Gibbons & Moreno 2002)	12
Fig. 6 Distribution of the main evaporate outcrops on the Iberian Peninsula (Gutiérrez et al. 2008) .	13
Fig. 7 Geological map with the three Lagunas Fuente de Piedra, Dulce & Salada (from North to South, indicated by the green points). This map was constructed with GIS on the basis of a geological map of the “SERVICIO DE PUBLICACIONES – MINISTERIO DE INDUSTRIA Y ENERGIA” of 1986.	15
Fig. 8 Legend for the geological map in Fig.7	16
Fig. 9 Geological map of the Laguna de la Ratosa, indicated by the green point. This map was constructed with GIS on the basis of a geological map of the “SERVICIO DE PUBLICACIONES – MINISTERIO DE INDUSTRIA Y ENERGIA” of 1986.	17
Fig. 10 Legend for the geological map with the Laguna de la Ratosa in Fig.9 (no translation available for words in quotation marks).....	18
Fig. 11 Geological Map of the Laguna del Gosque, indicated by the black point. This map was constructed with GIS on the basis of a geological map of the “SERVICIO DE PUBLICACIONES – MINISTERIO DE INDUSTRIA Y ENERGIA” of 1986.	18
Fig. 12 Legend for the geological map with the Laguna del Gosque in Fig.11	19
Fig. 13 Essential part of the International chronostratigraphic chart from the International Commission of Stratigraphy (v2013/01) for the geological site description	19
Fig. 14 Temperature distribution & zones in a thermally stratified lake;	20
Fig. 15 Cycle development from a flooded brackish lake to a dry pan (modified after (Lowenstein & Hardie 2006)	21
Fig. 16 Simplified model of factors affecting lake sediments modified after Cohen (2003)	22
Fig. 17 Pictures of coring with a vibracorer (a), of the floating platform (b), the open drill probes (c) & halves of liner tubes (d).....	25
Fig. 18 Geological map of the Laguna Salada & the Laguna Dulce with drilling points	26
Fig. 19 Picture from the Itrax XRF Core scanner (www.coxsys.se).....	27
Fig. 20 Mechanism for X-ray fluorescence of an atom (Kalnicky & Singhvi, 2001)	28
Fig. 21 Block diagram for a typical energy dispersive XRF spectrometer (Kalnicky & Singhvi 2001) ...	29
Fig. 22 Display panel of the Bartington MS2 (Dearing 1999)	30
Fig. 23 (A) Picture of waterbath (middle right side of the picture), (B) centrifugal, (C) Vortex Mixer, (D) safety equipment for HF-treatment, (E) HF-treatment & (F) ultrasonic bath with preparation equipment	33
Fig. 24 Last steps of pollen and pollen slide preparation	33
Fig. 25 Protocol for pollen preparation (part1)	34
Fig. 26 Protocol for pollen preparation (part2)	35
Fig. 27 Stratigraphy, further description and magnetic susceptibility of DUL-CO3	37

List of figures

Fig. 28 Plot of the stratigraphy, Rb-, Si-, Al- and K-content as well as the Rb/Al and Mn/Fe ratio of DUL-CO3, the Rb/Al and Mn/Fe ratio is presented at higher resolution. Highs and increases are illustrated in green, lows and decreases are illustrated with the blue boxes and arrows.....	38
Fig. 29 Plot of the stratigraphy as well of the Mg/Ca, Mg/Al, Sr/Ca, Sr/Al and Zr/Al Fe ratio in a higher resolution as in the previous figure of DUL-CO3. Highs and increases are illustrated in green, lows and decreases are illustrated with the blue boxes and arrows	39
Fig. 30 Stratigraphy, further description and magnetic susceptibility of SAL1	41
Fig. 31 Next plot of the stratigraphy as well of the Pb-, Rb-, Si- and Al content as well as the Rb/Al and Mn/Fe ratio in a higher resolution as in the previous figure. Highs and increases are illustrated in green, lows and decreases are illustrated with the blue boxes and arrows.....	42
Fig. 32 Plot of the stratigraphy as well of the K- content and the Mg/Ca, Mg/Al, Sr/Ca, Sr/Al and Zr/Al ratio in a high resolution. Highs and increases are illustrated in green, lows and decreases are illustrated with the blue boxes and arrows.....	43
Fig. 33 Stratigraphy, further description and magnetic susceptibility of SAL2	45
Fig. 34 Next plot of the stratigraphy, Rb-, Si-, Al- and K-content as well as the Rb/Al and Mn/Fe ratio of SAL2, the Rb/Al and Mn/Fe ratio is presented at higher resolution. Highs and increases are illustrated in green, lows and decreases are illustrated with the blue boxes and arrows.....	46
Fig. 35 Plot of the stratigraphy as well of the K- content and the Mg/Ca, Mg/Al, Sr/Ca, Sr/Al and Zr/Al ratio in a high resolution. Highs and increases are illustrated in green, lows and decreases are illustrated with the blue boxes and arrows.....	47
Fig. 36 Stratigraphy, further description and magnetic susceptibility of SAL3	49
Fig. 37 Plot of the stratigraphy as well as the Pb-, Rb-, Si- and Al content as well as the Rb/Al and Mn/Fe ratio of SAL3.....	50
Fig. 38 Plot of the stratigraphy as well of the K- content and the Mg/Ca, Mg/Al, Sr/Ca, Sr/Al and Zr/Al ratio in a high resolution. Highs and increases are illustrated in green, lows and decreases are illustrated with the blue boxes and arrows.....	51
Fig. 39 Stratigraphy, further description and magnetic susceptibility of SAL-CO5	53
Fig. 40 Plot of the stratigraphy as well of the Pb-, Rb-, Si- and Al content and the Rb/Al and Mn/Fe ratio in a high resolution. Highs and increases are illustrated in green, lows and decreases are illustrated with the blue boxes and arrows.....	54
Fig. 41 Plot of the stratigraphy as well of the K- content and the Mg/Ca, Mg/Al, Sr/Ca, Sr/Al and Zr/Al ratio in a high resolution. Highs and increases are illustrated in green, lows and decreases are illustrated with the blue boxes and arrows.....	55
Fig. 42 Pictures of the sample SAL2; 19-20 cm with the most representative pollen grains within this sample: Chenopodiaceae, Asteraceaea, Polygonum raai & Phyllirea.....	58
Fig. 43 From left to right: Salsola kali & Atriplex littoralis (2 times) (Beug 2004)	58
Fig. 44 Pictures of Chenopodiaceaea, right: Allenrolfea occidentalis, left: Maireana pyramidata (www.plantsystematics.org)	59
Fig. 45 Mineral remains, funghi & Lycopodium spores.....	59
Fig. 46 Picture of the Poaceaea Merostachys neesii (www.plantsystematics.org)	59
Fig. 47 Pictures of the sample SAL2; 0-1m; 0,59-0,60 m with the most representative pollen grains within this sample: Chenopodiaceae, Phyllirea	60
Fig. 48 Pictures of Phyllirea media (Beug 2004).....	60
Fig. 49 Pictures of the Crupina vulgaris of the group of the Asteraceae (Beug 2004)	61
Fig. 50 Pictures of the Asteraceae Aster novae-angliae (left) and Bellis perennis (right) (www.plantsystematics.org)	61

List of tables

Fig. 51 Pictures of the sample SAL2; 0-1m; 0,79-0,8 m with the most representative pollen grains within this sample: Asteraceae & Phyllirea (family of the Oleaceae)	62
Fig. 52 Picture of the Phyllirea angustifolia (www.plantsystematics.org)	62
Fig. 53 Pictures of the sample SAL-CO5; 0-1m; 0,42-0,43m with the most representative pollen grains within this sample: Asteraceae, Polygonum raii (Polygonaceae).....	63
Fig. 54 Pictures of Polygonum raii, left: pollen grains (Beug 2004), right: Eriogonum arborescens (www.plantsystematics.org)	63
Fig. 55 Map of the drilling locations of SAL,3 and SAL-CO5	67
Fig. 56 Comparison of the cores SAL2 and SAL-CO3 respective the PB-, Rb-, Si-, Al—and K-content and the Rb/Al, Mn/Fe, Mg/Ca, Sr/Ca, Sr/Al and Zr/Al ratio	70
Fig. 57 Comparison of the same elements and ratios as in the picture before but in addition of DUL-CO3	71

List of tables

table 1: some major evaporite minerals after Warren, 2010	23
table 2 Table of some minerals with magnetic susceptibility (Dearing 1999)	31
table 3 overview of the samples as well as their availability of pollen	57
table 4: Overview of elements and ratios used for interpretation	65

References

- Ábalos, B. et al., 2002. Variscan and Pre-Variscan Tectonics. In W. Gibbons & T. Moreno, eds. *The Geology of Spain*. Geological Society, London.
- Abrantes, F. et al., 2012. Paleoclimate Variability in the Mediterranean Region. In P. Lionello, ed. *THE CLIMATE OF THE MEDITERRANEAN REGION - FROM THE PAST TO THE FUTURE*. Elsevier Insights.
- Alcalá-García, F.J. et al., 2001. MINERALOGIA Y GEOQUIMICA DE LOS SEDIMENTOS DE ALGUNAS LAGUNAS DEL N DE LA PROVINCIA DE MALAGA (S DE ESPANA). *Estudios Geol.*, 57, pp.93–98.
- Alonso-Zarza, A.M. et al., 2002. Tertiary. In W. Gibbons & T. Moreno, eds. *The Geology of Spain*. Geological Society, London.
- Anderson, D.E., Goudie, A.S. & Parker, A.G., 2007. *Global Environments through the Quaternary - Exploring Environmental Change*, Oxford University Press.
- Azanón, J.M. et al., 2002. Alpine tectonics II: Betic Cordillera and Balearic Islands. In W. Gibbons & T. Moreno, eds. *The Geology of Spain*. Geological Society, London.
- Battarbee, R.W., 2000a. Palaeolimnological approaches to climate change, with special regard to the biological record. *Quaternary Science Reviews*, 19(1-5), pp.107–124.
- Battarbee, R.W., 2000b. Palaeolimnological approaches to climate change, with special regard to the biological record. *Quaternary Science Reviews*, 19(1-5), pp.107–124.

References

- Beug, H.-J., 2004. *Leifaden der Pollenbestimmung für Mitteleuropa und angrenzende Gebiete* 1st ed., Verlag Dr. Friedrich Pfeil München.
- Birks, H.H. & Birks, H.J.B., 2006. Multi-proxy studies in palaeolimnology. *Vegetation History and Archaeobotany*, 15(4), pp.235–251.
- Bischoff, J.L. et al., 1994. Karstification without carbonic acid Bedrock dissolution by gypsum-driven dedolomitization. *Geology*, 22, pp.995–998.
- Bolle, H.-J., 2003. Climate, Climate Variability, and Impacts in the Mediterranean Area: An overview. In H.-J. Bolle, ed. *Mediterranean Climate - Variability and Trends*. Springer Verlag.
- Borradaile, G.J., 1988. Magnetic susceptibility, petrofabrics and strain. *Tectonophysics*, 156(1-2), pp.1–20.
- Boyle, J.F., 2000. Rapid elemental analysis of sediment samples by isotope source XRF. *Journal of Paleolimnology*, 23, pp.213–221.
- Carrión, J.S. et al., 2010. The historical origins of aridity and vegetation degradation in southeastern Spain. *Journal of Arid Environments*, 74(7), pp.731–736.
- Cohen, A.S., 2003. *Paleolimnology - The History and Evolution of Lake Systems*, Oxford University Press.
- Cronquist, A., 1980. *Vascular flora of the southeastern United States*, The University of North Carolina Press.
- Dearing, J., 1999. *Environmental Magnetic Susceptibility. Using the Bartington MS2 System* 2nd editio., Chi Publishing, England.
- Dreßler, M. et al., 2010. Use of sedimentary diatoms from multiple lakes to distinguish between past changes in trophic state and climate: evidence for climate change in northern Germany during the past 5,000 years. *Journal of Paleolimnology*, 45(2), pp.223–241.
- Durán, J.J., López Martínez, J. & Vallejo, M., 1998. Distribución, caracterización y síntesis evolutiva del karst en Andalucía. In J. J. Durán & J. López-Martinez, eds. *Karst en Andalucía*. Instituto Tecnológico Geominero de Espana.
- Eusterhues, K., Heinrichs, H. & Schneider, J., 2005. Geochemical response on redox fluctuations in Holocene lake sediments, Lake Steisslingen, Southern Germany. *Chemical Geology*, 222(1-2), pp.1–22.
- FAO, 2013. FAO. (*Food and Agriculture Organization of the United Nations*). Available at: www.fao.org/sd/climagrimed/c_2_02.html [Accessed August 23, 2013].
- Fletcher, W.J., Boski, T. & Moura, D., 2007. Palynological evidence for environmental and climatic change in the lower Guadiana valley, Portugal, during the last 13 000 years. *The Holocene*, 17(4), pp.481–494.
- Fletcher, W.J. & Sánchez Goñi, M.F., 2008. Orbital- and sub-orbital-scale climate impacts on vegetation of the western Mediterranean basin over the last 48,000 yr. *Quaternary Research*, 70(3), pp.451–464.

References

- Fletcher, W.J. & Zielhofer, C., 2013. Fragility of Western Mediterranean landscapes during Holocene Rapid Climate Changes. *Catena*, 103, pp.16–29.
- Flügel, E., 2010. *MICROFACIES OF CARBONATE ROCKS - Analysis, Interpretation and Application* 2nd ed., Springer Verlag.
- García-Alix, a et al., 2013. Anthropogenic impact and lead pollution throughout the Holocene in Southern Iberia. *The Science of the total environment*, 449, pp.451–60.
- Gibbons, W. & Moreno, T., 2002. Introduction and overview. In W. Gibbons & T. Moreno, eds. *The Geology of Spain*. Geological Society, London.
- Giralt, S. et al., 1999. Late Glacial to Early Holocene environmental adjustment in the Mediterranean semi-arid zone of the Salines playa-lake (Alacante, Spain). *Journal of Paleolimnology*, 21, pp.449–460.
- Giralt, S. et al., 2011. Quantitative climate reconstruction linking meteorological, limnological and XRF core scanner datasets: the Lake Sanabria case study, NW Spain. *Journal of Paleolimnology*, 46(3), pp.487–502.
- Goñi, M.S. et al., 2002. Synchronicity between marine and terrestrial responses to millennial scale climatic variability during the last glacial period in the Mediterranean region. *Climate Dynamics*, 19(1), pp.95–105.
- Gutiérrez, F. et al., 2008. Geological and environmental implications of the evaporite karst in Spain. *Environmental Geology*, 53(5), pp.951–965.
- Gutiérrez-Elorza, M. et al., 2002. Quaternary. In W. Gibbons & T. Moreno, eds. *The Geology of Spain*. Geological Society, London.
- Harrison, S. & Digerfeldt, G., 1993. European lakes as palaeohydrological and palaeoclimatic indicators. *Quaternary Science Reviews*, 12, pp.233–248.
- Hicks, S., 2006. When no pollen does not mean no trees. *Vegetation History and Archaeobotany*, 15(4), pp.253–261.
- IPCC (Intergovernmental Panel on Climate Change), 2001. *Climate Change 2001. The Climate System*,
- Jalut, G. et al., 2009. Holocene circum-Mediterranean vegetation changes: Climate forcing and human impact. *Quaternary International*, 200(1-2), pp.4–18.
- Jiménez-Moreno, G. et al., 2013. Vegetation, fire, climate and human disturbance history in the southwestern Mediterranean area during the late Holocene. *Quaternary Research*, 79(2), pp.110–122.
- Kalnicky, D.J. & Singhvi, R., 2001. Field portable XRF analysis of environmental samples. *Journal of hazardous materials*, 83(1-2), pp.93–122.
- Kohfahl, C. et al., 2008. Characterising flow regime and interrelation between surface-water and ground-water in the Fuente de Piedra salt lake basin by means of stable isotopes, hydrogeochemical and hydraulic data. *Journal of Hydrology*, 351(1-2), pp.170–187.

References

- Koinig, K.A. et al., 2003. 9000 years of geochemical evolution of lithogenic major and trace elements in the sediment of an alpine lake—the role of climate, vegetation, and land-use history. *Journal of Paleolimnology*, 30, pp.307–320.
- Kylander, M.E. et al., 2007. Rare earth element and Pb isotope variations in a 52 kyr peat core from Lynch's Crater (NE Queensland, Australia): Proxy development and application to paleoclimate in the Southern Hemisphere. *Geochimica et Cosmochimica Acta*, 71(4), pp.942–960.
- Linares Girela, L. & Rendón Martos, M., 1998. La laguna de Fuente de Piedra (Málaga), un área endorreica de interés ecológico ligada al karst yesífero-salino. In J. J. Durán & J. López-Martinez, eds. *Karst en Andalucía*. Instituto Tecnológico Geominero de España.
- Lionello, P. et al., 2006. The Mediterranean Climate : An Overview of the Main Characteristics and Issues. In P. Lionello, P. Malanotte-Rizzoli, & R. Boscolo, eds. *MEDITERRANEAN CLIMATE VARIABILITY*. Elsevier - Developments in EARTH & ENVIRONMENTAL SCIENCES 4.
- López-Gómez, J., Arche, A. & Pérez-López, A., 2002. Permian and Triassic. In W. Gibbons & T. Moreno, eds. *The Geology of Spain*. Geological Society, London.
- Lowenstein, T.K. & Hardie, L.A., 2006. Criteria for the recognition of salt-pan evaporites. *Sedimentology*, 32.
- Luterbacher, J. et al., 2012. A Review of 2000 Years of Paleoclimate Evidence in the Mediterranean. In P. Lionello, ed. *THE CLIMATE OF THE MEDITERRANEAN REGION - FROM THE PAST TO THE FUTURE*. Elsevier Insights.
- Magny, M. et al., 2003. Contrasting patterns of hydrological changes in Europe in response to Holocene climate cooling phases. *Quaternary Science Reviews*, 22(15-17), pp.1589–1596.
- Martín-Puertas, C. et al., 2010. Late Holocene climate variability in the southwestern Mediterranean region: an integrated marine and terrestrial geochemical approach. *Climate of the Past*, 6(6), pp.807–816.
- Moreno, A. et al., 2012. The Medieval Climate Anomaly in the Iberian Peninsula reconstructed from marine and lake records. *Quaternary Science Reviews*, 43, pp.16–32.
- Murawski, H. & Meyer, W., 2010. *Geologisches Wörterbuch* 12th ed., Spektrum Akademischer Verlag Heidelberg.
- Okrusch, M. & Matthes, S., 2009. *Mineralogie. Ein Einführung in die spezielle Mineralogie, Petrologie und Lagerstättenkunde* 8th ed., Springer Verlag.
- Reed, J.M., 1998. Diatom preservation in the recent sediment record of Spanish saline lakes: implications for palaeoclimate study. *Journal of Paleolimnology*, 19, pp.129–137.
- Reed, J.M., 1996. The potential of diatoms, ostracods and other indicators for Holocene palaeoclimate research in southern Spanish salt lakes. *Limnética*, 12, pp.25–39.
- Reicherter, K., 2001. Paleoseismologic advances in the Granada basin (Betic Cordilleras, southern Spain). *Acta geológica hispánica*, 36, pp.267–281.

References

- Reicherter, K.R. & Peters, G., 2005. Neotectonic evolution of the Central Betic Cordilleras (Southern Spain). *Tectonophysics*, 405(1-4), pp.191–212.
- Rodó, X. et al., 2002. High-resolution saline lake sediments as enhanced tools for relating proxy paleolake records to recent climatic data series. *Sedimentary Geology*, 148, pp.203–220.
- Rodríguez-Rodríguez, M. et al., 2006. Estimation of ground-water exchange with semi-arid playa lakes (Antequera region, southern Spain). *Journal of Arid Environments*, 66(2), pp.272–289.
- Rothwell, R.G. et al., 2006. Turbidite emplacement on the southern Balearic Abyssal Plain (western Mediterranean Sea) during Marine Isotope Stages 1–3: an application of ITRAX XRF scanning of sediment cores to lithostratigraphic analysis. *Geological Society, ...*, 267, pp.79–98.
- Seppä, H. & Bennett, K.D., 2003. Quaternary pollen analysis: recent progress in palaeoecology and palaeoclimatology. *Progress in Physical Geography*, 27(4), pp.548–579.
- Sousa, A. et al., 2006. Post-Little Ice Age warming and desiccation of the continental wetlands of the aeolian sheet in the Huelva region(SW Spain). *Limnetica*, 25, pp.57–70.
- Stockhausen, H. & Zolitschka, B., 1999. Environmental changes since 13,000 cal. BP reflected in magnetic and sedimentological properties of sediments from Lake Holzmaar (Germany). *Quaternary Science Reviews*, 18, pp.913–925.
- Strahler, A.H. & Strahler, A.N., 1999. *Physische Geographie*, (UTB für Wissenschaft: Grosse Reihe) Verlag Eugen Ulmer Stuttgart.
- Tucker, M.E. & Wright, V.P., 1990. *Carbonate Sedimentology*, Oxford, UK: Blackwell Publishing Ltd.
- Valero-Garcés, B.L. & Moreno, A., 2011. Iberian lacustrine sediment records: responses to past and recent global changes in the Mediterranean region. *Journal of Paleolimnology*, 46(3), pp.319–325.
- Vanniere, B. et al., 2011. Circum-Mediterranean fire activity and climate changes during the mid-Holocene environmental transition (8500-2500 cal. BP). *The Holocene*, 21(1), pp.53–73.
- Wansard, G., 1996. QUANTIFICATION OF PALEOTEMPERATURE CHANGES DURING ISOTOPIC STAGE " IN THE LA DRAGA CONTINENTAL SEQUENCE (NE SPAIN) BASED ON THE Mg / Ca RATIO OF FRESHWATER OSTRACODS. *Quaternary Research*, 15, pp.237–245.
- Cohen, A.S.: Paleolimnology. The history and evolution of lake systems, Oxford University Press, New York, 2003.
- Engstrom, D. R. & H. E. Wright, 1984. Chemical stratigraphy of lake sediments as a record of environmental change. In Hayworth, E. Y. & J. W. G. Lund, Lake sediments and environmental history, University of Minnesota Press, Minneapolis, 411 pp.
- Bayly, I.A.E. & Williams, W.O. (1974) *Inland Waters and Their Ecology*. Longmans, London.
- Moreno, A., Cacho, I., Canals, M., Grimalt, J. O., S´anchez-Goñi, M. F., Shackleton, N., and Sierro, F. J.: Links between marine and atmospheric processes oscillating on a millennial timescale. A multi-

References

proxy study of the last 50 000 yr from the Alboran Sea (Western Mediterranean Sea), Quaternary land-ocean correlation, *Quaternary. Sci. Rev.*, 24, 1623–1636, 2005.

Guieu, C. and Thomas, A.: Saharan aerosol: from the soil to the Ocean, in: *The impact of desert dust across the Mediterranean*, edited by: Guerzoni, S. and Chester, R., Kluwer Academy Publishers, 207–216, 1996.

Further references for pictures:

Picture of the Itrax XRF Core scanner from: ; (27.08.2013)

Geological Maps are on the basis of: SERVICIO DE PUBLICACIONES – MINISTERIO DE INDUSTRIA Y ENERGIA (1986)

www.plantsystematics.org (09.09.2013; 15:00)